6th International Workshop on High-Resolution Depth Profiling HRDP6

Paris, France
June 27th-30th

SPONSORS

Agilent Technologies

INSTITUTIONAL SUPPORT

Supported by the Physics Faculty of UPMC

HRDP6 Lecture Hall

Sunday tutorial session

Posters and Sponsors,
coffees and lunches

Registration and Cocktails
21 rue de l'Ecole de Médecine
Sunday 26 June 18h00-20h00

Welcome to High Resolution Depth Profiling 6

We are very pleased to host this sixth High Resolution Depth Profiling Workshop in Paris. The program centers on use of ion beams to determine concentration depth profiles or atomic structure with nanometric or subnanmonetric depth resolution, covering MEIS, high resolution RBS and ERDA, and Nuclear Resonance Profiling. For this workshop, we have also invited experts to introduce some related techniques: in particular the established techniques of high resolution SIMS profiling and atom probe atomic location, and the emerging techniques around diffraction of grazing fast atoms.

The Workshop is preceded by a two day tutorial session on high resolution ion-beam depth profiling techniques, which has attracted 27 young participants, a number of whom plan to stay on and participate at the workshop.

The workshop and tutorial have been sponsored by the SPIRIT Integrated Infrastructure Intitiative of the European Union, which has provided resources to allow a number of doctoral students and early career researchers to participate, and we have benefitted from strong support from our industrial and institutional sponsors, whom we warmly thank here.

We wish you an invigorating conference, and very much hope that you will also be able to find time to sample some of the delights and attractions of Paris.

Ian Vickridge and the HRDP6 Organizing Committee

Paris, June 2011

HRDP6 Committees

International Committee

P. Bailey (UK)
J. O'Connor (Australia)
Y. Kido (Japan)
T. Koshikawa (Japan)
I. Vickridge (France)
M. Copel (USA)
T. Gustafsson (USA)
K. Kimura (Japan)
D. W. Moon (Korea)
D.P. Woodruff (UK)

Local Organizing Committee

Institut des NanoSciences de Paris

I. Vickridge (Chair) (Paris)
L. Bonnamy (Paris)
G. Deokar (Paris)
C. Deville-Cavellin (Paris)
S. Steydli (Paris)
E. Vickridge (Paris)
D. Benzeggouta (Paris)
E. Briand (Paris)
M. D'Angelo (Paris)
D. Schmaus (Paris)
I. Trimaille (Paris)
S. Younés (Paris)

Ece N. Aybeke

Program Committee

V. Esaulov (Orsay)
M. D'Angelo (paris)
D. Jalabert (Grenoble)
P. Roncin (Orsay)
D. Schmaus (Paris)
J-J. Ganem (Paris)

C. Deville-Cavellin (Paris)

HRDP6 Oral Program

Monday 27 June 2011

Chair : Daewon Moon

9h00	I 1	**Gustafsson**	*Medium Energy Ion Scattering from Novel Materials: High-k, SiC, Oxide Interfaces and Topological Insulators.*
9h35	O1	Primetzhoffer	High resolution Rutherford backscattering spectrometry: Depth profiling and composition analysis.
10h00	O2	Bauer	Information depth in Low Energy Ion Scattering

Coffee

Chair : Denis Jalabert

10h45	I 2	**Shutthanandan**	*High resolution depth profile analysis of interface mixing at the $LaAlO_3/SrTiO_3$ interface*
11h20	O3	Munnik	High-resolution RBS investigation of $LaLuO_3$ as candidate for a second-generation high-k material
11h45	O4	Chan	High-resolution Rutherford Backscattering Spectrometry investigation of solid phase epitaxial growth in Sn-implanted Si

Lunch

Chair : John O'Connor

14h00	I 3	**Blavette**	*Ultimate depth profiling using Atom Probe Tomography*
14h35	O5	Shuttanandan	Embedded Nanoparticle Analysis using Atom Probe Tomography and High-Resolution Electron Microscopy
15h00	O6	King	Surface Analysis of Samples Returned from the NASA Genesis Mission

Coffee

Posters and Sponsor Displays

Tuesday 28 June 2011

Chair : Kenji Kimura

09h00	I 4	**Goncharova**	*Transport and exchange of hydrogen and oxygen isotopes using medium energy ion scattering*
09h35	O7	Deokar	Investigation of oxygen exchange between CO_2 and thermally grown SiO2 network by Narrow Resonance Depth Profiling
10h00	O8	Py	Ultimate backside sample preparation for ultra thin high-k/metal gate stack depth profiling with ToF-SIMS, MEIS and pAR-XPS

Coffee

Chair : Pedro Grande

10h45	I 5	**Visikovskiy**	*Oxygen deficiency and excess of metal-oxide surfaces analyzed by MEIS and ERD*
11h20	O9	Woodruff	The V_2O_3(0001) surface termination crystallography: phase equilibrium revealed by medium- and low-energy ion scattering.
11h45	O10	Jalabert	Strain measurement in a thin silicon film using Medium Energy Ion Scattering.

Lunch

Chair : Lyudmila Goncharova

14h00	I 6	**Etgens**	*Layer-by-layer film growth monitored by Grazing Incidence Fast Atom Diffraction*
14h35	O11	Brongersma	Quantitative and non-destructive determination of the atomic composition of the outer surface and of in-depth profiles by HS-LEIS
15h00	O12	Goebl	Quantification of second layer contributions in Low Energy Ion Scattering

Coffee

Tuesday 28 June 2011(continued)

Chair : Peter Bauer

15h45	I7	**Noakes**	*Dealing with disorder, defects and amorphicity in medium energy ion scattering experiments*
16h20	O13	Bergmaier	Monte Carlo simulations of high resolution elastic recoil detetection depth profiles
16h45	O14	Ganem	Vicinage Effect and Coulomb explosion dynamics of hydrogen molecules in Silicon Nitride Films
17h10	O15	Hentz	A simple approach for simulating the 2D MEIS spectrum in crystalline materials

---

Wednesday 29 June 2011

Chair : Bruce King

09h00	I 8	Vandervorst	*High Resolution SIMS Depth Profiling*
09h35	O16	Ngo	Depth profiling of metal - organic samples by (low-energy) dynamic SIMS
10h00	O17	Meerschaut	Compositional analysis of NiO thin films grown by MOCVD

Coffee

Chair : Wilfried Vandervorst

10h45	I9	**Sánchez**	*Adsorption and thermal stability of organic films on surfaces monitored by Direct Recoil Spectroscopy*
11h20	O18	Itani	Depth Resolution in SIMS Depth Profiling with Oxygen Primary Ions
11h45	O19	Galtayries	ToF-SIMS depth profiling of nanometric Mg/Co/Zr stacks

Lunch

Outing

Gala Dinner

Thursday 30 June 2011

Chair : Phil Woodruff

09h00	I10	**Baddeley**	*Using MEIS to probe segregation effects in bimetallic nanoparticles.*
09h35	O20	Sortica	Nanostructures characterization using the MEIS technique.
10h00	O21	Sanchez	Structural characterization of buried nanostructured materials through Medium Energy Ion Scattering technique

Coffee

Chair : Torgny Gustafsson

10h45	I11	**Kimura**	*Improvement of sensitivity in high-resolution RBS by reducing detector noise*
11h20	O22	Bailey	A UHV-compatible, demountable heat transfer system.
11h45	O23	Moon	Development of imaging TOF- MEIS and Applications

Closing Remarks

Lunch

High-Resolution Depth Profiling

June 27th - 30th, 2011

Talk abstracts

I 1. Medium Energy Ion Scattering from Novel Materials: High-k, SiC, Oxide Interfaces and Topological Insulators.

T. Feng[1], H. D. Lee[1], C. Xu[1], X. Zhu[1], E. Garfunkel[2], L. C. Feldman[1], and T. Gustafsson[1]

gustaf@physics.rutgers.edu (corresponding author)

[1] *Department of Physics, Rutgers University, 136 Frelinghuysen Road, Piscataway, NJ 08854, USA*
[2] *Department of Chemistry, Rutgers University, 610 Taylor Road, Piscataway, NJ 08854, USA*

I will describe some recent depth profiling experiments on novel materials that have been done at Rutgers using medium energy ion scattering. Topics will include:

- High dielectric constant materials as gate dielectrics in state of the art devices.
- Interface structure of SiC and the role of carbon.
- Interfaces between oxides – what is the origin of the metallic conductivity in the $LaAlO_3/SrTiO_3$ system?
- Ultrathin films of topological insulators – interface structure and growth.

O1 High resolution Rutherford backscattering spectrometry: Depth profiling and composition analysis.

D. Primetzhofer[1], W. Roessler[1], P.J. Wagner[1], M. Yarema[2], W. Heiss[2] and P. Bauer[1]

daniel.primetzhofer@jku.at (corresponding author)

[1]*Institut für Experimentalphysik, Johannes Kepler Universitaet Linz, A-4040 Linz, Austria*
[2] *Institut für Festkörperphysik, Johannes Kepler Universitaet Linz, A-4040 Linz, Austria*

Rutherford backscattering spectrometry (RBS) is a versatile tool for analysis of composition and thickness of µm- and sub-µm-films. However, RBS is often claimed to have limited resolution, with respect to element identification, especially for multi-trace element targets [1]. The development of electrostatic or magnetic spectrometers [2] and construction of high resolution semiconductor surface barrier detectors (SSBD) [3] has pushed the limit in thickness analysis, and moreover also permits composition analysis with much higher accuracy. In the present work, we explore the potential of High Resolution RBS (HR-RBS) in identification and quantification of elements with very low concentrations in thin films. By analysis of a multi-element organic compound (human blood) the resolution and accuracy of the method is tested [4]. A comparison of HR-RBS with competing techniques will be presented. Furthermore, we also examine the analytical power of HR-RBS in thickness analysis. In this context, systems composed of multiple nm-films are investigated. Additionally, we studied ultrathin layers of semiconductor quantum dots deposited on Si.

The experiments were performed employing the AN-700 accelerator at the Johannes Kepler University of Linz. The accelerator provides monoenergetic beams of H, D and He ions with up to 700 keV primary energy. A LN2 cooled surface barrier detector and a low noise amplification system were used to record the spectra of backscattered projectiles [3]. The sample orientation with respect to the beam can be changed to improve depth resolution.

For the organic sample, it was possible to identify at least 10 chemical elements with high accuracy. For instance, the concentration of Fe was determined to 350 +/- 10 ppm equivalent to 400 mg/L in perfect agreement with standard blood test values. The detection limit for elements with atomic number higher than Fe is found to be below 20 ppm. Note that it would be possible to resolve a concentration gradient within the film by HR-RBS.

The depth profile analysis of the multi-layer structures sets new limits for the minimum layer thickness that can be resolved in HR-RBS experiments using a SSBD. In addition, the integral depth profile can be determined from experiments at primary energies well above the stopping maximum.

The results presented clearly indicate the potential of HR-RBS for both, thickness and composition analysis of thin films. The main advantage of using an elastic scattering technique is that relative and absolute elemental concentrations can be determined with very high accuracy. In other words, no matrix effects have to be expected.

References

W. Maenhaut. Nucl. Instr. and Meth. B **35** (1988) 388
K. Kimura, K. Nakajima, M. Mannami, Nucl. Instr. and Meth. B **136** (1998)1196
M. Geretschläger, Nucl. Instr. and Meth. B **204** (1983) 479
D. Primetzhofer, P. Bauer, Nucl. Instr. Meth. B, in print

O2 Information depth in Low Energy Ion Scattering

D. Primetzhofer1, S.N. Markin1, M. Spitz1, S. Rund1, D. Goebl1, D. Roth1, E. Taglauer2 and P. Bauer1

peter.bauer@jku.at (corresponding author)

[1]*Institut für Experimentalphysik, AOP, JKU Linz, A-4040 Linz, Austria*

[2] *Max-Planck-Institut für Plasmaphysik, EURATOM Association, D-85748 Garching bei München, Germany*

The basic idea of Low Energy Ion Scattering (LEIS) is to bombard a sample with noble gas ions and analyze the projectiles, which are backscattered into a certain solid angle dΩ. Typical incident energies E_0 of the ions range from 0.5 keV to 10 keV. In a typical experimental geometry, the angle of incidence α, measured with respect to the surface normal, is smaller than 60° and the scattering angle θ is ~ 130° or larger.

LEIS is known for its excellent surface sensitivity, when noble gas ions are used as projectiles and scattered ions are detected. Furthermore, the absence of matrix effects in the yield of scattered ions Y^+ is commonly accepted [1]. The extremely high surface sensitivity is based on the large scattering cross section and the very efficient neutralization of primary ions. Therefore, quantification of experimental LEIS data urgently requires a fundamental understanding of charge exchange.

For He^+ projectiles, different charge exchange mechanisms are active depending on the primary energy and the atomic species of the projectile [2]. Non-local Auger neutralization (AN) is possible at all primary energies. Collision induced neutralization (CIN) and reionization (CIR) can only contribute for sufficiently close interaction distance between projectile and target atom. In this process, the He 1s level is promoted to energies resonant with the conduction band, below or above the Fermi level, respectively. This minimum distance corresponds, for a given scattering geometry, to an energy threshold E_{th}.

In this contribution we present an analysis of the information depth deduced from P^+ data obtained for He^+ ions and metal surfaces (Cu, Au, Al) both, in the regimes of reionization and where only AN is possible [3].

Support by the Fonds zur Förderung der Wissenschaftlichen Forschung (project P20831) is gratefully acknowledged.

References.

[1] H.H. Brongersma, M. Draxler, M. de Ridder, P. Bauer, Surf. Sci. Rep. 62 (2007).
[2] R. Souda and M. Aono, Nucl. Instrum. Methods Phys.Res., Sect. B 15, 114 (1986).
[3] D. Primetzhofer, M. Spitz, E. Taglauer, and P. Bauer, submitted.

I 2. High resolution depth profile analysis of interface mixing at the $LaAlO_3/SrTiO_3$ interface

V. Shutthanandan[1], L. Qiao[1], A. Cohen[1], T. Feng[2], H.D. Lee[2], T. Gustafsson[2], E. Garfunkel[2]
S. Thevuthasan[1] and S. A. Chambers[1]

Shuttha@pnl.gov – corresponding author

[1]*Pacific Northwest National Laboratory, Richland, WA, USA*
[2]*Rutgers University, Piscataway, NJ, USA*

There is a strong and growing interest in complex oxide interfaces because of the wide range of functional properties exhibited. It is well known that the $LaAlO_3/SrTiO_3$ (LAO)/(STO) interface exhibits novel electronic conductivity when grown in certain ways. LAO and STO are both band insulators in the bulk, but their interface exhibits n-type electrical conductivity when LAO is grown on TiO_2-terminated STO. The observed conductivity has been attributed to formation of a two-dimensional electron gas on the $SrTiO_3$ side of the interface. Most of the papers published so far, assumed that the film is stoichiometric and the interface is abrupt without any interface mixing. In light of the potential importance of intermixing at the LAO/STO interface, we have combined high resolution analytical methods with a range of sensitivities to elemental concentrations and spatial separations to investigate the interfaces of films grown using pulsed laser deposition.

Detailed interface characterization were carried out in thinner (4 u.c) and thicker (25 u.c) films. For each thickness, we utilize techniques well suited to the thickness—RBS, ToF-SIMS and HAADF-STEM/EELS for 25 u.c. films, and HRBS, ARXPS and MEIS for 4 u.c films. MEIS and HRBS data collected at random direction (Figure 1.a) clearly indicated that La indiffused in to the STO substrate while Sr outdiffused into the LAO film [1]. MEIS spectrum

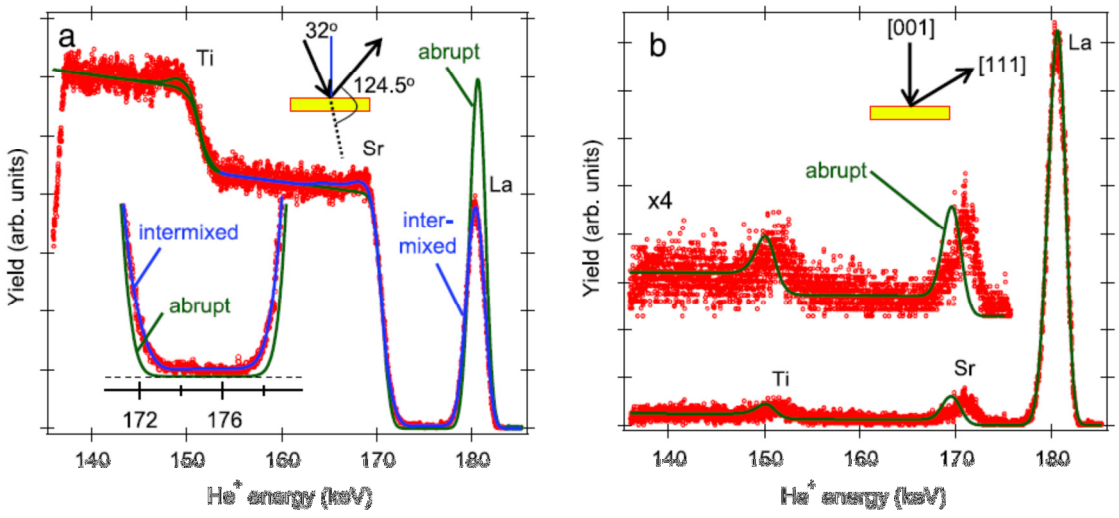

Figure 1. 198.6 keV He+ MEIS spectra in random (a) and aligned (b) geometries, along with simulations for abrupt and intermixed interface models, for a 4 u.c. Tokyo film [1].

collected in the channeling direction (Figure 1.b) reveals that Sr and Ti out diffused all the way to the first u.c of the LAO film. Since MEIS does not have enough sensitivity for the Al, we have also carried out angle resolved XPS to study the interface of this film. The ARXPS scans clearly deviate from simulations based on an abrupt interface and an optimized intermixed model is required to reproduce these data.

RBS (shown in Figure 2) and ToF SIMS (Figure 3) data collected on the 25 u.c sample clearly shows that La diffuses deep into the STO substrate. The clear presence of a shoulder

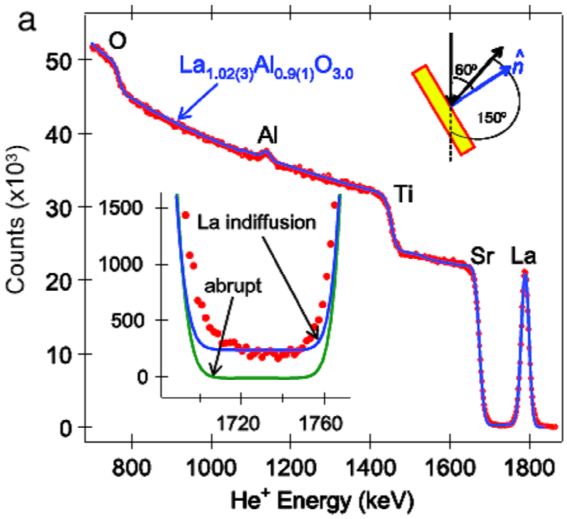

Figure 2. Experimental RBS spectra using 2 MeV He+ for 25 u.c. LAO/STO(001) at scattering angles of 96◦ along with optimized SIMNRA simulations [1]

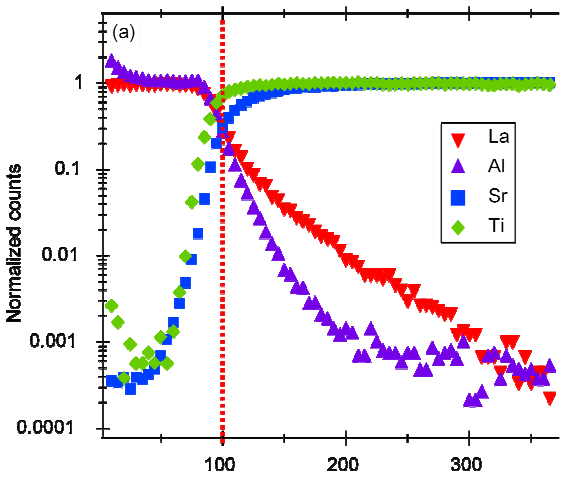

Figure 3. ToF-SIMS depth profiles for 25 u.c. LAO/STO(001. The count rates have been normalized to unity near the surface for La and Al. and deep in the bulk for Sr and Ti.

Between the low energy side of the La RBS peak and the high energy side of the Sr edge suggests La indiffusion, although this shoulder could also be caused by pulse pile up in the detector, straggling, and/or multiple/dual scattering effects. Therefore, RBS data were taken as a function of beam current, incident beam energy, and film thickness to determine if this shoulder is due to these artifacts, or La indiffusion (figure 4). It was determined that none of the aforementioned artifacts occur, thereby implicating La indiffusion. The presence of substitutional La at Sr sites in the substrate provides a plausible explanation for the observed n-type conductivity, as La is a shallow donor in STO. Hence, using several independent analytical methods, we have shown that there is a strong tendency for the LAO/STO interface to intermix rather than form an atomically abrupt interface.

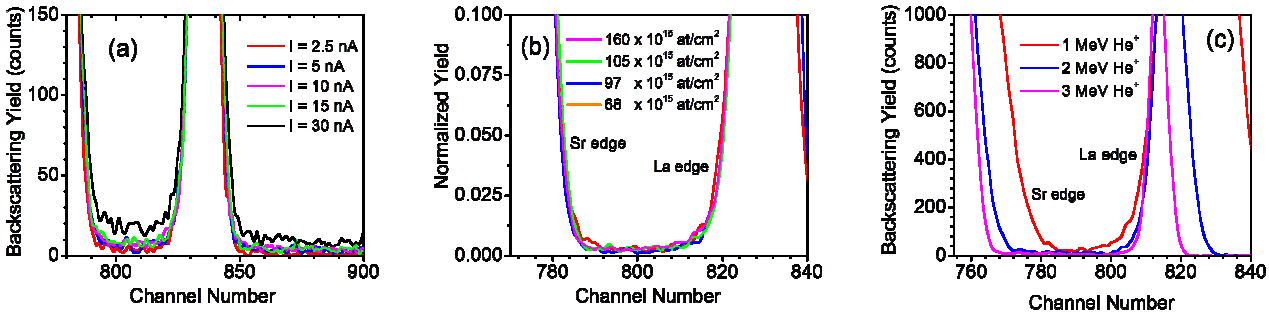

Figure 4: (a) Experimental RBS spectra using 2 MeV He+ for 25 u.c. LAO/STO(001) with various incident beam currents to illustrate the effect of pulse pile up (b) RBS valley between the La and Sr peaks at 2 MeV He+ for LAO/STO(001) films grown at a scattering angle of 150° for various LAO film thicknesses to illustrate the effect of straggling and (c) Valley between the La and Sr RBS peaks for 25 u.c. LAO/STO(001) as a function of incident beam energy to illustrate the effect o multiple scattering.

In this talk, we will present our detail analysis of this system using high resolution depth profile methods. Recently, we have undertaken a comprehensive experimental and theoretical investigation of the properties of MBE-grown $LaCrO_3$ (LCO) on STO(001). This system received considerable attention because the band gap and optical absorption properties are tunable by doping the LCO with Sr. Resent results from HRBS (Figure 5), STEM and XPS will also be presented.

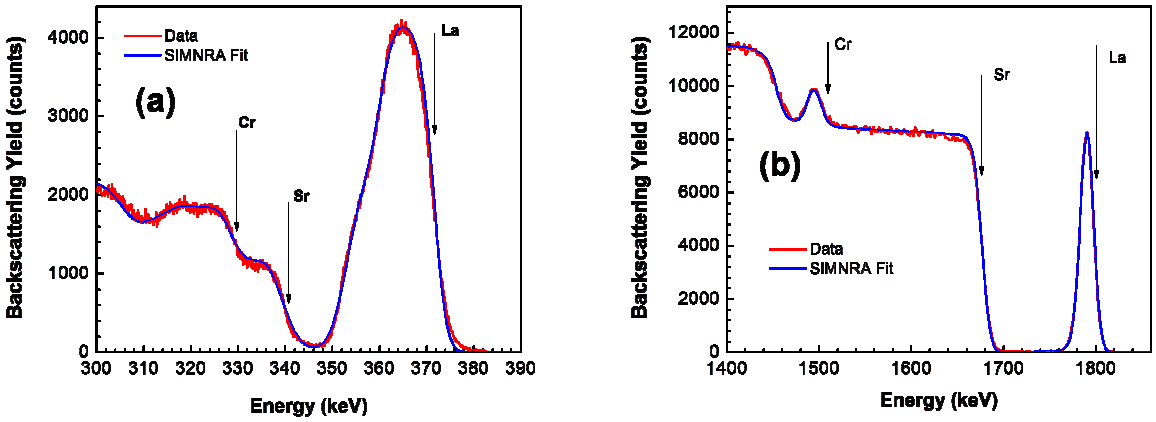

Figure 5: Comparison of HRBS (a) and normal RBS (b) spectrum obtained from LCO film on STO.

References:

[1] S.A. Chambers, M.H. Engelhard, V. Shutthanandan, Z. Zhua, T.C. Droubaya, L. Qiao, P.V. Sushko, T. Fengc, H.D. Lee, T. Gustafsson , E. Garfunkel , A.B. Shahd, J.-M. Zuod, Q.M. Ramassee, Surface Science Reports 65 (2010) 317–352

O3 High-resolution RBS investigation of $LaLuO_3$ as candidate for a second-generation high-k material

M. Kosmata, M. Zier, F. Munnik

f.munnik@hzdr.de (corresponding author)

Helmholtz-Zentrum Dresden-Rossendorf (HZDR), P.O.Box 510119, D-01314 Dresden, Germany

The ever-shrinking MOSFET (metal–oxide–semiconductor field-effect transistor) requires new materials that exhibit a higher dielectric constant compared to SiO_2, for the gate dielectric [1]. Currently underway is the search for second-generation high-k materials [2] with higher permittivity, superior thermodynamic stability in contact with Si [3], matching band alignment with Si [4] and processing compatibility with poly-Si and metal gate electrodes. A suitable candidate material is lanthanum lutetium oxide ($LaLuO_3$, LLO). During the so-called "gate first" manufacturing process, the gate oxide stack is subjected to thermal treatment. It is, therefore, important, to investigate the thermal stability of the deposited layer stack.

The samples under investigation are stacks of Si/$LaLuO_3$/Si made by FZ Jülich, before and after annealing at 900°C. The samples have been studied with standard RBS (Rutherford Backscattering Spectrometry), high-resolution RBS and high-resolution TEM (Transmission Electron Microscopy). Standard RBS measurements have been performed under a scattering angle of 170° and two different angles of incidence to the surface normal (0° and 70°), where the first provides good separation of La and Lu in the spectrum and the latter higher depth resolution. These two measurements give the total amount of La, Lu and O and to a minor degree the depth profile of these elements. However, the results indicate some mixing of Si into the LLO, but the depth resolution was insufficient to obtain unambiguous results. High-resolution TEM could not provide a definitive answer either. Therefore, high-resolution RBS has been employed to investigate this question.

The high-resolution RBS set-up [5] consists of a Browne-Buechner type magnetic spectrometer and a position sensitive detector coupled to a 3 MV Tandetron accelerator. A 2.024 MeV C^{2+} ion beam has been used. The spectrometer is located at a forward scattering angle of 35° to maximise the depth resolution and scattering cross-section, achieving an energy resolution of $< 0.1\%$. Due to the limited length of the position sensitive detector, only a narrow energy window of $< 0.1\ E_0$ can be analysed. Therefore, not all elements and also often not the whole width of one layer in the sample can be measured in one run and several measurements with a shifted energy window have to be performed. These individual spectra can be analysed simultaneously using WiNDF [6] or in a more intuitive approach, all partial spectra are combined in one complete spectrum. For this purpose, the counts were re-binned into new energy bins of 1 keV width, considering a different channel to energy calibration for each spectrum. For an internal self-consistency check the partial spectra overlap a certain amount and the final spectrum is obtained by averaging the overlapping data.

The resulting spectra for a sample before and after thermal treatment clearly show a redistribution of Si during annealing. This work will be continued with an investigation of the annealing temperature dependence and different annealing processes on the intermixing of Si.

References

[1] http://www.itrs.net/links/2009itrs/home2009.htm.
[2] M. Li et al. Adv. in Sci. and Techn. 45 (2006) 1342.
[3] E.P. Gusev et al. Microelectronic Engineering 59 (2001) 341.
[4] J. Robertson. Appl. Surf. Sci. 190 (2002) 2.
[5] R. Grötzschel et al. Nucl. Instr. Meth. B219 (2004) 344.
[6] N.P. Barradas, C. Jeynes, R.P. Webb, Appl. Phys. Lett. 71 (1997) 291.

O4 High-resolution Rutherford Backscattering Spectrometry investigation of solid phase epitaxial growth in Sn-implanted Si

T. K. Chan[a], A. Markwitz[b], F. Fang[b], T. Osipowicz[a]
phyctk@nus.edu.sg (Corresponding author)
[a] *Centre for Ion Beam Applications (CIBA), Department of Physics, National University of Singapore, Blk S7, 2 Science Drive 3, 117542 Singapore*
[b] *Institute of Geological and Nuclear Sciences (GNS), 1 Fairway Drive, Avalon 5010 PO Box 30-368, Lower Hutt 5040, New Zealand*

Si-Sn alloys potentially allow for band gap tuning over a very wide energy range, with anticipated applications in the manufacture of novel devices. However, introduction of Sn into Si usually creates damage in the Si lattice, and crystal regrowth via solid phase epitaxy is required since good crystallinity is essential for proper band gap characteristics. In this paper, the solid phase regrowth process of ultra-thin Sn-implanted Si samples was investigated using channeling High-resolution Rutherford Backscattering Spectrometry. Silicon samples implanted with and without the Si substrate undergoing prior self-amorphization process were investigated. (100) Si was used, and the pre-amorphization was done by 25 keV self implantation. Solid phase regrowth was induced by electron beam annealing at 429 °C and 529 °C for durations in the range of 50 – 5000 seconds. Result show markedly different behavior for the two sets, and are discussed in terms of melt-induced crystallization process introduced in [1].

References

[1] R.P. Thornton, R.G. Elliman and J.S. Williams, J. Mater. Res. 5 (1990) 1003

I 3. Ultimate depth profiling using Atom Probe Tomography

D. Blavette[1,2] , S. Duguay[1], and E. Cadel[1]

Corresponding author : Didier.blavette@univ-rouen.fr

[1] *GPM UMR CNRS 6634, Université de Rouen, UFR Sciences, BP12, 76801 St Etienne u Rouvray cedex*
[2] *Institut Universitaire de France, Paris*

The design of the three-dimensional atom probe twenty years ago has been an important breakthrough in the advents of high resolution analytical microscopes. The first prototypes of this instrument were developed at Oxford, GB ("the position sensitive atom probe") and Rouen, France ("the tomographic atom probe") [1,2]. For the first time it has been possible to map out the distribution of chemical species at the atomic scale in 3D (fig. 1).

Atom Probe has been one of the rare methods able to provide depth profiles at the ultimate scale. The instrument combines a very high spatial resolution (better than 0.1 nm in depth) with the quantitativity of composition measurements. Many key results were provided by this new instrument, for instance Cottrell atmospheres (segregation of solute elements to dislocation lines) were imaged in 3D at the atomic-scale for the first time [3]. Depth profiles along an arbitrary direction can be derived from 3D images such as shown in figure 1. The composition of individual planes can be measured. It is hence possible to determine the preferential sites of addition elements in ordered phases (fig.2).

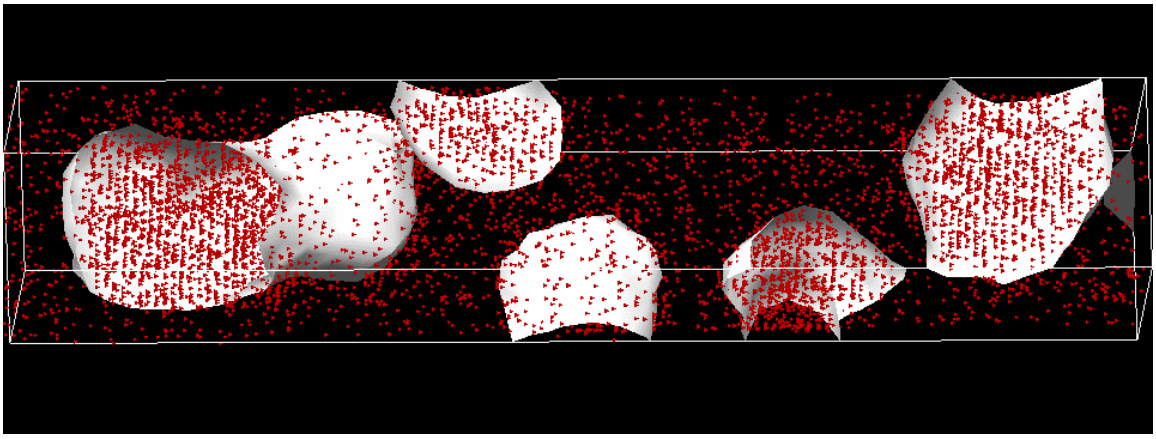

Figure 1. Three dimensional reconstruction of the small volume analysed in a model superalloy (V = 8×8×45 nm^3). Only Al is represented for the sake of clarity. Al-enriched γ' precipitates are observed in the Al-depleted γ solid solution (parent phase). Al isosurfaces (grey envelopes, threshold: C_{Al} = 10 at. %) provide the approximate location of γ-γ' interfaces. The volume has been tilted parallel to [001] direction to exhibit the ordered structure of small precipitates, i.e. the alternation of Al-enriched planes with Al-depleted planes (Ni_3Al, L12 ordered structure). The interplanar distance (lattice parameter) is 0.36 nm.

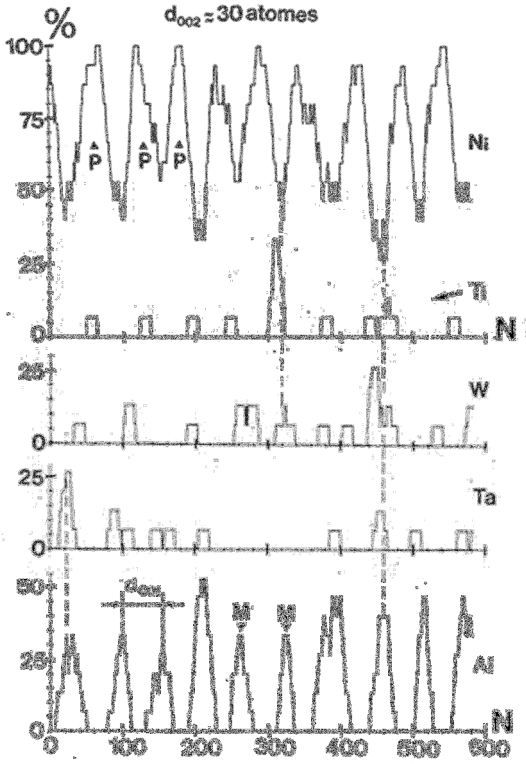

Figure 2. Depth profiles along <001> direction in the ordered γ′ phase of a single crystal nickel base superalloy (MC2) showing the site preferences of solute elements. Ti, Ta and W are observed preferentially in Al-enriched planes suggesting that these elements substitute preferentially to Al in the Ni_3Al ordered structure of the γ′ phase (L12 ordered structure, see below). Possible artefacts caused by the preferential retention of refractory elements (W, Ta) from one plane to the following cannot be ruled out and may bias results.

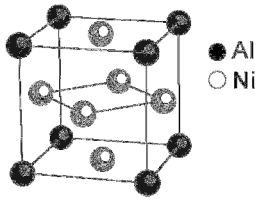

With the recent implementation of ultra-fast pulsed laser to the instrument instead of electric pulses, a new breakthrough has been achieved. Previously limited to metals, semiconductors as well oxides can now be analysed. This challenging innovation has made APT a unique approach for atomic-scale investigations in nanosciences (e.g. tunnel junctions) and nanoelectronics (clustering of boron or arsenic in implanted silicon, segregation of dopants (B, As) to crystal defects in polycrystalline silicon, reactive diffusion Ni-Si (contacts in microelectronics) [4,5,6,7]). The two versions of this instrument developed in the lab [4] and in USA [5] are now both marketed by CAMECA–AMETEK that is leader in this field.

Performance of APT versus SIMS (secondary ion mass spectrometry) is illustrated in figures 3 and 4. The 3D atomic map of boron atoms in silicon samples containing boron deltas (ultra-thin boron-rich layers, figure 3) shows the presence of four deltas. The related depth profile taken perpendicular to boron layers is compared to SIMS profile in figure 4. A good agreement is observed. As expected, the boron layers are separated by 18 nm and a peak concentration around 10^{21} boron atoms/cm^3 is measured for each delta. Let us mention the larger steepness of APT profiles compared to SIMS, illustrating the higher depth resolution of APT. However, the base level of boron between deltas is lower in SIMS profiles. APT has a lower sensitivity compared to SIMS because of the overall larger noise (statistical fluctuations as well as intrinsic background noise ~ 10^{19} at/cm^3 in this experiment).

Compared to other methods (e.g. SIMS), APT has the drawback of its advantage: due to the small analyzed area (50x50 nm^2 in the last generation instruments), profiles are shown to be subjected to larger statistical fluctuations. These larger sampling errors (~2σ with σ the standard deviation) are caused by the much smaller volume (i.e. smaller number (N) of atoms) on which atom-probe estimates relies on. Profiles such as shown in figure 4 were constructed by moving a thin slice (thickness e, d^2 the analysed area) in a direction perpendicular to delta layers. The amplitude of sampling errors is given by the standard deviation $\sigma = (C(1-C)/N)^{1/2}$ with $N = QV/\Omega$ with Q the detection efficiency (~0.5), V the volume of slice ($V=e.d^2$) and Ω

the average atomic volume (~ 0.02 nm^3 in Si). For an analyzed area of d^2= 20x20 nm^2, a thickness e=0,4 nm, one finds N ~ 4000 atoms. For C=10%, σ ~ 0.5 at.% so that sampling errors (~2σ) are close to 1%. In addition to these statistical errors, systematic errors may arise. Preferential retention of high binding energy elements form one layer to the following may damage the depth resolution as well. Other detrimental sources may also interfere.

In this presentation, the unique capabilities of APT in depth profiling will be highlighted on the basis of some salient illustrations related to precipitation, ordering and segregation to crystal defects (interfaces, dislocations) in metallic alloys and semiconductors, reactive diffusion in Ni-Si thin films, magnetic multilayers. Advantage as well as limitations of the instrument will be discussed.

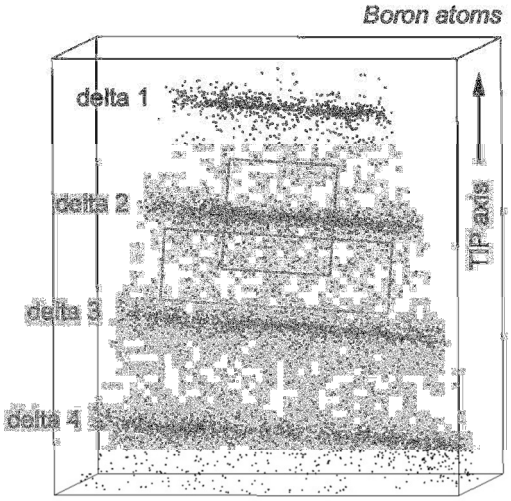

Figure 3. 3D reconstruction of boron distribution in silicon samples containing thin boron deltas (a few nm thick). For clarity, only boron atoms are shown. Four boron deltas distant of 18 nm are exhibited.

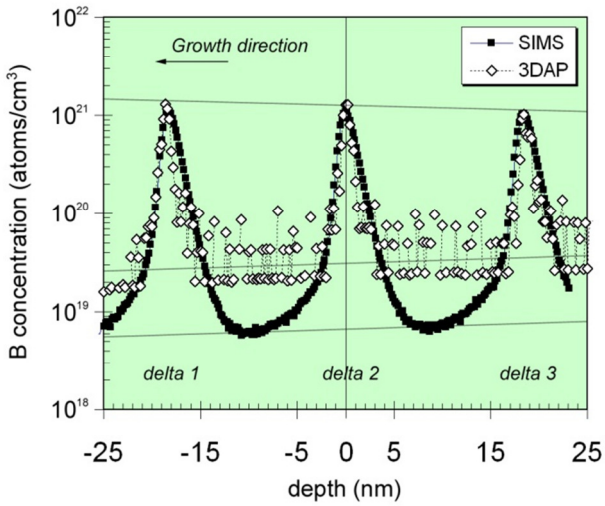

Figure 4. Concentration profile of boron derived from 3D map (figure 4). A thin slice 0.2 nm thick was moved in a direction perpendicular to boron deltas. The surface area of the sampling box is 25 nm x 25 nm. SIMS profile is superimposed to APT profile.

References.

[1] A. Cerezo, I. J. Godfrey and G. D. W Smith, 1988, Rev. Sci. Instr. 59 (6), 862
[2] D. Blavette, A. Bostel, J.M. Sarrau, B. Deconihout and A. Menand, 1993, Nature 363, 432
[3] D. Blavette, E. Cadel, A. Fraczkiewicz, A. Menand, 1999, Science 17, 2317
[4] B. Gault, F. Vurpillot, A. Vella, M. Gilbert, A. Menand, D. Blavette, B., 2006, Rev. Sci. Instr. 77, 043705
[5] T. F. Kelly and M. K. Miller, 2007, Rev. Sci. Instrum. 78, 031101
[6] O. Cojocaru-Mirédin, D. Mangelinck, K. Hoummada, E. Cadel, D. Blavette, Scripta Mater. 57, 5 (2007) 373-376
[7] S. Duguay, T. Philippe, F. Cristiano, D. Blavette, 2010, Apll. Phys. Lett. 97, 242104

O5 Embedded Nanoparticle Analysis using Atom Probe Tomography and High-Resolution Electron Microscopy

S. Thevuthasan1, Satyanarayana V. N. T. Kuchibhatla1 V. Shutthanandan1, B.W. Arey1, L. Kovarik1, C.M. Wang1, T. J. Prosa2, R. M. Ulfig2, B. P. Gorman3

1EMSL, Pacific Northwest National Laboratory, Richland, WA – 99354
2Cameca Instruments Inc., Madison, WI – 53711
3Colorado School of Mines, Golden, CO – 80401

Contact: satya@pnl.gov

One of the major challenges before the materials scientists today is the ability to "determine the positions (in 3D) and chemical identity of individual atoms in any materials system". It is envisioned that the combination of atom probe tomography, APT, and the advances in high-resolution electron microscopy paves the way towards this goal. APT is primarily a combination of point-projection microscopy and time-of-flight mass spectrometry [1]. The three dimensional atomic structure of the sample tips can be obtained through a reconstruction of the experimental data generated by a progressive layer-by-layer evaporation of the atoms from the needle-shaped tip and accounting for the time-of-flight of the ions. Recently, the development of laser-assisted evaporation of materials has unveiled the great potential of APT to analyze the insulating materials. APT is shown to provide chemical identity of the samples with atomic-scale resolution with a field-of-view better than 100nm x 100nm x 100nm. Despite these interesting features, there exist various challenges in terms of data analysis and the assumptions made while carrying out the reconstruction process. It is hence possible to compliment the APT data with high-resolution electron microscopy and thereby obtain a more realistic picture of the material under consideration.

Here, we explore the possibility of the intelligent marriage between APT and TEM/STEM to obtain the three-dimensional chemical imaging of Au-nanoparticles embedded in a dielectric (such as MgO) matrix. Ion beam implantation of Au^+ (2 MeV) in oxides and post-implantation annealing treatments have been shown to result in in situ nanoparticle formation. Previously, it was indicated by the researchers that the embedded structures are of pure-Au, based on the electron microscopy and optical absorption analyses [2]. However, the recent atom probe tomography (APT) analysis of the Au-implanted MgO samples questions these results and the first set of conclusions indicate that the nanoclusters formed within the MgO matrix may consist of a mixture of Au, Mg and O as opposed to 100% Au as reported and further validation is in progress.

Detailed APT analysis is underway at the EMSL, Environmental Molecular Sciences Laboratory, to gain the clear understanding about the chemical composition of these nanoclusters as they may have implications in sensors and catalysis related research. The samples were analyzed under different laser pulse energies (0.3 nJ – 0.8 nJ, 542 nm), which indicate that the higher laser energies may lead to various artifacts including non-stoichiometric MgO mass fractions. Further analysis was carried out on the sample run at 0.3 nJ pulse energy and the iso-concentration surface analysis revealed that the Au- particle size is similar to that observed from TEM and STEM. While the size of the clusters is shown to

increase with the increasing depth of implantation, the 1D-compositional analysis of the clusters indicates that the largest cluster may contain a maximum of up to 50 – 60% Au

with the others having relatively lower concentration of Au. The interface between the nanoparticle and the MgO matrix is often rich with Mg and O and the Au-particles were observed to contain stoichiometric Mg and O. No significant clustering was observed in the case of MgO. Some of the interesting observations during this analysis also include the variations in the mass resolution as a function of Au concentration.

In order to validate the data further, atom probe tips were prepared on half-cut TEM grids utilizing the focus ion beam technique and [3] analyzed in both high-resolution electron microscope and APT. High- resolution STEM analysis revealed the coherent nature of the Au-nanoparticles in the MgO matrix. The results will be discussed in detail while drawing the attention towards the "strengths" of complimentary imaging.

References

[1] M.K. Miller et al., Atom Probe Field Ion Microscopy, Oxford University Press, Oxford, 1996.
[2] Wang et al., Applied Physics Letters 87, 153104, 2005
[3] B. P. Gorman et al., Microscopy Today, June/July 2008

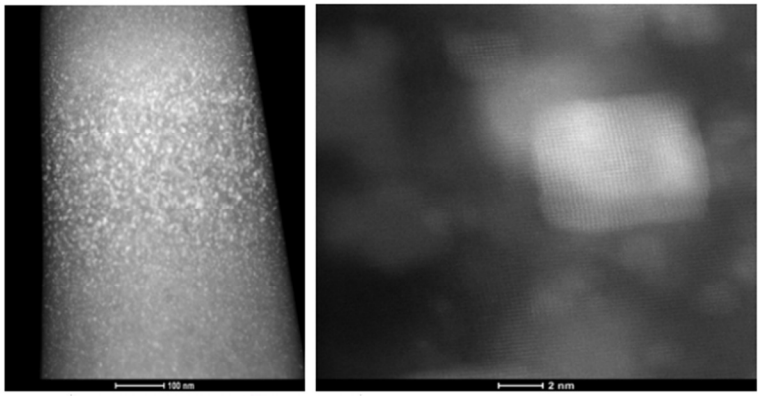

Typical STEM – HAADF images obtained from aberration corrected TITAN instrument at EMSL.

Left: Image of an APT tip

Right: High-magnification image showing the coherent Au-particle in MgO

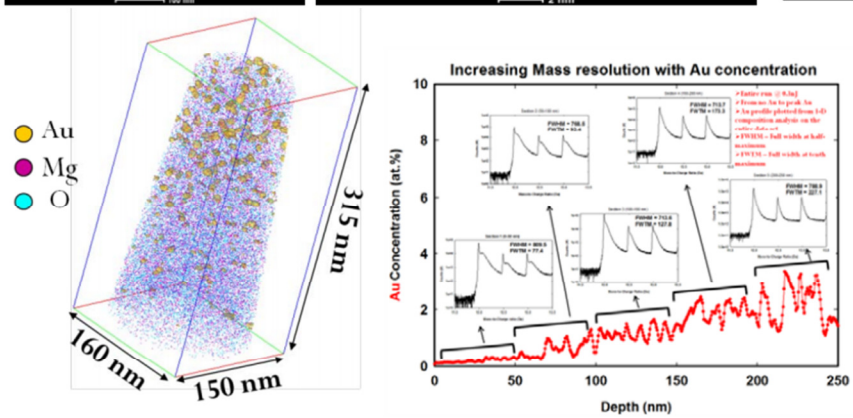

Left): 3-D reconstructed image of APT sample showing the Au-iso-concentration surfaces

Right): View graph indicating the variation in the mass resolution with increasing Au-concentration

O6 Surface Analysis of Samples Returned from the NASA Genesis Mission

B.V.King,[1,2] I.V.Veryovkin[2], M.J. Gladys[1], C. Glover[3]

bruce.king@newcastle.edu.au(corresponding author)

[1] *University of Newcastle, Callaghan 2308, Australia*
[2]*Materials Science, Argonne National Laboratory, Argonne IL, USA*
[3] *Australian Synchrotron, Clayton Vic 3333, Auistralia*

There are few analytical techniques that combine surface sensitivity with elemental sensitivity. Two of these are secondary ion mass spectrometry (SIMS) and its variants (including RIMS, resonant ionisation mass spectrometry [1]) and total X-ray fluorescence microscopy (TXRF) [2]. While these techniques don't have the ultimate depth resolution of techniques such as LEIS, they do permit analyses of elemental areal densities below 10^{10} atoms cm^{-2}. In this presentation, TXRF and RIMS are use to measure the near surface composition of samples returned from the NASA Genesis mission.

In the NASA Genesis mission [3], a spacecraft orbited the sun between Earth and Venus for 27 months, collecting solar wind atoms into wafers. The solid wind comprises mainly ionised H with smaller amounts of He, O, N, C, Ne, Mg, S, Fe and other elements all travelled towards the Earth as velocities ranging form $250kms^{-1}$ to $800kms^{-1}$. These ions are typically implanted 30nm below the surface of the wafer at ppm to ppt concentrations during the mission. On return to Earth, the spacecraft crashed and the wafers surviving the crash were contaminated with debris from other wafers or terrestrial contamination. The goal of surface analytical techniques is to separate the contamination on the surface from the solar wind buried just below the surface. If the solar wind can be measured to 10% accuracy then new data on the solar composition can be obtained which is relevant to the formulation of models of solar system evolution.

We have used the XAS beamline at the Australian Synchrotron (7.5 – 14 keV X-rays with a flux of 10^{12} photons s^{-1} into an area of 0.17mm (H) x 0.3mm (V)) to measure the fluorescence from a Genesis sample, compared to a $2x10^{13}$ ions cm^{-2} 168keV Fe^{+} implant standard (fig 1). The signals from the implant are much higher than those from the Genesis flight sample. The 6.8keV Fe Kα X-ray fluorescence was used to determine the Fe concentration in the Genesis sample to be approximately $1.5x10^{12}$ cm^{-2}. This value agrees well with SIMS measurements of Fe concentration [4]. The minimum detection level for our experiment was found to be $8x10^{9}$ cm^{-2}, primarily due to incomplete charge collection in the germanium energy dispersive detector used to collect the X-ray spectra. The data in fig 1 was collected at an X-ray incidence angle of 0.22°, corresponding to the critical angle for reflection. Above and below this angle the Fe fluorescence intensity drops (fig 2) in the flight sample, indicating that the Fe signal is coming from just below the sample surface. In contrast the implant sample shows high intensity at small incidence angles, indicating that there is significant material on and above the sample surface. This contamination from above the sample surface is presumably responsible for the large fluorescence peaks in fig 1 for the elements apart from Fe.

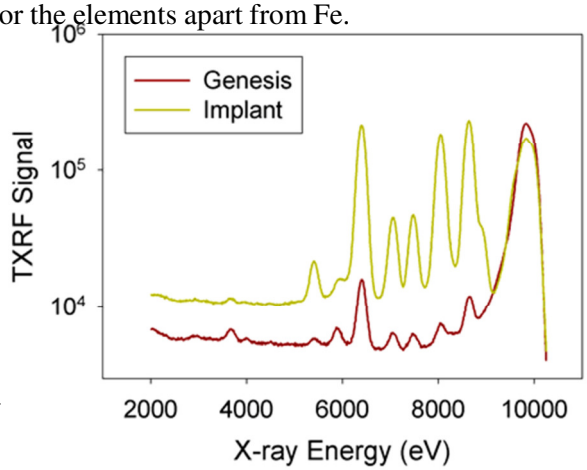

Fig 1 TXRF spectra for 600 s count time show scattering incident X-rays (at 10keV)

and fluorescence from Ni, Cu, Fe, Ni, Ca, Ti and Zn in the sapphire Genesis sample (bottom trace) and the Fe implanted sample (top trace).

Fig 2 Angular scans of the intensity of the Fe peak from the Genesis flight sample (circles) and the Fe implant (triangles)

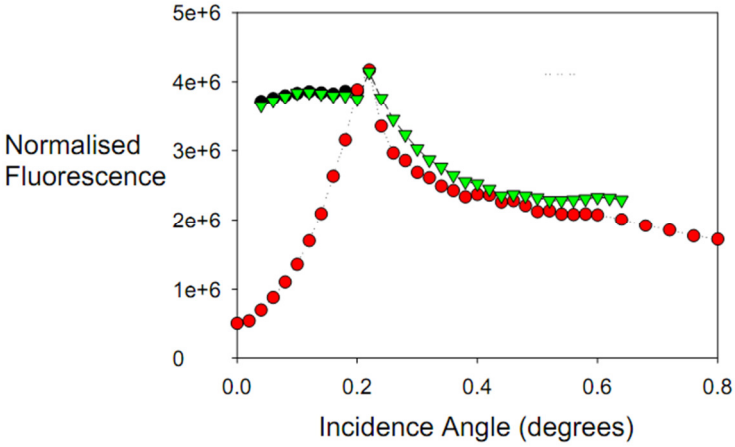

Figure 3 RIMS depth profile of Mg from a Genesis flight sample 60179 which is uncleaned (top trace) and cleaned by irradiation with a 10keV Ar_{5000}^{+} cluster ion beam (bottom trace). The solar wind implant peaks at a depth 60nm below the surface and at a level much smaller that the surface Mg concentration. Cleaning the sample with a cluster ion beam reduces background by an order of magnitude.

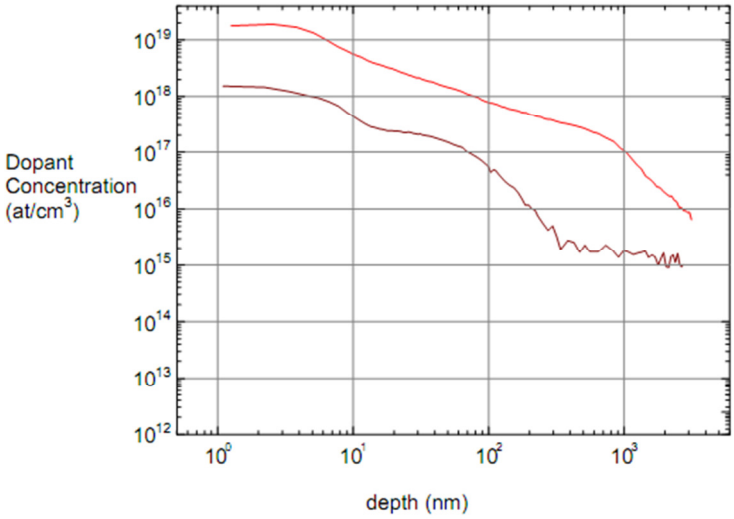

We have also used RIMS depth profiling to measure the Mg depth distribution in a silicon Genesis light sample. Lasers tuned to 285.296nm and 360.635nm were used to resonantly ionise Mg atoms desorbed from the surface using 10keV Ar sputtering. Before profiling, mesas were ion beam cut into the sample so crater edge effects and hence backgrounds in subsequent depth profiles were minimised. Fig 3 shows that the characteristic solar wind implant "bump" around 60nm depth becomes much clearer after surface cleaning using a 10keV Ar_{5000}^{+} cluster beam which was used to remove the top 8nm of the surface. The Mg concentration in the Genesis Si flight sample was found to be 1.5-2 $x10^{12}$ cm.
In conclusion, TXRF and sputter depth profiling using RIMS analysis are complementary techniques capable of analysing Fe and Mg compositions in the near surface region with high sensitivity.

References.

[1] Analyzing individual presolarg rains with CHARISMA. MR Savina, MJ Pellin, CE Tripa, IV Veryovkin, WF Calaway, AM Davis, Geochimica et Cosmochimica Acta 67 (2003) pp 3215-3225.
[2] Total reflection X-ray fluorescence and grazing incidence x-ray spectrometry – Tools for micro- and surface analysis. A review. A von Bohlen, Spectrochimica Acta B64 (2009) pp 821-832
[3] The Genesis Discovery mission : Return of solar matter to Earth. DS Burnett etal, Space Science Rev. 105 (2003) pp509-534
[4] Elemental Abundances of the Bulk Solar Wind : Analyses from Genesis and ACE, DB Reisenfeld etal Space Sci Rev 130 (2007) pp 79-86

I 4. Transport and exchange of hydrogen and oxygen isotopes using medium energy ion scattering

J. Liu, S.N. Dedyulin, L.V. Goncharova

lgonchar@uwo.ca (corresponding author)

Department of Physics and Astronomy, University of Western Ontario, London, Ontario, N6A 3K7 Canada

Thermally driven transport and exchange of hydrogen and oxygen isotopes in silicon-based metal-oxide-semiconductor (MOS) device-related structures were experimentally investigated using medium energy ion scattering. The motivation for this work was twofold: (i) importance of light elements quantification to obtain accurate stoichiometry, and (ii) general importance of hydrogen in semiconductor devices (for instance, giant hydrogen isotopic effect on hot-electron degradation mechanism).

Medium energy ion scattering (MEIS) is capable to give quantitative information on the structure and composition of shallow layers with sub-nm depth resolution near the surface, although of heavy impurities and light substrates [1]. MEIS with isotopic tracing was used to examine oxygen exchange and the mechanism of interfacial growth in hafnium-based ultra-thin dielectric films. The primary route for oxygen delivery to the interface responsible for the SiO_2 growth is via exchange, however, direct oxidation by molecular oxygen cannot be discounted completely. Concurrent with the exchange, interfacial SiO_xN_y is grown due to the supply of the displaced ^{16}O (as well as ^{18}O) that migrates toward the Si substrate; both oxygen isotopes are present at the interface in near-equal abundance. It is potentially interesting to extend MEIS to perform elastic recoil detection analysis (ERDA) using electrostatic energy analyzer (ESA) in medium energy range. In the past this approach has been already demonstrated successfully by Copel, et al [1], using time-of-flight approach, and Nishimura, et al [2], using modified version of ESA. Our implementation (ME-ERDA) is based on using ~300-500keV N^+ or Si^+ ions as projectiles and detecting negative hydrogen (H-) recoils using existing ESA detector. We applied this technique to the analysis of H-terminated Si (001), self-assembled monolayers, and 2–5 nm thick HfO_2 and $HfSiO_x$ films grown by atomic layer deposition on Si(001).

We were able to obtain hydrogen profiles for hafnium silicate films described above. In order to determine the absolute quantity of H on Si by this approach, the charge fraction of H^-, (which is dependent on the energy) must be measured in advance. Quantitative analysis of hydrogen content in these thin films is complicated by the presence of residual hydrogenated species after expose to air and in vacuum system, giving rise to so-called hydrogen surface peak. Comparison between ME-ERDA, ERDA and SIMS results will be discussed, as well as the limitations of such analyses.

References.

[1] L.V. Goncharova, M. Dalponte, T. Feng, et al. Phys. Rev. B 83 (2011) 115329.
[2] M. Copel, R.M. Tromp, Rev. Sci. Instrum. 64 (1993) 3147-3152.
[3] T. Nishimura, A. Ikeda, T. Koshikawa, et al. Surf. Sci. 409 (1998) 183-188.

O7 Investigation of oxygen exchange between CO_2 and thermally grown SiO_2 network by Narrow Resonance Depth Profiling

C. Deville Cavellin[1,2] , G. Deokar[1], M. D'Angelo[1], I. Trimaille[1], J.J. Ganem[1], I. Vickridge[1]

deville@u-pec.fr

[1] *Institut des Nanosciences de Paris, UPMC, UMR 7588 CNRS, 4 place Jussieu, 75005 Paris, France.*
[2] *Faculté des Sciences et Technologie, UPEC, 61 av. General De Gaulle, 94010 Créteil, France.*

CO_2 interacts with silica via exchange of oxygen during diffusion at 1100°C. We establish this phenomena using ^{18}O as isotopic tracer and $^{18}O(p,\alpha)^{15}N$ narrow nuclear resonance profiling (NRP) at 151 keV [1].

Single crystal silicon wafers of three different orientations have been used as substrates. Silica films were grown by dry thermal oxidation using $^{16}O_2$. These samples were then annealed at 1100°C under $C^{18}O_2$ at various pressures (60, 100 and 200mbar) and for different durations (1h, 2h30, 4h and 6h).
To interpret the NRP spectra, we propose a model for diffusion and interaction of CO_2 with SiO_2. It was assumed that two types of processes are involved. Close to surface, oxygen diffusion should be mediated through SiO_2 network defects. While simultaneously, CO_2 diffuses through the silica and exchanges oxygen all along its diffusion path. Combined solution of the equations corresponding to these two processes has been used to fit (via SPACES [2] software) all the NRP data with only 3 adjustable parameters.

From these, the CO_2 diffusion coefficient in thermal silica at 1100°C has been determined : $D_{CO2} = 1.4 \pm 0.3\ 10^{-9}$ cm2/s. This value is close to the CO diffusion coefficient at 1100°C in thermal silica $D_{CO} = 2.0 \pm 0.3\ 10^{-9}$ cm^2/s that we established previously by the same method [3].

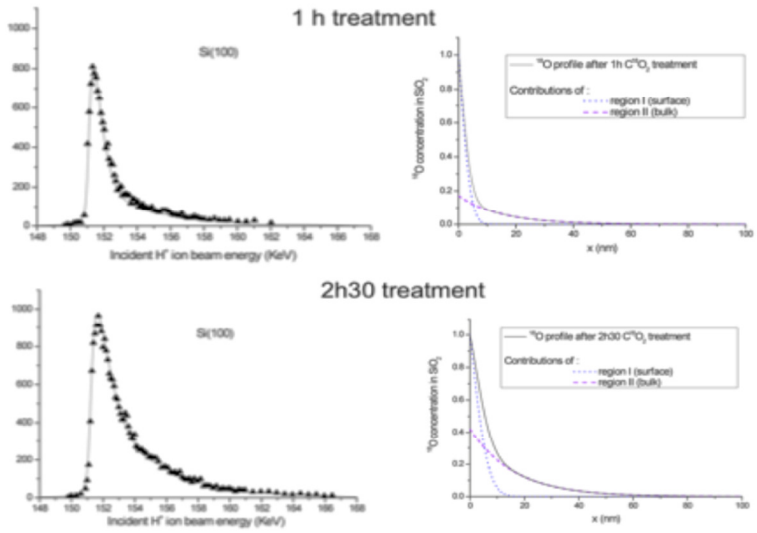

[1] B. Maurel, G. Amsel, J. Nadai, Nucl. Inst. Methodes Phys. Res. 197 (1982) pp 1-13. [2] I. Vickridge, G. Amsel, Nucl. Instrum. Meth. Phys. Res. B 45 (1990) pp 6-11.
[3]. C. Deville Cavellin, I. Trimaille, J.-J. Ganem, M.D'Angelo, I. Vickridge, A. Pongrácz, G.Battistig J. App. Phy. 105(3) (2008).: 033501.

O8 Ultimate backside sample preparation for ultra thin high-k/metal gate stack depth profiling with ToF-SIMS, MEIS and pAR-XPS

M. Py[1], M. Veillerot[1], J.M. Fabbri[1], F. Pierre[1], R. Boujamaa[1, 2], D. Jalabert[3], C. Roukoss[4], B. Pelissier[4], J.P. Barnes[1], F. Bertin[1]

matthieu.py@cea.fr

[1] *CEA-Leti, MINATEC Campus, 17 rue des Martyrs, 38054 GRENOBLE Cedex 9, France*
[2] *STMicroelectronics, 850 rue de Jean Monnet, 38926 Crolles, France*
[3] *CEA-INAC/UJF-Grenoble1 UMR-E, SP2M, LEMMA, Minatec Grenoble, F-38054*
[4] *LTM-CNRS/CEA-LETI, 17 rue des Martyrs, 38054 GRENOBLE Cedex 9, France*

Over the past decade it has become increasingly common to resort to backside analysis to overcome weaknesses such as ion mixing and preferential sputtering in SIMS depth profiling [1-3], and to bring the layer of interest as close as possible to the surface for XPS analysis. However backside analysis remains challenging since only a fraction (~20 nm) of the 750 µm thick silicon substrate must remain while maintaining a smooth, flat surface suitable for analysis. Recent developments have used Silicon on Insulator (SOI) substrates where the buried thick (145 nm) SiO_2 is used as an etch stop layer [4].

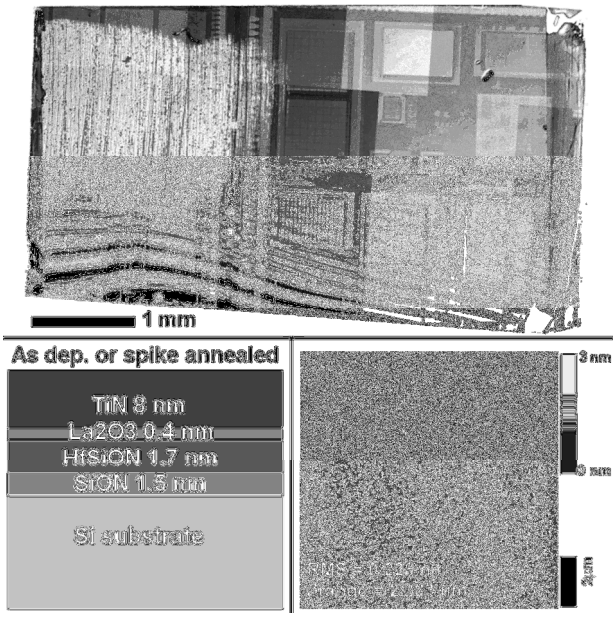

FIGURE 1. [Top] Optical image of a sample after backside preparation. The silicon wafer is completely removed except for the top left corner of the sample. Patterns on the surface of the support wafer are seen by transparence through the layers of interest (~12 nm) and the glue (~1-2 µm). [Bottom left] Schematic structure of the samples studied. [Bottom right] Topography of the surface of the sample after preparation.

Here we present a backside sample preparation method adapted to samples with an extremely thin etch stop layer. It consists in a two step preparation: a mechanical polishing up to a few remaining microns, followed by a dedicated TMAH etch. This method yields an extremely flat and smooth surface, without remaining silicon after preparation (see Figure 1). We therefore used it to prepare two samples consisting of a high-k/metal gate stack for 32 nm node CMOS devices, before and after activation anneal. On these samples the etch stop layer consists of a 1.5 nm thick SiON layer as shown in Figure 1. This preparation has allowed precise depth profiling of the different elements in the stack and thus investigation of stack behaviour upon annealing with ToF-SIMS, MEIS and parallel AR-XPS. The results of the different analysis will be discussed and compared with conventional "frontside" analysis). We will highlight the improvements brought by the backside preparation as well as some typical features of the studied stacks upon annealing.

References.

[1] W. Vandervorst, J. Bennett, C. Huyghebaert, T. Conard, C. Gondran, and H. De Witte, Appl. Surf. Sci. 231-232, 569 (2004).
[2] C. Hongo, M. Takenaka, Y. Kamimuta, M. Suzuki, and M. Koyama, Appl. Surf. Sci. 231-232, 594 (2004).
[3] C. Hongo, M. Tomita, and M. Takenaka, Appl. Surf. Sci. 231-232, 673 (2004).
[4] M. J. P. Hopstaken, J. C. Cabral, D. Pfeiffer, C. Molella, and P. Ronsheim, AIP Conf. Proc. 1173, 94 (2009).

Acknowledgments: This work was partially supported by the European EUREKA/CATRENE program in the frame of the CT206 UTTERMOST project and by the National Research Agency (ANR) through the French "Recherche Technologique de Base" Program.

I 5. Oxygen deficiency and excess on rutile TiO_2(110) surfaces studied by ion scattering and elastic recoil detection analyses

Yoshiaki Kido, Hideki Okumura, Kei Mitsuhara and Anton Visikovskiy

Corresponding author: ykido@se.ritsumei.ac.jp

Department of Physics, Ritsumeikan University, Kusatsu, Shiga-ken 525-8577, Japan

In this talk, we present two topics, (1) what is the primary source of the defect state in the band gap of reduced rutile TiO_2(110) surfaces and (2) what is the partner of the reaction of CO taking place on O-rich TiO_2(110) surfaces. Oxygen deficiency and excess intimately related to subsurface electronic charge play a key role in chemical reactions occurring on metal-oxides surfaces. The number of O atoms adsorbed on TiO_2(110) surfaces was determined by medium energy ion scattering (MEIS) using an isotopically labeled $^{18}O_2$ gas and that of O vacancies created was measured by H_2O exposure followed by elastic recoil detection (ERD) of H using medium energy Ne^+ ions[1]. Figure 1 shows the MEIS spectrum observed for the O-rich surface obtained by exposing a reduced surface to $^{18}O_2$. The inset corresponds to the magnified spectrum around the scattering component from ^{18}O atoms. The ERD spectrum obtained for 147 keV Ne^+ impact on the reduced surface after H_2O exposure is shown in Fig. 2. The sensitivity to ^{18}O and H is estimated roughly ~0.5×10^{13} atoms/cm^2. Employing the MEIS and ERD techniques, we try to clarify the above two issues.

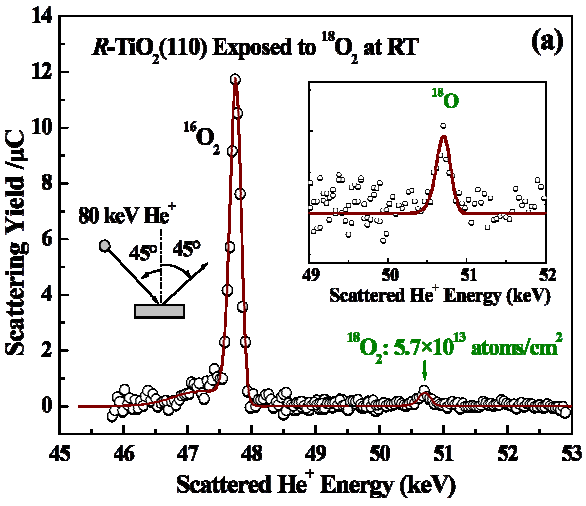

Fig. 1. MEIS spectrum observed for reduced TiO_2(110) after $^{18}O_2$ exposure.

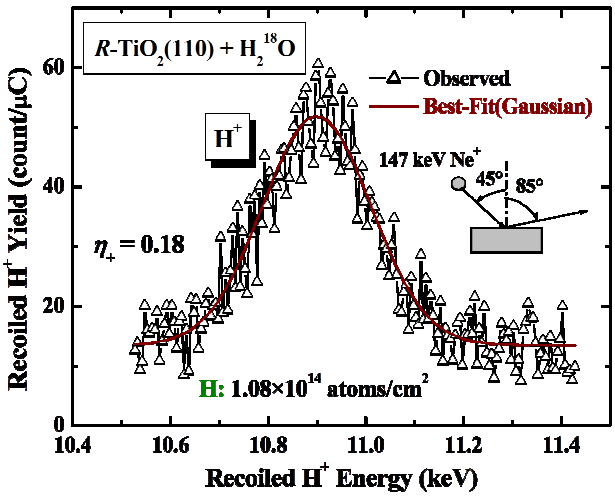

Fig. 2. ERD spectrum measured for reduced TiO_2(110) surface after H_2O dose.

[1] K. Mitsuhara, T. Kushida, H. Okumura, H. Matsumoto, A. Visikovskiy and Y. Kido, Surf. Sci. **604** (2010) L48.

O9 The V_2O_3 (0001) surface termination crystallography: phase equilibrium revealed by medium- and low-energy ion scattering.

A.J. Window[1], A. Hentz[1], D.C. Sheppard[1], G.S. Parkinson[1], H. Niehus[2], D. Ahlbehrendt[2], T.C.Q. Noakes[3], P. Bailey[3], D.P. Woodruff[1]

d.p.woodruff@warwick.ac.uk

[1] *Physics Department, University of Warwick, Coventry CV4 7AL, UK*
[2] *Humboldt-Universität zu Berlin, Institut für Physik, Newtonstr. 15, D-12489 Berlin, Germany*
[3] *STFC Daresbury Laboratory, Warrington WA4 4AD, UK*

The (0001) faces of corundum-phase structures, notably V_2O_3, α-Al_2O_3, and Cr_2O_3, are particularly interesting because there are several distinctly different atomic layers at which the bulk structure might be terminated. The bulk structure comprises alternate buckled metal layers, described as two half-layers, each with one atom per surface unit mesh, and single O_3 layers (…MM'O_3MM'O_3...). The simplest possible stoichiometric terminations are thus half-metal (…MM'O_3M), full-metal (…MM'O_3MM'), or O_3 (…MM'O_3MM'O_3) One fundamental question that is particularly relevant to the structure of these surfaces is whether, in practice, a surface can be created that is truly in equilibrium with its surroundings under preparation conditions. Starting from a bulk crystal of the oxide, it may be difficult to overcome the kinetic barriers to achieve equilibrium under conditions of temperature and oxygen partial pressure accessible to surface science experiments. Alternatively, epitaxial growth of the oxide on a suitable substrate, by deposition of metal vapour in the presence of a partial pressure of oxygen, may offer a better means of achieving this gas-solid equilibrium, despite growth being intrinsically a non-equilibrium process. Nevertheless, previous structural studies of the surface of bulk crystals of α-Al_2O_3 and Cr_2O_3, and of Cr_2O_3 produced by oxidation of metallic Cr, *do* appear to be consistent with the expected equilibrium structure of a so-called half-metal termination or, in the case of Cr_2O_3 at higher O_2 partial pressures, a half-metal termination capped with O atoms to produce chromyl, Cr=O, surface species [1].

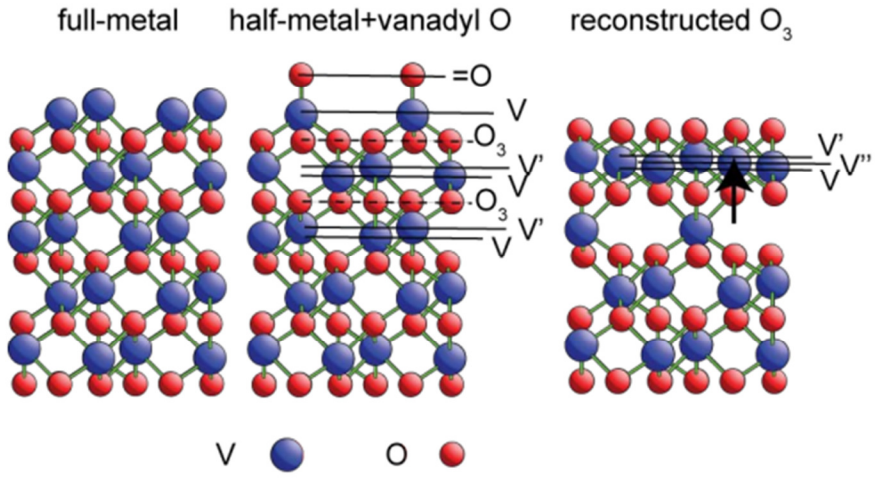

Fig. 1 Some possible terminations of the V_2O_3(0001) surface. Spectroscopic and chemical studies favour the vanadyl termination but DFT calculations indicate the reconstructed O_3 termination should be the equilibrium phase under most conditions. (see Fig. 2)

By contrast, spectroscopic, imaging, and chemical studies of the $V_2O_3(0001)$ surface of epitaxial films grown *in situ* have been interpreted in terms of a half-metal termination with each surface V atom capped with an atop O atom to produce a vanadyl (V=O)-covered surface (e.g. [2]), but this is *not* the equilibrium O_3 termination predicted by (DFT) theory.

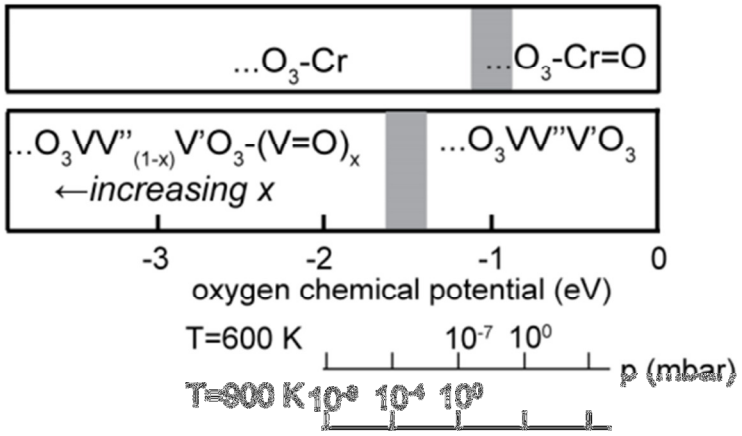

Fig. 2
Simplified phase diagram of the equilibrium termination structure of $Cr_2O_3(0001)$ [3] and $V_2O_3(0001)$ [4] as a function of oxygen chemical potential in the gas phase as provided by DFT calculations.

Here we will present results which challenge this conventional wisdom and indicate that the $V_2O_3(0001)$ surface termination *is* consistent with the predictions of DFT calculations. Specifically, we will report the results of two complementary, but independent, medium-energy ion scattering and(low-energy) noble gas impact-collision scattering spectroscopy (MEIS and NICISS) studies of the (0001) surfaces of V_2O_3 films grown on Pd(111), Au(111), and $Cu_3Au(100)$ that reveal the surface to have the reconstructed full O_3-layer termination predicted to be the equilibrium structure by DFT calculations. We find this structure, in which the reconstruction leads to a VO_2 surface trilayer, gives the best description of surfaces of V_2O_3 films grown under conditions that are both similar to, and distinctly different from, those used in the earlier explorations of the properties of these surfaces. Moreover, our results are clearly *not* consistent with the previously-supposed (1x1) V=O vanadyl termination (which DFT calculations indicate should *never* be the equilibrium structure at any combination of oxygen partial pressure and temperature. We show that the results of the earlier (non-structural) studies of this surface can be reconciled with the predicted equilibrium structure, and do not require that the surface has a (1x1) vanadyl termination as was previously supposed. They also allow us to understand our previous photoelectron diffraction results [5] that showed that hydroxylation of this surface leads to H atom bonding to in-plane surface O atoms, and not to atop vanadyl O atoms.

Reference:

[1] O. Bikonda, W. Moritz, X. Torrelles, H.J. Kim, G. Thornton, R. Lindsay, Phys. Rev. B. **81**, 205439 (2010)
[2] S. Surnev, M. G. Ramsey, F. P. Netzer, Prog. Surf. Sci. **73**, 117 (2003).
[3] A Rohrer, J. Hafner, G. Kresse, Phys. Rev. B 7**70**, 125426 (2004)
[4] G. Kresse, S. Surnev, J. Schoiswohl, F. P. Netzer, Surf. Sci. 555 (2004) 118.
[5] E. A. Kröger, D. I. Sayago, F. Allegretti, M. J. Knight, M. Polcik, W. Unterberger, T. J. Lerotholi, K. A. Hogan, C. L. A. Lamont, M. Cavalleri, K. Hermann, D. P. Woodruff, Surf. Sci. 602 (2008) 1267.

O10 Strain measurement in a thin silicon film using Medium Energy Ion Scattering.

D. Jalabert[1], D. Pelloux-Gervais[2], A. Béché[1,†], J. M. Hartmann[3], P. Gergaud[3], J. L. Rouvière[1], B. Canut[2]

denis.jalabert@cea.fr

[1] CEA/INAC/SP2M/LEMMA, 17 Rue des Martyrs, 38054 Grenoble cedex 09, France.
[2] Université de Lyon ; Institut des Nanotechnologies de Lyon INL-UMR5270, CNRS, INSA de Lyon,Villeurbanne, F-69621, France.
[3] CEA/LETI, MINATEC Campus, 17 Rue des Martyrs, 38054 Grenoble cedex 09, France.
[†] Now at FEI Company, Achtseweg Noord 5, 5600 Eindhoven, The Netherlands.

The depth strain profile in silicon from the Si (001) substrate to the surface of a 2 nm thick Si/12 nm thick SiGe/Si heterostructure grown by RP-CVD has been determined by Medium Energy Ion Scattering (MEIS). We have found that the SiGe layer is fully strained with respect to the silicon substrate and that the 2 nm Si top film presents a decreasing strain profile. The presence of Ge diffusion in the Si cap has also been highlighted. A strain profile has been deduced from the elastic theory taking into account the chemical composition experimentally determined in the Si top film. This calculated strain profile and the one obtained from MEIS blocking experiment presents exactly the same behavior. XRD measurements have been carried out to check the validity of MEIS results. It has been found that the ion beam is responsible for the substrate strain state change. Although such statement implies further investigations like TEM and additional MEIS measurements at different ion doses, we have demonstrated the capability of MEIS for profiling strain with both high depth resolution (< 1 nm) and good strain sensitivity (1×10^{-3}).

I 6. Probing semi-conductors surfaces with fast atom diffraction: a new in situ technique to investigate the surface structure during epitaxial growth

Paola Atkinson[1], Mahmoud Eddrief[1], Victor H. Etgens[2,1], Anouchan Momeni[3], Maxime Mulier[3], Hocine Khemliche[3] and Philippe Roncin[3]

victor.etgens@insp.jussieu.fr (corresponding author)

[1] *Institut des NanoSciences de Paris, UPMC, CNRS UMR 7588, 140 rue de Lourmel, Paris F-75015, France.*
[2] *Fédération Lavoisier Franklin-Université de Versaille Saint Quentin en Yvellines-France.*
[3] *ISMO UMR8214 CNRS-Université Paris-Sud Orsay 91400 France*

We have developed a new surface sensitive technique allowing studies of thin films growth, in situ and in real time, based on scattering of grazing incidence medium energy atoms. This technique has been named GIFAD for Grazing Incidence Fast Atom Diffraction[1, 2].

In its geometry, GIFAD is very similar to RHEED (reflection high energy electron diffraction) with atoms instead electrons. An ion source produces a 200-1000 eV He^+ beam that is neutralized to produce a neutral He beam. After collimation, the beam enters the UHV chamber and is diffracted by
the sample surface under an incident angle close to one degree. The full diffraction pattern is collected on a phosphor screen after the sample. The energy of the projectiles normal to the surface does not exceed one eV that excludes sub-surface interaction and makes GIFAD exclusively sensitive to the topmost surface layer. So in respect with other surface techniques, GIFAD is less invasive, more surface sensitive and readily interpretable quantitatively. In order to test its fully potentialities, we have customized a commercial type molecular beam epitaxy (MBE) growth machine.
First, the basis of this new technique will be presented with a short review of literature results followed by results we have obtained for a prototypical semiconductor II–VI compound, ZnSe(001). Besides providing lattice parameter with high accuracy, GIFAD gives straightforward access to the surface valence electron density profile, allowing clear identification of an electron transfer from Zn to Se (Figure 1)[3].
Finally, the on going results will be presented with this new MBE–GIFAD growth equipment on surface and growth studies of arsenic compounds[4].

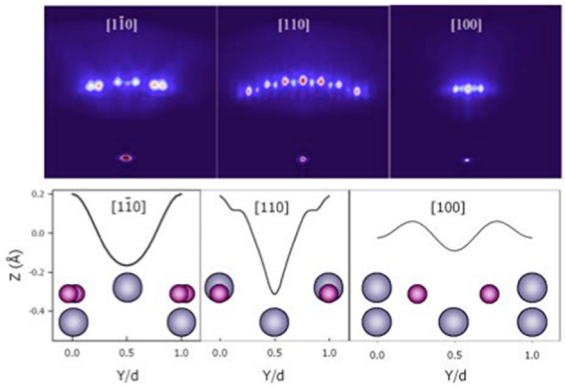

Figure 1: *Diffraction patterns recorded for 400 eV He on a ZnSe(001) surface aligned along the [1-10], [110] and [100] respectively [taken from ref. 3]. The line drawn below are the shape of the corrugated hardwall (see text) that fits the diffracted intensities. The atomic model superimposed is that corresponding to the so-called Z_n-vacancy model.*

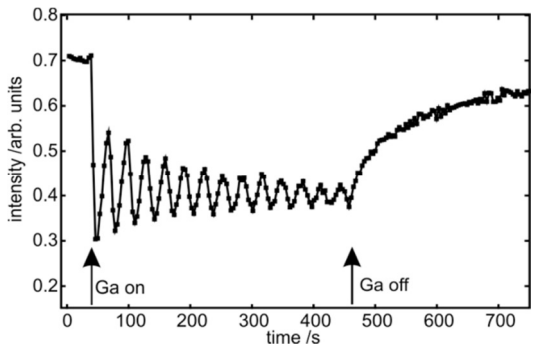

Figure 2 *: GaAs growth oscillations*

Finally, we have demonstrated that GIFAD profiles provide well-resolved specular intensity oscillations characteristic of a layer-by-layer growth (Figure 2) that allow growth dynamics to be probed.

Acknowledgement
This work has been supported by ANR contract ANR-07-BLAN-0160.

References.

[1] P. Rousseau et al, Phys Rev. Lett. 98, 016104 (2007).
[2] A. Shculler et al, Phys Rev. Lett. 98, 016103 (2007).
[3] H. Khemliche et al, Appl. Phys. Lett. 95, 151901 (2009).
[4] Ohtake, Surf. Sci. Reports 63, 295 (2008)

O11 Quantitative and non-destructive determination of the atomic composition of the outer surface and of in-depth profiles by HS-LEIS

Hidde H. Brongersma[1,3], Thomas Grehl[1], Marinus J.P. Hopstaken[2], Michael Fartmann[3], Hendrik R.J. ter Veen[3] and Veronique I.T.A. de Rooij-Lohmann[4]

H.H.Brongersma@tue.nl

[1]*ION-TOF GmbH, Heisenbergstr. 15, 48149 Münster, Germany*
[2]*IBM T.J. Watson Research Center, Yorktown Heights, NY 10598, USA*
[3]*Tascon GmbH, Heisenbergstr. 15, 48149 Münster, Germany*
[4]*FOM Institute for Plasma Physics Rijnhuizen, P.O. Box 1207, 3430 BE Nieuwegein, The Netherlands*

In modern technology new (sub-) nanometer materials and preparation techniques are being developed. Advancement heavily relies on the availability of analytic techniques that can validate and support the preparation. One of the new analytic techniques that is being used is High- Sensitivity Low Energy Ion Scattering (HS-LEIS). Its unique surface sensitivity makes it possible to selectively determine the atomic composition of the outer atoms of the surface. Thus precisely the atoms that control ALD growth, catalysis, and adhesion. The improved mass resolution even
permits the separation of heavy elements like Pt and Au. Nowadays, HS-LEIS can also be used for non-destructive ("static") high-resolution in-depth analysis down to about 6 nm below the surface. It will be shown that, using simple reference samples, the quantification of the atomic composition of the outer atomic surface and depth profiles of ultra-thin layers is relatively straightforward. Thus precisely in situations where the rapidly changing matrix hampers the quantification by SIMS, and the in-depth resolution of XPS is insufficient.

The thickness uniformity of grown ultra-thin layers is largely determined in the transient regime, this is in the period before closure of the layer is reached. Depending on the composition of the layers and the growth mode in the transient regime, the number of cycles that is needed in ALD for closure can vary widely (typically 6 – 150 cycles). For the growth of HfO_2 on Si(100) with ultra- thin SiO(N) interlayers (IL) layer closure and growth mode were determined by LEIS in combination with an integral areal dose technique (RBS). Evaluation of the absolute LEIS surface coverage as a function of the RBS areal dose allowed for assessment and modeling of the growth mode. In a comparison between MOCVD and ALD the better thickness uniformity was achieved with ALD, potentially giving scalability and leakage benefits.
In studies of $Mo/B_4C/Si$ multilayers, used as mirrors in extreme ultraviolet lithography applications, in-situ LEIS analysis during heating experiments enabled the determination of interdiffusion coefficients.

O12 Quantification of second layer contributions in Low Energy Ion Scattering

D. Goebl, D. Primetzhofer, M. Spitz, and P. Bauer

dominik.goebl@jku.at

Institute for Experimental Physics, Johannes Kepler University Linz, Linz, Austria

Low Energy Ion Scattering (LEIS) is a surface analysis technique, very well known for its supreme surface sensitivity [1, 2]. Especially when noble gas ions are used as projectiles, which are very efficiently neutralized inside the target, valuable information on composition and structure of the outermost atomic layer can be obtained. Nevertheless, depending on target material, projectile and primary energy of the ion beam, one can also identify substantial contributions from deeper layers. In order to quantify the contribution of ions backscattered from second layer atoms, simulations of He^+ scattered from a $Cu_{0.5}Au_{0.5}$ crystal were performed and compared to recent experiments.

A $Cu_{0.5}Au_{0.5}$ crystal is an excellent target for this kind of investigation, as in the (001) orientation, the sample consists of alternating layers of Au and Cu, with Au in the outermost atomic layer. A sketch of the $Cu_{0.5}Au_{0.5}(001)$ surface is given in Fig. 1; the crystal has a tetragonal geometry, with lattice spacing a = 3.872 and c/a = 0.924 [3]. The large difference in mass between Au and Cu permits a straightforward evaluation of the ion peaks and, consequently, the individual contributions of first and second layer in the resulting spectrum. Primetzhofer et al. performed an experimental investigation of this crystal [4]. For scattering along the [110] azimuth direction, the first and second layer are completely visible to the detector. Here, the ratio of the Au and Cu ion yield, A_{Au}^+ / A_{Cu}^+ was determined to 10. The ion yield A^+ of a given element i is given by:

$$A_i^+ = \underbrace{N_0 \cdot n_i \cdot \left(\frac{d\sigma}{d\Omega}\right)_i \cdot d\Omega \cdot \eta_i}_{Y_B} \cdot P_i^+ \qquad (1)$$

where, N_0 denotes the number of impinging projectiles, n represents the areal surface density, d /d refers to the scattering cross section, d identifies the detector solid angle and stands for the detector efficiency. P^+ represents the ion fraction, which is defined as the fraction of positive ions amongst the projectiles backscattered to the detector. The index i denotes the specific element under consideration; in the present case either Au or Cu. The first part of the equation corresponds to the yield, Y_B, of particles backscattered from one monolayer. For the energies considered in this investigation, the detection efficiency can be approximated as 1 and is therefore neglected in the following. From the ratio of the ion yields, it is possible to deduce the ratio of the ion fractions, when the ratio of backscattered yields is known:

$$\frac{A_{Au}^+}{A_{Cu}^+} = \frac{Y_{B,Au} \cdot P_{Au}^+}{Y_{B,Cu} \cdot P_{Cu}^+} \qquad (2)$$

To determine the backscattered yield for the different elements, MD simulations were performed with the simulation package KALYPSO [5]. Fig. 2 presents a comparison of simulated (red, dashed line) and experimental (black, solid line) spectra for 2 keV He^+ scattered from $Cu_{0.5}Au_{0.5}(001)$ in the [110] azimuth direction. The pronounced peaks in

the simulated data can be attributed to trajectories including only a single scattering event with a first layer Au atom or a second layer Cu atom, respectively.

The simulated data was normalized to reproduce the experimental peak for Au. The ratio of the backscattered yields was deduced from the areas of the single scattering peaks, which were

modeled by Gaussian functions. Features of the spectrum, which are due to multiple scattering and scattering from deeper layers (e.g. the small peak slightly below 1800 eV) were neglected, as those projectiles are not visible in the spectrum of backscattered ions, due to efficient neutralization within the target. The calculated ratio of the backscattered yields amounts to $Y_{B,Au}/Y_{B,Cu}$ = 2.13. From this, one can deduce a significant focusing effect from first to second layer since the ratio of the scattering cross sections $(d\sigma/d\Omega)_{Au}/(d\sigma/d\Omega)_{Cu}$ is 3.10. The fact that in the experimental spectrum backscattering from Cu results in a peak slightly shifted to lower energies with respect to the simulated one may be traced back to electronic stopping, which is not considered in the simulation.

.

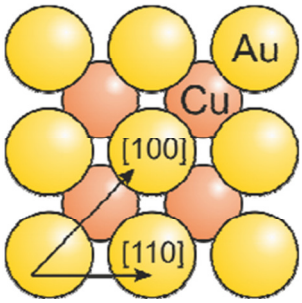

Fig. 1: (001) face of a $Cu_{0.5}Au_{0.5}$ single crystal.

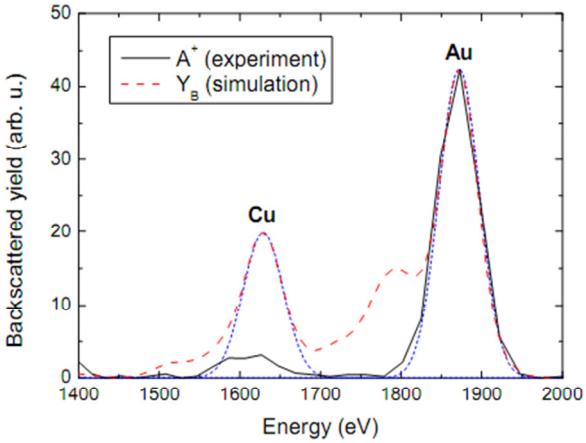

Fig. 2: Simulated and experimental spectrum of 2 keV He^+ scattered from CuAu(001) in the [110] azimuth direction.

Considering the measured ion yield ratio of 1/10, evaluation of eq. (2) results in P_{Cu}^+/P_{Au}^- = 0.213. From experimental data P^+ for Au was deduced to 0.196 [4]. Thus, the absolute ion fraction for 2 keV He^+ scattered from Cu in the second layer amounts to 0.042. Although the absolute values for P^+ decrease for higher primary energies, the relative importance of contributions from ions backscattered from the second layer increases. The same procedure applied to data obtained for 3 keV He^+ results in a much more pronounced relative contribution of He ions backscattered from Cu in the second layer. This finding points to a higher probability for neutralization in the backscattering collision from Au in comparison to Cu.

These results make clear that the charge exchange probabilities must be known if one aims at a quantitative analysis of surface composition using LEIS. On the other hand, comprehensive knowledge of these quantities allows to perform even quantitative depth profiling with good accuracy.

Support by the Austrian Science Fund (FWF), project P20831, is gratefully acknowledged.

Refernces.

[1] H.H. Brongersma, M. Draxler, M. de Ridder, P. Bauer, Surf. Sci. Rep. 62 (2007) 63.
[2] H. Niehus, W. Heiland, E. Taglauer, Surf. Sci. Rep. 17 (1993) 213
[3] W.B. Pearson, Handbook of lattice spacings and structures of metals and alloys, Pergamon, Oxford (1967)
[4] D. Primetzhofer, M. Spitz, S.N. Markin, E. Taglauer, P. Bauer, Phys. Rev. B 80, 125425 (2009)
[5] M.A. Karolewski, Nucl. Instrum. Meth. B 230 (2005) 402–405.

I 7. Dealing with disorder, defects and amorphicity in medium energy ion scattering experiments

T.C.Q. Noakes

tim.noakes@stfc.ac.uk (corresponding author)

STFC Daresbury Laboratory, Daresbury Science and Innovation Campus, Keckwick Lane, Daresbury, Warrington, Cheshire, WA4 4AD, UK

The crystalline nature of many solid materials is one of the first lessons learnt in solid state physics. However, in the real world perfect crystals never exist because of the presence of a wide range of defects such as vacancies, interstitials and edge and screw dislocations. On a more macroscopic level it is possible to have other imperfections, such as grain boundaries between crystalline regions, disordered regions within a crystalline matrix or even amorphous regions where the bond lengths and angles are all different even though the average remains the same as for the crystalline equivalent.

In many applications the ability to grow good quality crystalline materials with the minimum amount of disorder is important, a good example being the epitaxial growth of semiconductor quantum well structures. However, in some applications crystallinity may need to be suppressed to achieve the best performance (e.g. high dielectric constant gate oxide films). In other systems, such as magnetic metal/metal and metal/metal oxide multilayers crystalline order clearly plays an important role, although it is not always clear whether perfect ordering is either required or necessarily desirable. Clearly the ability to asses the degree of crystalline order is important for a range of technologically important applications, so a technique that can provide this information in a quantitative or at least semi quantitative fashion is desirable for experiments in areas such as these.

Traditionally, diffraction techniques have been used to investigate crystalline materials, X-ray diffraction (XRD) for bulk solids, and more surface sensitive techniques such as reflection high energy electron diffraction (RHEED) and low energy electron diffraction (LEED) for thin film growth. For these techniques the majority of information is contained in the spots and streaks observed, which essentially come from the crystalline part of the sample, the disordered regions simply contributing to the diffuse background. However, in a medium energy ion scattering (MEIS) experiment the structural information comes from the position of blocking dips in the angular spectra. At the bottom of a blocking dip the intensity is low for a crystalline material, but will be much higher for materials containing significant disorder. For this reason MEIS data and in particular the blocking dip amplitudes are a sensitive probe of disorder in crystalline materials and thin films.

Whilst the sensitivity of the technique is indisputable there remains the problem of extracting quantitative or at least semi quantitative information from the MEIS angular spectra. Fitting angular spectra is normally carried out using the VEGAS Monte Carlo simulation code [1] where perfect crystalline order is often assumed, allowing a small unit cell with periodic boundary conditions to be employed and thus minimising computation time. This assumption was certainly beneficial in the early days of MEIS data analysis when computing power was much more limited. Whilst it is now possible to run much larger models where accurate representations of various kinds of disorder are recreated (e.g. [2-3]),

there are still advantages of using approaches which involve smaller models, not least the saving in time it takes to set up a model using many thousands of atoms. Over the years a number of different approaches have been used to try and model disorder in a simple and straightforward manner using VEGAS; these will be described along with some of their advantages and disadvantages.

Some of the earliest work to model disorder used essentially flat signal to represent the disordered part of the sample, with the results from a VEGAS simulation of a relatively small model providing the crystalline part. In this procedure it is important to match the amount of flat signal with the number of layers in the VEGAS simulation and the depth range of the extracted data. This very simple procedure has been successfully used on numerous occasions to compare the relative crystallinity of different samples [4-5]. However, there are several disadvantages of this method; it assumes a crystalline matrix with completely amorphous inclusions and does not allow for any partly crystalline regions and it also assumes complete illumination of the disordered regions and ignores any dechanneling through them. The method is also seen to only reduce the amplitude of blocking dips and not the width even though this is often observed experimentally. Getting the width of the blocking dips wrong can cause problems with fitting, particularly when other parameters such as strain are included in the modelling. For these reasons the method certainly can not be considered to be truly quantitative, but does provide a 'disorder parameter' which critically can be determined with an associated error using our established fitting techniques with chi-squared reliability factors. Hence it is possible to tell whether he difference in the amount of disorder between samples is statistically relevant or not.

Because of the limitations of the previous method, attempts were made to look for alternative ways of fitting disorder. One method was to apply random shifts to the atom positions which might be particularly useful for systems which display partially amorphous character. A table of random numbers for all three dimensions was generated and applied as shifts to the crystal model with a scaling factor which acts as the fit parameter. Here a somewhat larger model is required. For small values of the scaling factor both the amplitudes and widths of the blocking dips were seen to reduce. One interesting question is how large the mean displacements need to be before the dips disappear entirely. However, it was not possible to investigate this because for larger values of the scaling factor the VEGAS program was seen to crash. Investigations into the reason for this initially concentrated on the proliferation of groups in the auxiliary lattice used in the ion propagation algorithm because the original version of the code had clear limits on the possible number that could be tolerated. However, even with this rectified the code failed to run for large values of the scaling factor. Another possible reason for the failure of the code was thought to be the ion propagation algorithm itself, but because this is so fundamental to the way VEGAS works it was not possible to rectify this problem and hence the random displacement method was effectively abandoned.

Another approach is to use dynamic displacements of the atoms to simulate the static displacements seen for disordered materials. Since the time scale of the interaction between the ion and the surface is much shorter than that for thermal vibrations the ions effectively take a snapshot of the atoms in fixed positions where deviations from the average positions as a result of the thermal vibrations are present. It is therefore possible to simulate static disorder by simply increasing the vibrational amplitudes. One issue here is how to separate static and dynamic displacements and the simplest way is to calculate the theoretical vibrational amplitude from the Debye temperature and subtract this from the fitted value.

This approach has been successfully applied in metal-on-metal growth experiments [6]. However, Debye temperatures are not always known with great accuracy, particularly for alloys and compounds. An alternative approach is to take data and fit it at a range of sample temperatures and extrapolate to absolute zero to extract the static disorder component. The problem here is the large amount of additional time required for data collection which may make this approach impracticable for many applications.

In summary, different approaches have been investigated to fit disorder in MEIS data, of which two have been demonstrated to be useful. While they clearly have their distinct advantages and disadvantages, both have been successfully used to exploit the sensitivity of the MEIS technique to this important parameter in solid state materials.

References

[1] J.F. Frenken, J.F. van der Veen and R.M. Tromp, Nuclear Instruments an Methods in Physics Research B 17 (1986) 334

[2] J.A. Smerdon, J. Ledieu, R. McGrath, T.C.Q. Noakes, P. Bailey, M. Draxler, C.F. McConville, T.A. Ross and T.A. Lograsso, Physical Review B 74 (2006) 035429

[3] M.A. Munoz-Marquez, R.E. Tanner and D.P. Woodruff, Surface Science 565 (2004) 1

[4] T.C.Q. Noakes, P. Bailey, D.T. Dekadjevi and M.A. Howson, Physical Review B 68 (2003) 155425

[5] T.C.Q. Noakes and P. Bailey, Thin Solid Films 394 (2001) 16

[6] M.D. Cropper, T.C.Q. Noakes, M.T. Butterfield and P. Bailey, 594 (2005) 212

O13 Monte Carlo simulations of high resolution elastic recoil detetection depth profiles

A. Bergmaier[1], S. Auer[1], G. Dollinger[1], F. Schiettekatte[2]

andreas.bergmaier@unibw.de

[1] *Universität der Bundeswehr München, LRT 2, Werner-Heisenberg-Weg 39, D-85577 Neubiberg, Germany*
[2] *Regroupement Québécois sur les Matériaux de Pointe, Département de Physique, Université de Montréal, Montréal, QC, Canada H3C 3J7*

Measuring high resolution ERD depth profiles with the Q3D magnetic spectrograph at the Munich tandem accelerator, energy and depth resolution is not longer defined by the detector energy resolution but just by physical limits. These are e.g. energy straggling, angular straggling and plural and multiple scattering effects.

We perform Monte Carlo (MC) simulations in order to include all physical effects in spectrum simulation using CORTEO program [1] and to extract true elemental profiles. We show simulated and measured oxygen profiles of a 7 nm thick SiO_2 layer on silicon substrate (in semiconductor quality) using a 40 MeV Au beam, scattering angle of 15^o and an incident angle of 4^o that gives a depth resolution at the surface of less than 0.5 nm. In contrast, the width of the interface is about 2.5 nm. The only way to decide if this interface width is due to the sample – inhomogeneities of the layer thickness or an oxygen gradient at the interface – or due to the physical limits of the measurement, is to perform the Monte Carlo (MC) simulations. In the first instance, MC simulations and measurements show good correlations. However some discrepancies remain which we attribute to some unresolved plural scattering effects of the projectiles. The increase in quality of the data evaluation will be discussed.

References.

[1] F. Schiettekatte, Fast Monte Carlo for Ion Beam Analysis Simulations, Nucl. Instr. Meth. B266 (2008) 1880.

O14 Vicinage Effect and Coulomb explosion dynamics of hydrogen molecules in Silicon Nitride Films

A. L'Hoir, J. J. Ganem, I. Trimaille, I. Vickridge

Jean-Jacques.Ganem@insp.jussieu.fr

SAFIR, Institut des NanoSciences de Paris, UMR 7588 du CNRS, Case courrier 84, Université de Pierre et Marie Curie, 4 Place Jussieu, 75005 Paris, France.

When a molecular ion travels through matter with a velocity V, the stopping force on the molecule depends on the distance R between its nuclei. When R is much larger than the adiabatic cut-off $R_{ad} = V/\omega_p$ (ω_p, medium plasma frequency), each nucleus can be considered as an isolated particle, whereas for $R < R_{ad}$, each nucleus travels in a medium perturbed by the neighboring nuclei of the molecule (vicinage effect), usually resulting in a higher stopping force per nucleon S(R). As soon as a molecular ion enters a solid the cross sections for impact ionization of the molecule are sufficiently high that the molecule rapidly loses remaining bound electrons and its constituent nuclei are submitted to repulsive forces, resulting in a Coulomb explosion.

In previous work [1], we studied the transmission of molecular beams (H_2^+, H_3^+) in SiO_2 films highly enriched in ^{18}O, exploiting the isolated nuclear narrow resonance $^{18}O(p,\alpha)^{15}N$ occurring at E_R=151 keV and the resulting excitation curves $Y(E_b)$ obtained when scanning the beam energy E_b about E_R. It has been shown that the dynamics of Coulomb explosion and vicinage effect can be well described using the dielectric model and a reasonable screening potential for SiO_2 at this energy.

In the present work we present new results obtained on Si_3N_4, at higher velocity. For this experiment we grew homogeneous amorphous films of Si_3N_4 highly enriched in ^{15}N (99.9% labeling), of thickness ~100 nm, on Silicon (100) substrates. Excitation curves were obtained with high statistics about the Γ=120 eV wide resonance at 429 keV in $^{15}N(p,\gamma)^{16}O$ for H^+, H_2^+, and $H_3^+$are shown in Figure 1.

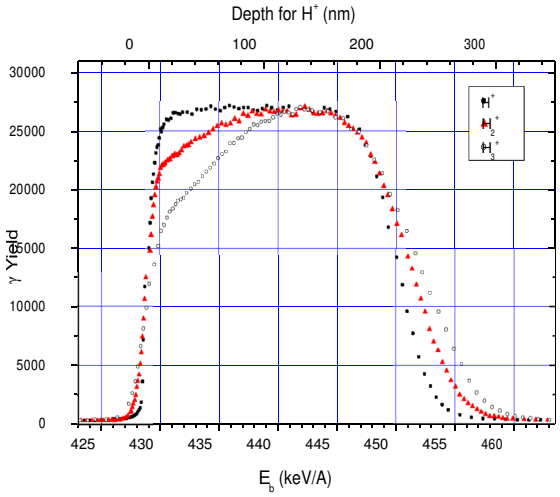

Figure 1 : Excitation curves recorded on a 81 nm thick Si_3N_4, on Si, tilted at 68° (apparent thickness 216 nm), for the 3 different beams using the $^{15}N(p;\gamma)^{16}O$ reaction.

It can be shown that, neglecting energy fluctuations, the γ-yield is inversely proportional to the stopping force S(R). One observes a low γ-yield at low energy (in the first 100-nm of the superficial region) for H_2^+ and even lower for H_3^+, a signature of the vicinage effect (here, a higher stopping force). The high-energy edges of the excitation curves (at the Si_3N_4/Si interface) show increasing energy broadening, essentially due to the variations of the velocity projected on the beam direction for individual protons caused by the Coulomb explosion of the molecules. Once the nuclei become independent ($R > 2R_{ad} = 2V/\omega_p$) the excitation curves reach a plateau (440-445 keV).

In order to quantitatively interpret the linked vicinage effect and Coulomb explosion, we again employed the dielectric model here, using the Energy Loss Function (ELF) of ref.[2]. We described the Coulomb explosion by a Yukawa type repulsive potential with a screening radius r_s. The lateral displacements due to small angle multiple scattering of the nuclei in the exploding molecules was included via a Monte-Carlo code.
The leading edge slope of $Y(E_b)$ is related to energy fluctuations at the layer entrance. The greater incident energy spread observed for molecular ions compared to that of isolated protons is due to the thermal Doppler effect, indicating that molecules produced by the accelerator RF ion source are in high vibrational excited states.

The best fit of the high-energy region of the γ yield curve for H_3^+ (fig. 2-a) is obtained for $r_s = 2R_{ad}$. The low energy region, where vicinage takes place, is also well described using this screening (which governs the molecule explosion) and the ELF of ref. [2]. With the same parameters, the yield curve for H_2^+ is also well reproduced (fig. 2-b). However, a still better fit of the high energy descending slope may be obtained when using a still larger r_s value (less screening).

According to fig. 1, it seems that vicinage effect takes place over similar depths (100 nm) for both molecular ions, a surprising result since the repulsive force is much higher

for H_3^+ than for H_2^+. We show in fact that energy fluctuations play a major role in the whole shape of the $Y(E_b)$ curves, in particular in the low energy part. The simplistic scaling law stating that $Y(E_b)$ is proportional to $1/S(R)$ is substantially modified by energy fluctuations : the full theoretical description of the process shows indeed that vicinage effect disappears faster for H_3^+ than for H_2^+, in good agreement with the experimental observations.

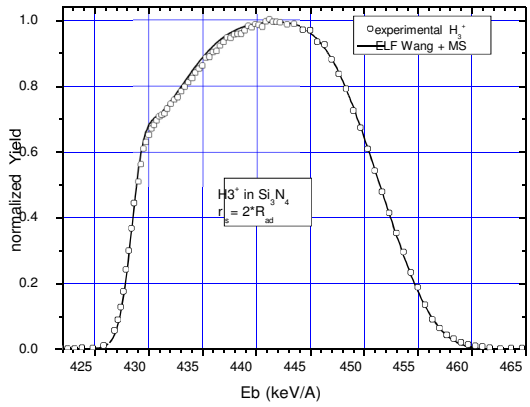

Figure 2-a: Solid line: fit for H_3^+ molecules

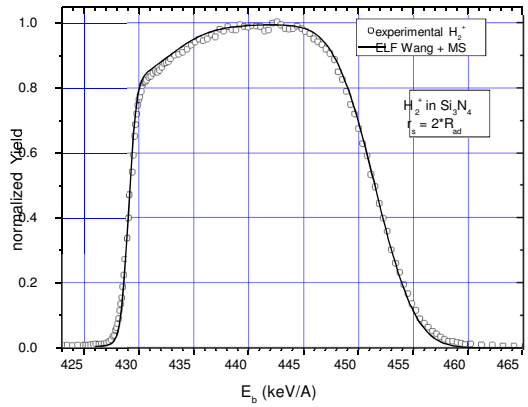

Figure 2-b: Solid line: fit for H_2^+ molecules

References.

1. A. L'Hoir, J.J. Ganem, I. Trimaille and I. Vickridge, Nucl. Instr. And Meth. B 268 (2010) 2850.
2. H. Wang, Y. Chen, Y. Kaneta and S. Iwata, J. Phys. Condens. Matter, 18 (2006) 10663.

O15 A simple approach for simulating the 2D MEIS spectrum in crystalline materials.

A. Hentz[1], P. L. Grande[1], D. P. Woodruff[2]
agenor@if.ufrgs.br

[1] *Instituto de Física, Universidade Federal do Rio Grande do Sul, Av. Bento Gonçalves 9500, Porto Alegre, Brazil*
[2] *Physics Department, University of Warwick, CV4 7AL, Coventry, UK*

We have recently shown [1] the effect of trajectory-dependent energy loss in Medium Energy Ion Scattering – MEIS – experiments for the clean Cu(111) surface under shadowing/blocking conditions. Specifically, the results show the influence of 'skimming' trajectories suffered by ions scattered from sub-surface layers and emerging close to a blocking dip after passing close to near-surface atoms. One key component of this previous result was the use of an impact-parameter dependent energy-loss distribution from coupled-channel calculations due to ionization and excitation processes.

Although the Coupled-channel calculations present the a full solution for the determination of the energy-loss distribution as a function of the impact parameter, they are computationally very time-consuming and their use requires one to deals with large tables of data (energy-loss distributions as a function of ion and target atomic species, ion energy, and impact parameter). In the present work we have tackled this issue by using an analytical asymmetric distribution function, called EMG – Exponentially Modified Gaussian [2]-, to model the energy-loss distribution according to the results from *ab-initio* calculations as well as from experimental data [3,4]. This information is then used in a modified version of the standard VEGAS program, widely used to model MEIS blocking curves to predict not only the scattered ion intensity, but also the scattered ion energy spectrum, as a function of scattering angle for a specific incidence direction at a crystalline surface. This approach allows for the use of the VEGAS program to generate the full 2D MEIS spectrum without using the time-consuming coupled-channel calculations.

Here we present the results of a combined experimental and theoretical investigation that demonstrates both clear and direct experimental evidence of the influence of trajectory-dependent inelastic energy loss in scattering from the outermost few atomic layers of a single crystal, and shows that this can be correctly modeled computationally. We show also the comparison between the simulated spectra obtained through the use of both analytical (EMG fitting) and tabulated (Coupled-channel calculations) energy-loss distributions.

References.

[1] Direct Observation and Theory of Trajectory-Dependent Electronic Energy Losses in Medium-Energy Ion Scattering. A. Hentz, et al. Phys. Rev. Lett. 102 (2009) 096103.
[2] An analytical energy-loss line shape for high depth resolution in ion-beam analysis. P.L. Grande, et al. Nucl. Instr. And Meth. B 256 (2007) pp 92-96.
[3] Inelastic energy loss in 100-keV H+ scattering from single atoms: Theory and experiment for K, Rb, and Cs. A. Hentz, et al. Phys. Rev. B 74 (2007) 125408.
[4] Asymmetric line shapes for medium energy H and He ions undergoing a large-angle collision. M. Hazama, et al. Phys. Rev. B 78 (2008) 193402.

I 8. Sims depth profiling with sub-nm resolution (?).

W.Vandervorst[1] B.Douhard, J.Delmotte, B.Vincent

vdvorst@imec.be (corresponding author)

Imec, Kapeldreef 75, B-3001 Leuven, Belgium
[1]also : Instituut for Kern- en Stralingsfysica, KULeuven,B-3001Leuven, Belgium

Secondary ion mass spectrometry (SIMS) is the cornerstone in many materials studies within the semiconductor community due to its unparalleled sensitivity, quantification accuracy and depth resolution. In recent years the application towards the analysis of very shallow (< 10nm) profiles or complex thin films like HfSiO/SiO_2/Si, SiGe/Si, metal gates,... has increased the demand for SIMS with very high depth resolution. A simple analysis shows that one needs a decay length (which is the correct definition of depth resolution) of less than 0,5 nm/dec in order to solve important technological problems [1].

Based on these requirements it is clear that one needs to reconsider all the fundamental SIMS mechanisms contributing to the quantification, depth scale errors, depth resolution,... and reduce the potential errors they might introduce. These mechanisms can be identified by realizing that in addition to the desired process i.e. the mass analysis of a sputtered, partially ionized, particle flux which can be converted into an intensity profile, concurrent processes occur as SIMS is essentially a (very) high dose implantation with an energetic (reactive) beam (Figure 1). Hence one needs to consider the modification of the near-surface composition of the sample by the incorporation of the reactive species (oxygen, cesium, C_{60},...(compound formation) as well as the impact of the continuous energy deposition leading to substantial atomic displacements below the surface. As these modify the (instantaneous) internal profile they impact directly on the attainable depth resolution.

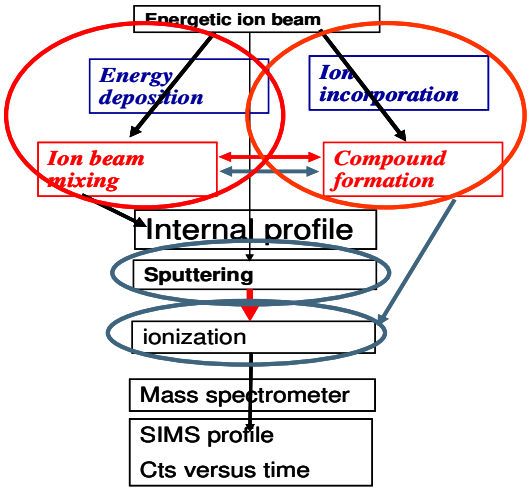

Figure 1 : *Basic interactions during SIMS profiling.*

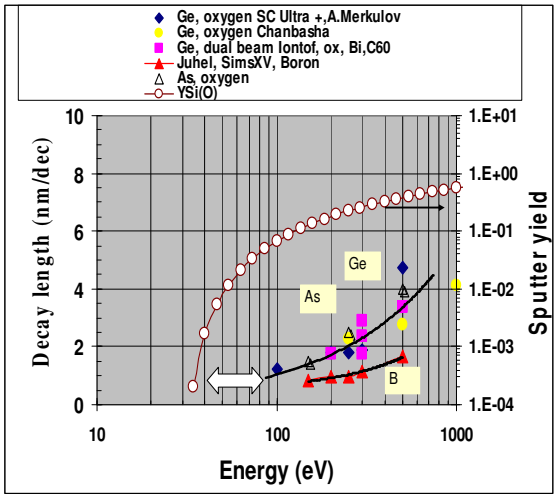

Figure 2 *: Decay length for B, As and Ge in Si versus impact energy. Open squares are the Si-sputter yield values (note the log axis for the sputter yield).*

Hence lowering *the extent of the collision cascade* (by lowering the impact energy) improves the depth resolution. Although this relation is true for all elements, one observes at the same time a pronounced element dependence WITHIN the same matrix (Figure 2). In addition to

the extent of the collision cascade one needs also to consider the *amount of energy deposited* within the collision cascade. This can be inferred from the depth resolution studies (Figure 3) comparing the decay length obtained for similar penetration depths using different primary ions.

As these can only be achieved with higher/lower energy for the heavier/lighter ion, a different energy deposition density and thus number of displacements will be induced leading to substantial differences in depth resolution. Finally one needs to recognize that the element dependence is also (partly) linked to element dependent displacements as the *energy transfer between a recoiling matrix element and the impurity and the distance travelled by* this element for a given energy transfer are element specific.

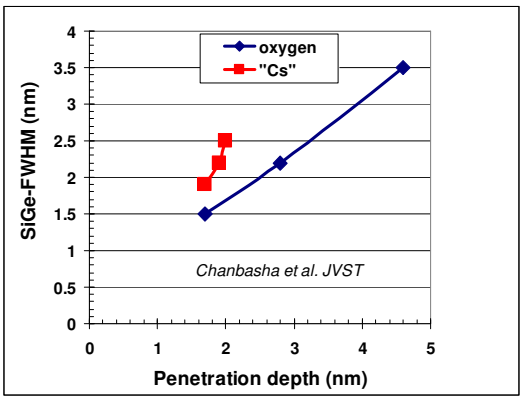

Figure 3 *: FWHM of a SiGe marker layer vs the penetration depth of the primary ion.*

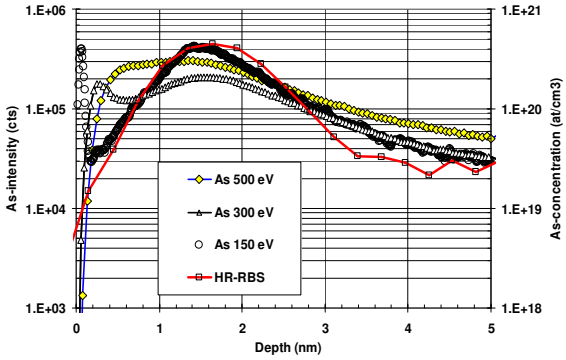

Figure 4 *: As-interfacial profile as observed with different primary beam energies and HR-RBS.*

The results in figure 1 indicate that in order to reach the 0.5 nm/dec decay length target, the primary beam energy needs to be reduced substantially. A lower limit is imposed by the threshold energy for sputtering (~30-40eV) and the need to maintain a practical erosion rate (> 0.1 nm/min) despite the strong reduction in sputter yield and poorer performance of most ion sources at reduced energies. The recent development of plasma based ion sources for SIMS has alleviated this problem and enabled the introduction of EXL(I)E-SIMS (extremely low energy SIMS) [2] operating at energies 100-150 eV routinely. The reduction from the "normal" energies (250-500 eV) to 150 eV leads to a dramatic improvement in profile resolution as indicated Figure 4. The profiles vary from an apparently uniform distribution in the oxide (for a 500 eV analysis) to a clearly defined peak at the interface for 150 eV in complete agreement with the high resolution RBS –profile (cfr prof K.Kimura).. The benefit of the SIMS relative to RBS lies of course in the much higher sensitivity as can be observed in the rest of the profile. An equally important side effect of the reduced impact energies is the complete disappearance from any matrix effect in the SIMS quantification. In fact the profiles shown in fig 4, are solely representing the raw data and were not processed with any matrix dependent calibration factor accounting for differences in ionization probabilities.

Extensive studies on SIMS depth resolution have been using delta layers of dopant layers. Rather than using the concept of FWHM to characterize broadening effects (as done in IBA, XPS,..), it is much more instructive to analyze the results in terms of the slope at the leading and trailing edge. Whereas the slope of the trailing edge is normally dominated by the ion beam mixing process, the leading edge is always much sharper (2-3x) and shows a much weaker energy dependence. The leading edge is much more a reflection of the true profile and

dominated by effects such as surface roughness and eventually the escape depth of a sputtered ion. Using the delta layer concept we have analyzed the energy dependence of these decay lengths for Boron, cfr Figure 5. It is now interesting to see that the extrapolation towards zero-energy indicates a minimal value of 0.33 nm/dec comparable to the slope of the leading edge at low energy (fig.6). This convergence may indicate that one starts to approach the intrinsic depth resolution value as imposed by the escape depth of the sputtered particle and the statistical nature of the particle emission.

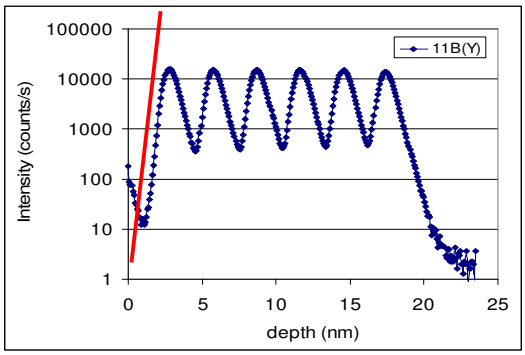

Figure 5 : *Sims profile of B-delta layer. Note the steeper upslope vs down slope.*

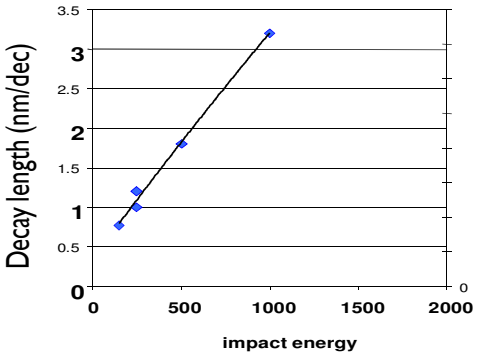

Figure 6 : *Decay length (trailng edge) of B delta in Si.*

The availability of EXLE-Sims has opened a new application range, previously unaccessible. For instance the concept of replacing Si by a higher mobility material such as Ge, has necessitated the development of novel interface passivation concepts as the Ge-oxide is of much poorer quality than SiO_2. One successful concept is based on passivating the Ge-surface with a FEW monolayers of Si. The optimum lies between 5-8 ML whereby one still needs to certify that no Ge-updiffusion occurs during the Si-growth [2]. Such a structure is at the same time an ideal test to probe the SIMS capabilities. The results in figure 7 show the Si (Ge) profile of a Ge-substrate covered with 9 ML of Si. As the Si forms a native oxide (~ 1 nm) , removing the latter by HF and letting it reoxidize effectively removes 0.5 nm of Si cap layer. As indicated in figure 7 the latter thickness difference is easily identifiable in the SIMS profiles. Tthe results in figure 8 demonstrate the ability to probe also small differences in Ge-uptake resulting from the Si-deposition process. The differences in Ge slope can be linked to differences in Ge-segregation (not diffusion) during the growth of the cap with different deposition gases. Note not only the different slopes in the Ge-profiles (in a 1 nm layer!) but also the presence of a small surface segregation peak. Finally the results indicate that it is possible to detect extremely very small differences in layer thickness (< 1 ML).

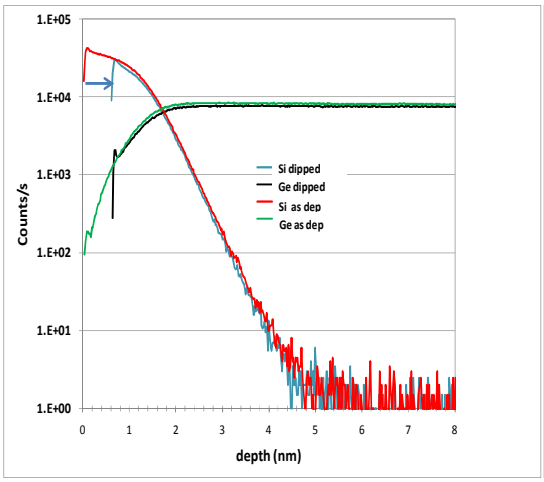

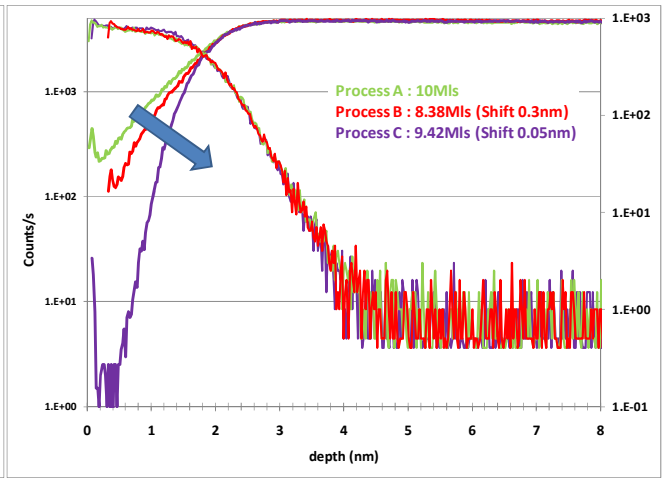

References.

[1] Semiconductor profiling with sub-nm resolution: challenges and solutions, W. Vandervorst, Applied Surface Science 255 (2008) 805-812

[2] Si passivation for Ge pMOSFETs: Impact of Si cap growth conditions, B.Vincent et al. Solid-State Electronics 60 (2011) 116–121

O16 Depth profiling of metal - organic samples by (low-energy) dynamic SIMS

K.Q. Ngo[a], P. Philipp[a], Y. Jin[b], S. Nola[b], M. Shtein[b], J. Kieffer[b], T. Wirtz[a]

ngo@lippmann.lu

[a] *Department "Science and Analysis of Materials" (SAM), Centre de Recherche Public – Gabriel Lippmann, 41 rue du Brill, L-4422 Belvaux, Luxembourg*

[b] *Department of Materials Science and Engineering, University of Michigan, Ann Arbor, Michigan 48109-2136*

Recently, the increasing sophistication of organic optoelectronic devices (e.g. organic light-emitting diodes and organic photovoltaic cells, etc.) requires molecular-level dimensional control in the fabrication of multi-layered structures with specifically engineered interfaces. In a current project, we address this challenge by advancing the development of low-energy secondary ion mass spectrometry (LE-SIMS) for the analysis of organic-based optoelectronic materials systems [1, 2].

In the current research, we investigated the formation and evolution of surface topography at the crater bottoms as well as interface resolution for some bi-layered samples sputtered by LE- SIMS. The samples, presenting a silver and an organic layer deposited onto a Si substrate, are analyzed by a 500 eV Cs^+ beam on a Cameca Sc-Ultra instrument [3]. Characterization of the surface roughness is carried out by AFM. The roughness is investigated as a function of depth, both, with and without sample rotation.

The samples were prepared by vacuum thermal evaporation (VTE). The experimental conditions have been reported somewhere else [1, 2]. Two VTE systems have been used: a standard Angstrom system and a lab-built supperlattice system. The cryo sample B has been deposited using a cooling substrate during the deposition. Altogether, two different organic molecules used in optoelectronic devices, Tris(8-hydroxyquinolinato) aluminium (Alq_3) and Copper Phthalocyanine (CuPc), different layer thicknesses and deposition methods are studied (Table. 1). Metal and organic layer have always the same thickness.

Name	Sample	Layer thickness	Depositing system	Sample substrate
A	Ag / Alq_3	30 nm	Angstrom	Room temperature
B	Ag / CuPc	13 nm	Angstrom	Cooling substrate
S1	Ag CuPc	12 nm	Supper-lattice	Room temperature
S2	Ag / CuPc	48 nm	Supper-lattice	Room temperature

Table 1: List of sample and details.

In the SIMS depth profiles (Fig. 1-3), the organic layers are identified by high intensities of the CN^- cluster ions (the blue dash line), while the Si substrate is characterised by Si^- intensities of 10^7 to 10^8 count/s (the dark yellow dash-dot-dot line). For the different samples, the depth resolution at interfaces between Ag and organic layers as well as between organic layer and Si substrate are calculated from the CN^- and Si^- depth profiles.

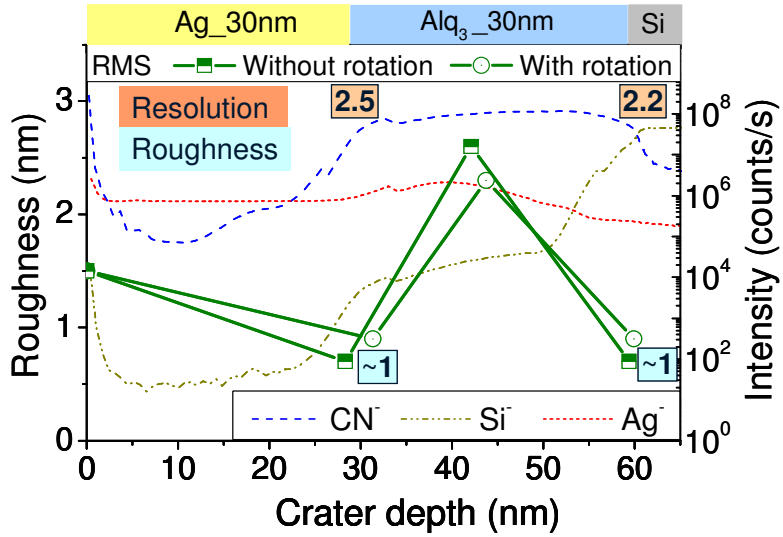

Figure 1. Roughness and depth resolution of sample A, with and without rotation during sputtering.

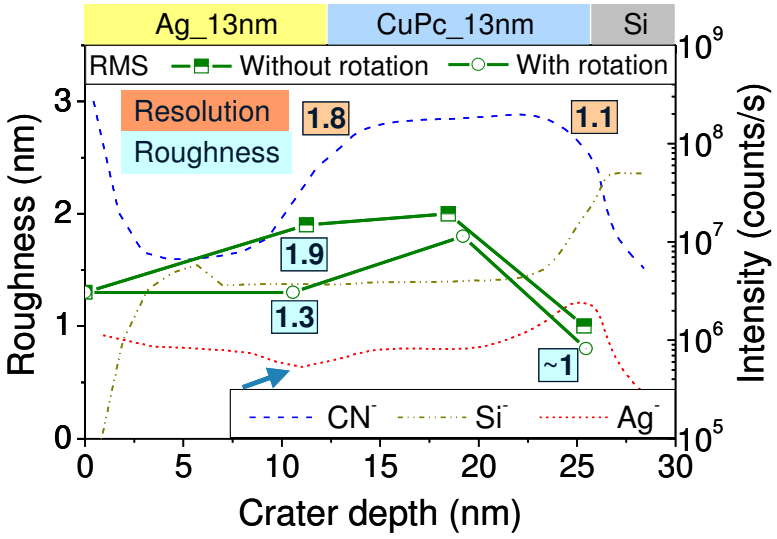

Figure 2. Roughness and depth resolution of sample B, with and without rotation during sputtering.

However, the intensity of Ag^- does not present well the shape of the Ag layer (the red dot line). For sample B (prepared by using cooling substrate), the Ag^- intensity is quite stable in both metal and organic layer but the depth profile shows a small minimum point at the interface between Ag and CuPc layer (cf arrow to red dot line in Fig. 2). This behavior is seen only in the cryo sample. For the samples A, S1 and S2 prepared at room temperature, the Ag^- intensity is increasing inside the organic layer (Fig. 1, 3). The presence of Ag in organic layers could be caused by a rough interface due to the sample preparation conditions or by radiation-induced roughening of the craters or Ag diffusion during sputtering in SIMS. In order to verify the role of surface roughening, the roughness was investigated at certain depths by AFM. SIMS depth profiles were stopped at different depths, and then the craters were transferred to AFM to measure the surfaces.

For both samples A and B, roughness could be reduced by using sample rotation during the SIMS analysis (Fig. 1, 2). Thus, using rotation helps to better resolve interfaces. Roughness is always slightly higher (less than 2nm) in the middle of the organic layer than in the other SIMS craters. Roughness shows a similar tendency in sample S1 (Fig. 3) (prepared in the lab-built instrument): the roughness does not change much in the Ag layer, and increases in the organic layer. For the sample S2,

(thickness of each layer 48nm), roughness shows a slightly different behavior: first increase in the metal film, and then decrease in the organic layer.

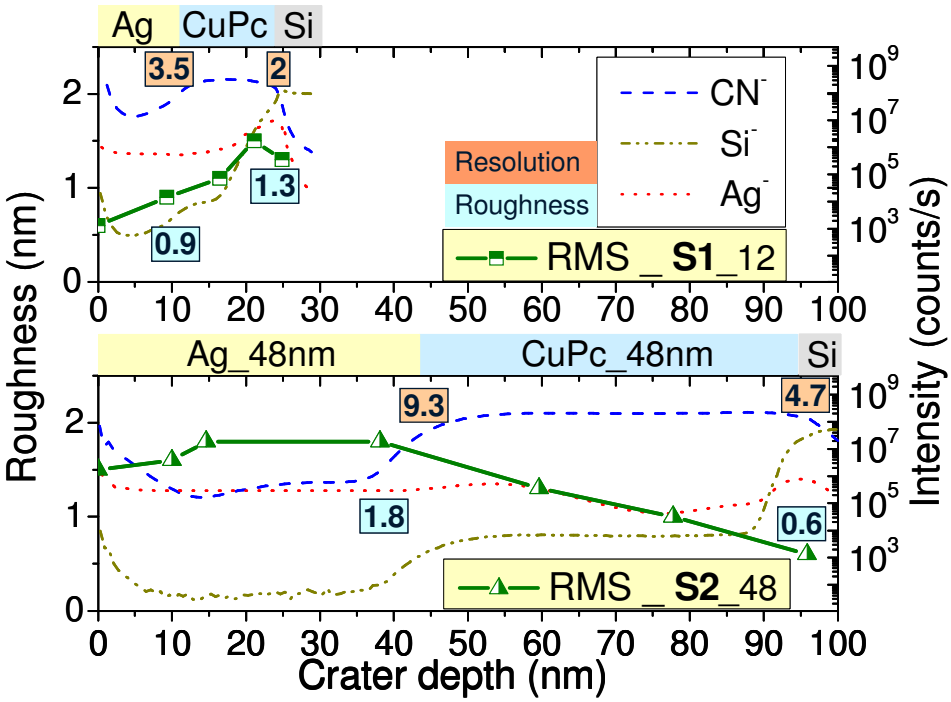

Figure 3. Roughness and depth resolution of samples S1 (top) and S2 (bottom)

However, in all situations, roughness at the organic/Si interface is lowest. In this study, roughness at the different interfaces is also smaller than the depth resolution calculated from SIMS depth profiles. Thus, characterization of the organic multilayered samples is not limited by the formation of roughness in the SIMS craters and the Ag^- depth profile is largely shaped by atomic mixing and diffusion of this element during the analysis or during the deposition into the organic layer.

References.

[1] Analysis and fragmentation of organic samples by (low-energy) dynamic SIMS. K.Q. Ngo, P.Philipp et al. Surf. Interface Anal. 43 (2011) pp 88-91.

[2] Analysis of organic multilayered samples for optoelectronic devices by (low-energy) dynamic SIMS. K.Q. Ngo, P.Philipp et al. Surf. Interface Anal. 43 (2011) pp 194-197.

[3] Ultra low energy Cs bombardment in a magnetic sector SIMS instrument. E.De Chambost, B. Boyer, B. Rasser, M. Schuhmacher. Proceeding of the twelfth International Conference on Secondary Ion Mass Spectrometry (SIMS XII). (1999) pp 533.

O17 Compositional analysis of NiO thin films grown by MOCVD.

J. Meersschaut

johan.meersschaut@imec.be

Imec, Kapeldreef 75, BE-3001 Leuven, Belgium

The resistive switching effect is considered to be a promising pathway to improve on high-density non-volatile memory applications. The functionality of resistive switching memories is based on the ability to switch resistance between a low and a high value through the application of current and voltage pulses [1]. Although resistive switching has been shown to occur for several metal oxides, the frequently observed unipolar transition and low programming voltage and current [2-5] for NiO makes this material particularly interesting.

We developed a metal-organic chemical vapor deposition process for the application of NiO thin films in resistive switching random access memory devices. The deposition process was developed on blanket 300 mm p-type Si(100) substrates. A 1 nm SiO_2 layer was grown through oxidation of H-terminated crystalline Si(100) substrates. The deposition of NiO films using $Ni(dmamb)_2$ and molecular oxygen as the oxidizer is investigated for substrate temperatures between 280°C and 375°C. Contaminants that remain from the incomplete decomposition or removal of the ligands from the metal-organic precursor are often a concern with chemical vapor deposition techniques. The amounts of hydrogen, carbon, and nitrogen contaminants therefore are of particular interest. It has also been reported that the electrical transport properties and the resistive switching effect are critically dependent on the Ni:O compositional ratio [4,6]. We have thus used X-ray photoelectron spectroscopy (XPS), elastic recoil detection analysis (ERDA), and secondary ion mass spectroscopy (SIMS) to gain information on the chemical composition of the layers.

The X-ray photoelectron spectra (XPS) are a fingerprint of the chemical bonding of the elements. If the X-ray photoelectron spectroscopy is combined with surface sputtering, one is able to quantitatively determine the depth dependent chemical profile of the thin film. X-ray photoelectron spectroscopy was carried out on a Theta300 system from Thermo Electron. The measurements were performed using a monochromatized Al Kα X-ray source (1486.6 eV) and a spot size of 400 microns. The energy resolution was ~0.8 eV (full width at half maximum measured at the Si $2p_{3/2}$ photoemission peak). The data are measured at a 22 degree exit angle as measured from the normal of the sample. The signal intensities are extracted from integration of the peak area after background subtraction. Standard sensitivity factors (photoionisation cross section, transfer function of the analyzer and depth sensitivity) were used to convert peak areas to atomic concentrations. XPS sputter depth profiling was done using a 500 eV Ar^+ ion beam at 45° incidence.

The elastic-recoil detection technique relies on the elastic nuclear interaction between the ion beam in the MeV energy range and the screened Coulomb potential of the nuclei in the sample. The advantage of the technique is that no sputtering is needed to probe the bulk of the film, and that it avoids the artifacts that are associated with preferential sputtering or with matrix effects that affect the secondary ion yield. The elastic recoil detection analysis (ERDA) experiments were performed with a time-of-flight telescope in combination with a Si detector.

Timing gates based on the electrostatic mirror design were used with a flight path of 845 mm. The experiments were done using 6 MeV Cl^{4+} ions accelerated by a 2 MV Pelletron accelerator. The scattering and recoil angles used were 39˚, whereas the exit angle of sample surface to detector was 5˚.

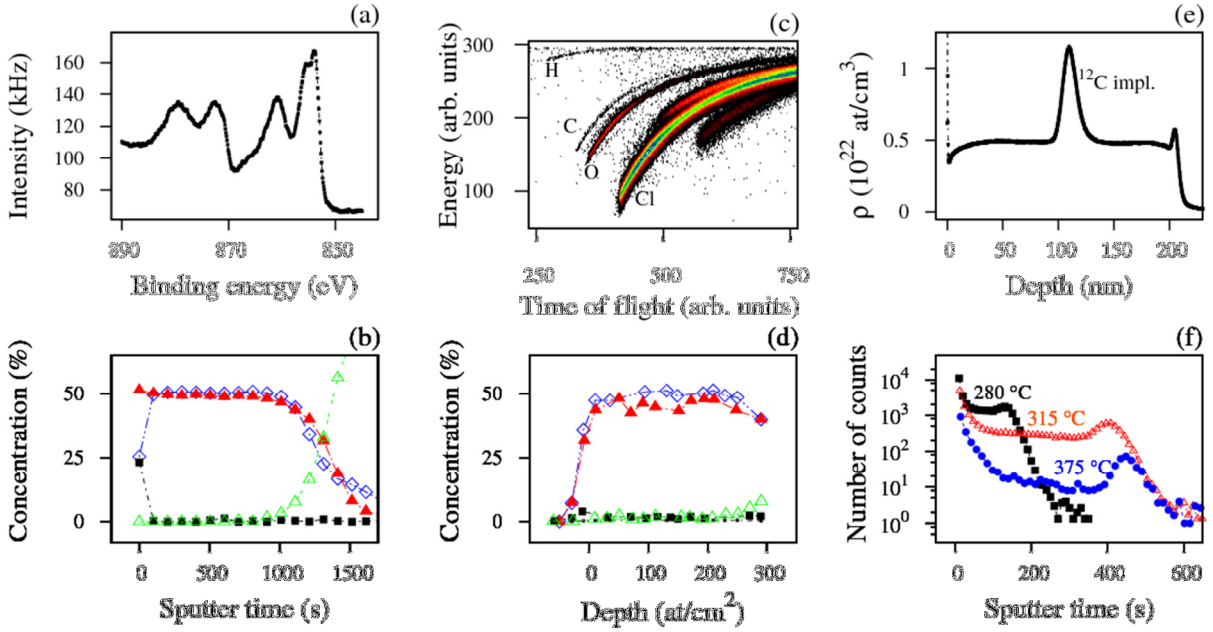

Figure 1 :
(a) High-resolution X-ray photoelectron spectrum (Ni 2p region) of a NiO film deposited at 315˚C.
(b) Sputter XPS profile of 15 nm NiO film: blue Ni 2p; red O1s; black C 1s; and green Si 2p signal.
(c) Elastic recoil detection data for a 25 nm thick NiO film on SiO_2/Si deposited at 315˚C.
(d) Reconstructed depth profile from ERDA: blue Ni; red O; black C; and green Si.
(e) SIMS depth profile of the ^{12}C signal for a sample that was implanted with 10^{16} ions/cm^2 after the deposition of 100 nm NiO, additionally covered with 100 nm NiO.
(f) ToF-SIMS depth profiles of CN for films deposited at 280˚C (black), 315˚C (red), and 375˚C (blue)

ToF-SIMS experiments were performed on a dual beam ION-TOF IV instrument. Both positive and negative ions were measured using a Ga beam (15 keV) for analysis and a Xe^+ beam for sputtering (500 eV). Sputtering depth profiles are obtained through rastering the Cs+ ion beam on a 200 X 200 µm^2 area and the Ga+ ion beam on a 50 X 50 µm^2 area.

A general assessment of the chemical profile is obtained via X-ray photoelectron spectroscopy. In figure 1(a), the energy range around the Ni 2p peak of the surface photoelectron spectrum obtained on a 15 nm thick NiO film grown on a (1 nm)SiO_2/Si substrate is shown. The binding energy positions of the main and the satellite peak, and the line shapes of the Ni 2p peaks indicate the formation of a fully oxidized NiO. The spectra obtained here are reminiscent of the spectra obtained earlier on NiO polycrystalline powder [7] and on thin films deposited via atomic layer deposition [8] or DC magnetron sputtering [6].
In figure 1(b) the XPS depth profile for the 15 nm thick NiO film is shown. After sputter-cleaning the sample for less than 100 seconds by an Ar ion beam to remove the surface contamination, the results show a uniform film. Unless the matrix effects are known, it is not possible to extract absolute values for the composition. Nevertheless, for comparison with literature data, we note that no carbon or other contamination was observed within the detection limit of the XPS measurement. Also, the XPS results are indicative of a slightly Ni-rich Ni:O stoichiometry.

It is known that elastic recoil detection analysis (ERDA) may allow one to determine the standard-free quantitative elemental composition of thin films. The raw data as a function of time-of-flight and energy are shown in the figure 1(c). The signals originating from hydrogen, carbon, oxygen, silicon, chlorine and nickel are identified in the plot of the raw data. Bulk ERDA compositions were obtained by averaging over the central part of the films, where no influence of surface and substrate are observed. The elemental depth profile on a thin NiO film deposited at 315˚C indicates that the Ni:O ratio approximately is 1.1:0.9. It is found that the hydrogen and nitrogen contamination remain below the percentage level. The ERDA results indicated a carbon contamination of the order of 2%.

An alternative quantification of the carbon contamination is attempted with secondary ion mass spectroscopy (SIMS) using a sample that was specifically designed for these purposes. After first depositing 100 nm NiO at 315˚C, the sample was implanted with 10^{16} carbon ions/cm^2, and finally complemented with another 100 nm NiO. The SIMS depth profile, figure 1(e), was performed on an Atomica tool using 500 eV Cs+ sputter ions and incidence angle of 45 degrees. Apart from the surface contamination, the sample also exhibits a maximum at the depth of 100 nm. Having related the area of this peak with the known dose of implanted ^{12}C, we are able to quantitatively determine the carbon content in the background as $5x10^{21}$ ions/cm^3, or as ~4% of the bulk NiO atom density.

The carbon contamination determined by SIMS exceeds the ERDA results. An overestimation of the C concentration in SIMS potentially may result from carbon re-deposition during the measurement. We investigated the effect of carbon re-deposition by using various current densities, obtained by varying the raster size or current. However, neither current values ranging from 14 nA to 80 nA nor raster sizes ranging from 250 to 600 have shown a variation in the layer-intrinsic carbon content. Therefore, the carbon contamination via SIMS is believed not to be influenced by re-deposition effects. Further wordk is needed to clarify the origin of the discrepancy between ERDA and SIMS.

Impurity and chemical depth profiles were also obtained by ToF-SIMS measurements. While the absolute quantification of the contaminants by TOFSIMS is difficult, it is found that the observed levels are typical for MOCVD-grown oxides. Apart from surface contamination effects, the profile was constant throughout the film. The C signal was found to be very small. The CN signal, acquired in negative polarity, attains a considerable level. The result of the ToF-SIMS depth profile on the CN signal is shown in figure 1(f). The results illustrate that the CN levels are decreasing substantially with increasing deposition temperature.

To summarize, NiO films produced by MOCVD of Ni(dmamb)$_2$ and molecular oxygen have been characterized using x-ray photoelectron spectroscopy, elastic recoil detection spectroscopy, and secondary ion mass spectroscopy. The Ni:O ratio is estimated to be approximately 1.1:0.9 from ERDA measurements. From SIMS experiments, we estimate the carbon contamination around 4%. ToF-SIMS results indicate decreasing CN levels with increasing deposition temperature. From ERDA, we obtained that the process at 315˚C results in H contamination and N contamination of 0.4% and 0.8% respectively. Therefore, this work shows that the chemical vapor deposition of NiO using the Ni(dmamb)$_2$ precursor and oxygen reactive gas is a promising route for applications in non-volatile resistive switching memory devices. The report illustrates how XPS, ERDA, and SIMS complimentarily yield information on the chemical composition of the metal oxide.

References.

[1] R. Waser and M. Aono, Nature Mater. **6** (2007) 833
[2] I.G. Baek, et al., Tech. Dig. Int. Electron Devices Meet. (2004) 587
[3] M.-J. Lee, et al. Adv. Mater. **19** (2007) 3919.
[4] S. Seo, et al., Appl. Phys. Lett. **85** (2004) 5655.
[5] Y.-H. You, et al, Appl. Phys. Lett. **89** (2006) 222105.
[6] M.J. Lee et al. J. Appl. Phys. **103** (2008) 013706
[7] A.P. Grosvenor, et al. Surface Science **600** (2006) 1771
[8] T.S. Yang, et al., J. Vac. Sci. Technol. A **23** (2005) 1238

I 9. Adsorption and thermal stability of organic films on surfaces monitored by Direct Recoil Spectroscopy.

L. Salazar-Alarcón[1], L.N. Serkovic Loli[1], L.J. Cristina[1], L. Chen[2], S. Shen[2], V.A. Esaulov[2], J.E. Gayone[1], E.A. Sánchez[1], O. Grizzi[1]

esanchez@cab.cnea.gov.ar

[1] *Centro Atómico Bariloche -Comisión Nacional de Energía Atómica, Instituto Balseiro – Universidad Nacional de Cuyo, CONICET, 8400 San Carlos de Bariloche, Río Negro, Argentina.*

[2] *CNRS, UMR 8625, Institut des Sciences Moléculaires d'Orsay, ISMO, Bâtiment 351, Université de Paris Sud-11, 91405 Orsay, France .*

The adsorption and self-assembly of organic molecules on a variety of substrates such as noble metals, transition metals with incomplete d-shells and semiconductors, is a subject of great activity in surface science and applied chemistry due to the possibility of using them as building blocks with specific electronic properties, or linkers between metallic contacts to produced optoelectronic devices. Π- conjugated or aromatic organic molecules are highly attractive building blocks as their electronic properties, the molecular arrangement and the functionality of these structures can be custom tailored through the rich chemistry of organic systems.

In this work we report results on the study of the adsorption process and of the thermal stability of a EP-PTCDI (N,N'-bis(1-ethylpropyl)-perylene-3,4,9,10-tetracarboxdiimide – $C_{34}H_{10}O_4N_2$) and BDMT (1, 4-benzene dimethanetiol – SH-CH_2-C_6H_4-CH_2-SH) ultrathin films grown on Au and Ag, by means of Direct Recoil Spectroscopy with time-of-flight mass analysis (TOF-DRS). This technique is particularly suitable to study organic molecules [1] because a) it detects hydrogen, an element that is present on organic molecules but that is not detected by the standard surface analysis techniques, b) it is sensitive to the topmost layer of the surface, c) both neutral and ion scattered and recoiling particles are detected with similar sensitivity thus avoiding uncertainties due to the electron exchange processes, and d) the TOF analysis combined with a multichannel technique allows the use of low density currents (10^8–10^9 ions.s^{-1}.cm^{-2}) producing undetectable damage within a typical analysis time.

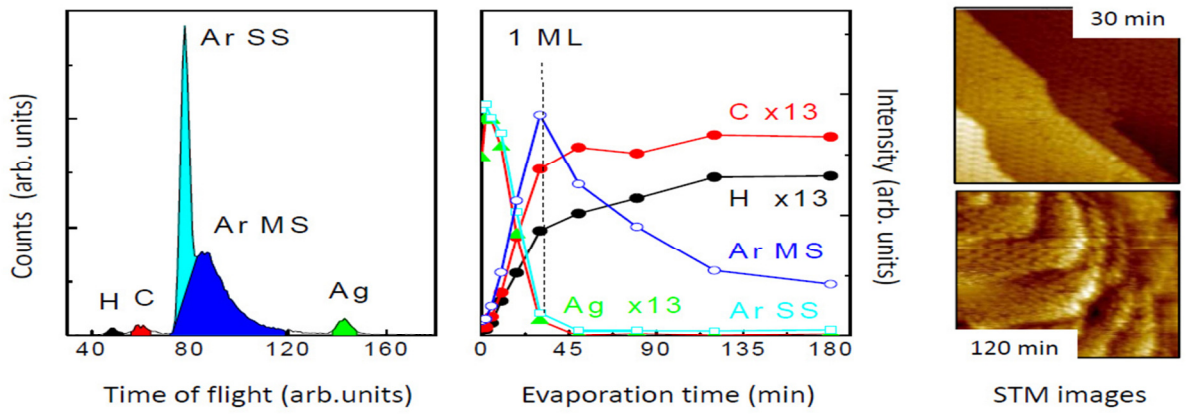

Figure 1: EP-PTCDI adsorption on Ag(111).

A typical spectrum of the deposition of EP-PTCDI molecules from a Knudsen cell on Ag(111) is shown on the left of Figure 1. In this picture the colored areas indicate the integral areas used to get the intensity of each element detected on the surface (H, C and Ag),

as well as the scattered Ar atoms through single (SS) or multiple (MS) collisions. The evolution of these intensities as a function of the evaporation time (at constant flux deposition) is shown in the central panel of Fig. 1. Note that the growth of H and C up to 30 min is linear, indicating that the sticking coefficient, i.e. the ratio of the number of molecules that do adsorb on a surface to the total number of molecules that impinge upon that surface, is constant. Combining these results with the STM observations shown on the right we conclude that the growth rate is constant, without favoring 3D island formation until completion of the first monolayer (30 min). For coverages higher than one monolayer is difficult to correlate TOF-DRS information with the growing evolution, in this case the STM image of 120 min (about 3 to 4 ML) shows a 3D island formation [2].
The desorption process of a EP-PTCDI multilayer grown on Ag is followed by TOF-DRS on the left panel of Fig.2, where a collection of spectra as a function of the substrate temperature are grouped with their intensities represented by a color palette (the blue is the higher, the black is zero). The desorption experiment shows that the film is stable up to 150 °C where a rapid desorption of the multilayer takes place. Beyond 170 °C the N and O signals rapidly decrease while the H intensity reduces slowly with a less decreasing of the C amount, suggesting a decomposition of the EP-PTDCI molecule. Finally, at about 400 °C the TOF-DRS results, together with the STM image shown on the right side of Fig.2, indicate the dissociation of the EP-PTCDI molecule leaving a well ordered monolayer of the perylene core [2].

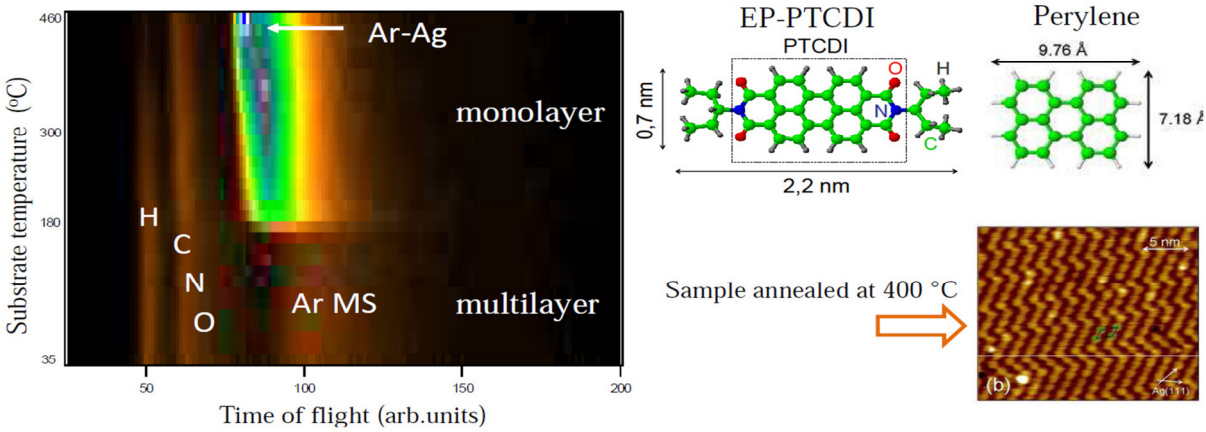

Figure 2: Desorption and dissociation of EP-PTCDI molecules.

The second example is the study of the adsoption of BDMT on Au(111) performed by dosing the molecules with a leak valve connected to the ultra high vacuum chamber. The spectra taken at different incidence angles and the intensities of the peaks as a function of the gas exposure are presented in Fig. 3. At grazing incidence angles the technique is more sensitive to top surface atoms, while at 20^{o} the heavy ions can penetrate the layer providing information also on the atoms lying below the top ones.

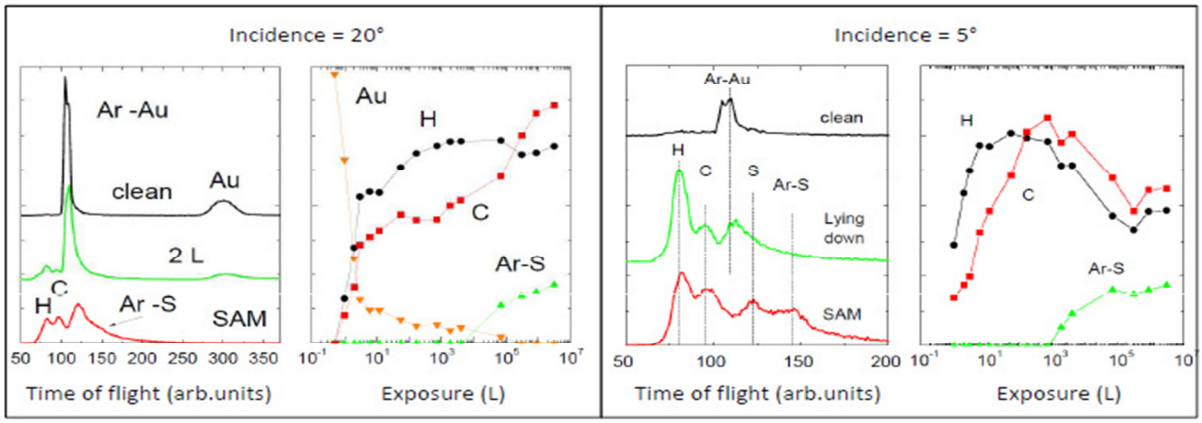

Figure 3: BDMT adsorption on Au(111).

One can distinguish two adsorption regimes. The first one that is characterized by a fast uptake of the molecules without showing S atoms, but with an important contribution of Ar atoms scattered from the substrate. The second one is characterized by the appearance of S atoms mainly on top of the layer (well seen at 5° incidence), with less signal of Ar atoms scattered off the substrate, and changes in the relative intensities of H and C atoms. These trends show that a lying down phase with both S atoms bonded to the surface is formed at low exposures, which precedes the standing up SAM phase where one sulphur atoms is bonded to the surface, while the other one is at the film vacuum interface [3,4].

To get information about the thickness of the SAM we simulated the multiple scattering events with SRIM 2006 code. On the left panels of Fig.4 the comparison of the calculation with the experimental results indicates that the SAM is formed by one single molecular standing up monolayer. A multilayer was observed for film depositions at lower temperatures (-20°C), as seen in the right panel of Fig. 4.

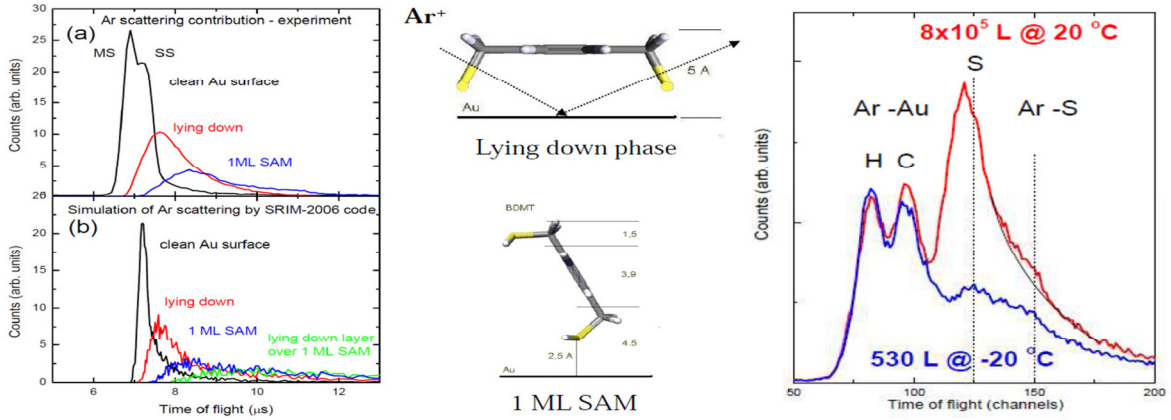

Figure 4: Calculation of the scattering contribution for different molecular configurations; and TOF-DRS spectra taken at two surface temperatures.

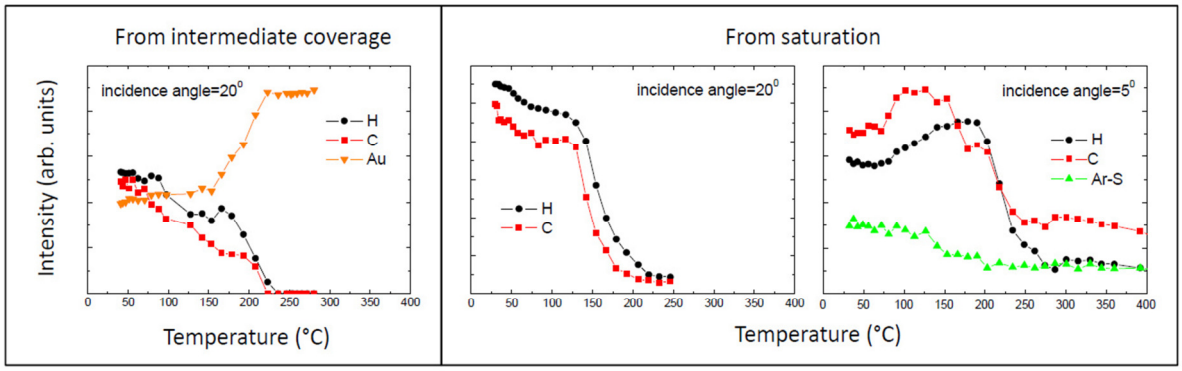

Figure 5: TOF-DRS intensities for desorption of BDMT molecules from intermediate and saturate coverages.

With respect to the thermal stability of the films, the trends presented in Fig. 5 show that these layers are stable up to near 80 °C where a transition takes place that removes the S atoms from the top of the layer, most probably implying a standing up to lying down transition. The remaining layer starts to desorb around 150°C. No molecule products remain on the surface if the desorption started from an intermediate or lying down phase, whereas some constituents where observed after SAM desorption.

Acknowledgments: We acknowledge financial support from: MINCyT (pict 06-715 & PAE (22708), PAE(22771)), CONICET (PIP 112-200801 - 00958), UNC (06/C323 and 06/C317), and the Laboratorio Internacional Franco-Argentino de Nanociencia (LIFAN).

References

[1] L.M. Rodríguez, J.E. Gayone, E.A. Sánchez, O. Grizzi, B. Blum, R.C. Salvarezza, L. Xi, and W.M. Lau, J.Am. Chem. Soc. 129(25) (2007) pp 7807-7813.

[2] L.N. Serkovic Loli, J.E. Gayone, M.L. Martiarena, E.A. Sánchez, O. Grizzi, L. Pasquali, B. Doyle, S. Nannarone, H. Hamoudi, C. Dablemont and V.A. Esaulov, J. Phys. Chem. C 113 (2009) pp17866-17875.

[3] L. Pasquali, F. Terzi, R. Seeber, S. Nannarone, D. Datta, C. Dablemont, H. Hamoudi, M. Canepa, and V.A. Esaulov, Langmuir *27* (8) (2011) pp 4713-4720.

[4] L. Salazar Alarcón,† L. Chen, V.A. Esaulov, J.E. Gayone, E.A. Sánchez, and O. Grizzi, J. Phys. Chem. 114 (2010) pp 19993–19999.

O18 Depth Resolution in SIMS Depth Profiling with Oxygen Primary Ions

T. Itani, K. Yamazaki, Y. Kataoka

itani@jp.fujitsu.com (corresponding author)

Fujitsu Laboratories Ltd., 10-1 Morinosato-Wakamiya, Atsugi 243-197, Japan

1. Introduction

Oxygen bombardment is a technique for introducing the oxygen into the target surface and converting the surface to an oxide. The bombardment technique is routinely used for depth profiling in Secondary Ion Mass Spectrometry (SIMS). The formation of an oxide layer at the bombarded surface causes high yields of positive secondary ions and provides low detection limits for most trace elements in the parts per billion range. However, the surface oxidation of the sputter eroded sample leads to a degradation of depth resolution and a number of artifacts in measured depth profiles[1-4]. Significant improvement in the situation was expected by the use of bombardment energies below 1 keV. The bombardment in the region of low and ultra-low energies, however, complicates the phenomena even further. The structure of the altered surface, i.e., the thickness of the oxide layer and the structure immediately below the oxide layer, are highly sensitive factors in understanding these effects. In this study, six boron delta layers with interlayer spacings of 5 nm were grown by Molecular Beam Epitaxy (MBE) on Si (100) and the relationship between depth resolution and oxygen bombardment conditions was examined. Furthermore, silicon oxide layers were formed on Si (100) by O_2^+ bombardment at ultra-low energies (250 eV–1 keV), and the dependence of silicon oxide thickness and the interface structure on bombardment parameters was investigated using High-resolution Rutherford Backscattering Spectrometry (HRBS). The aim of this study was to explore the structure of Si surface altered by ultra-low energy oxygen bombardment in more detail and to achieve improved understanding in SIMS depth profiling with oxygen bombardment.

2. Experiment

SIMS depth profiling of the boron delta layers and the oxygen bombardment on the Si (100) were performed using two commercial SIMS instruments, ATOMIKA 4500 and Cameca 4550, equipped with floating low-energy ion guns. For the depth profiling of the boron delta layers, the O_2^+ ions were used at 150 eV–1.25 keV and over a wide range of impact angles, from normal (0°) to glancing incidence (70°). Boron was detected as $^{11}B^+$, and $^{30}Si^+$ and $^{44}SiO^+$ served as a matrix reference species. For the oxide layer formation, the O_2^+ bombardment was performed at 250 eV–1 keV and 0°–40°. The $^{30}Si^+$ and $^{16}O^+$ signals from the bombarded surface were monitored during the bombardment. The bombardment was stopped after the signals reached at a stationary state. In each case, the oxygen dose was high enough to form a continuous SiO_2 layer, i.e., above a dose of 5×10^{17} O_2^+ atoms/cm^2. The beam currents were 5 nA (at 1.25 keV) to 40 nA (at 150 eV). The raster scan area in the (x_0,y_0) plane normal to the beam axis was 300 μm × 300 μm for the depth profiling and 1000 μm × 1000 μm for the oxide layer formation. The HRBS system used, HRBS 500, can obtain depth profiles with a depth resolution of a few tenths of a nanometer. In the instrument, ions scattered from the specimen are energy-analyzed by a magnetic spectrometer and detected by
a micro channel-plate position-sensitive detector (MCP-PSD) placed at the focal plane of the spectrometer. This allows the measurement of the energy spectrum without sweeping the

magnetic field. The HRBS spectra were measured using a 300-keV He^+ beam. The [101] channeling condition (the angle of incidence θ was 45º with respect to the surface normal) was used for all the layers at a scattering angle of 57º to reduce the signals from the Si (100) substrate.

3. Results and discussion

Two examples of the SIMS depth profiles for the boron delta layers are shown in Fig. 1 for 500-eV O_2^+ bombardment at two different impact angles, 0° and 60°. At an impact angle of 0°, the $^1B^+$ profile is well defined with a constant spacing. In contrast, at an impact angle of 60°, the maximum-to-minimum ratio of the $^{11}B^+$ signals decrease with increasing O_2^+ dose. For quantifying the changes in depth resolution, a resolution constant R_c is defined as

$$R_c = \frac{I_{max} - I_{min}}{I_{max} + I_{min}}, \quad (1)$$

where I_{max} and I_{min} are the local signal maxima (peak) and minima (valleys) in the $^{11}B^+$ profile, respectively. Energy depended results for various impact angles are presented in Fig. 2. The data is related to the fifth delta layer from the surface. In Fig. 2, several aspects deserve attention. (i) R_c decreases linearly with increasing O_2^+ energy for impact angles between 0° and 30°. The plotted data for each angle are fitted by a linear regression. (ii) For an impact angle of 40°, R_c deviate from the regression line at O_2^+ energies above 500 eV. (iii) For impact angles between 50° and 70°, R_c exhibits values lower than those for 0°–30°and decreases rapidly at some O_2^+ energies. The energy at which R_c exhibits a rapid decrease shifts toward a low energy region with increasing impact angle.

The decrease of R_c, linearly for 0°–30° and rapidly for 50°–70°, is attributed to atomic mixing and surface roughing by O_2^+ bombardment. In the analysis using Atomic Force Microscopy (AFM), for an impact angle of 50°, ripple structure was observed on the O_2^+ bombarded surface at 250 eV and the wavelength of ripple was seen to be longer at 500 eV than that at 250 eV. The observed results support the conclusion that the lower value and the rapid decrease of R_c are attributed to the ripple formation. However, no structure was observed on the surface bombarded at 750 eV and 40°. The result suggests the ripple formation is not responsible for the deviation from the linear dependence for an impact angle of 40°.

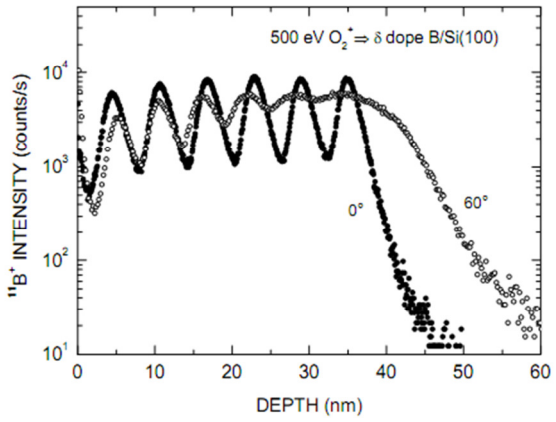

Figure 1. SIMS depth profiles of $^{11}B^+$ in boron delta layers measured by 500 eV O_2^+ bombardment at 0° and 60°.

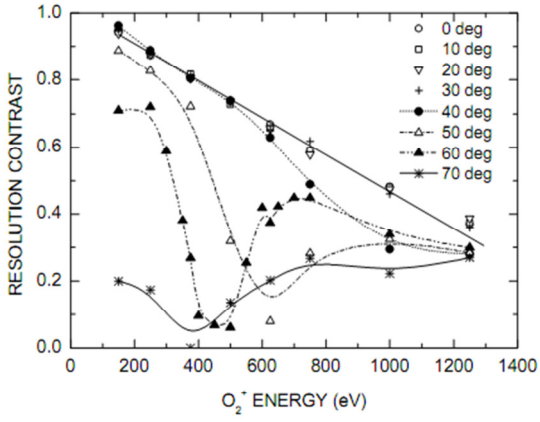

Figure 2. Resolution contrast R_c of $^{11}B^+$ profile versus O_2^+ energy for various impact angles.

HRBS analyses were performed to investigate the mechanism of the deviation for an impact angle of 40°. Two examples of the observed HRBS spectra for the Si (100),

bombarded at 750 eV O_2^+, are shown in Fig. 3 (at 0° and 40°). Both spectra clearly show the formation of surface oxide layers. The thickness of the oxide layer depends on O_2^+ bombardment conditions, i.e., bombardment energy and impact angle. From the simulation using Yang's empirical formulae for energy loss straggling, the thickness of the oxide layers is determined to be 5.5 and 3.6 nm at 0° and 40°, respectively. The areal densities of silicon and oxygen were calculated from the HRBS spectra for different thicknesses of SiO_2 layer formed under various conditions of O_2^+ bombardment and dry oxidation. The areal density of oxygen is plotted versus the areal density of silicon for both O_2^+ bombardment and dry oxidation in Fig. 4. The value of oxygen areal density is proportional to the thickness of SiO_2 layer. The dotted line represents the relation expected for an ideal interface composed of perfect Si single crystal and stoichiometric SiO_2. The data sets except for 750 eV can be fitted with a straight line of the same slope as stoichiometric SiO_2. The intercept on the vertical axis suggests the possibility of excess Si, i.e., disordered Si, in the interface region between Si single crystal and the SiO_2 layer, although the data include the effect of the surface peaks. The amount of excess Si increases with increasing O_2^+ energy and the variation shows linear increase. At an O_2^+ energy of 750 eV, the data for 0°–30° are plotted close to the line of stoichiometric SiO_2 and the amount of excess Si would be constant. For only 40°, the amount of excess Si is larger than that for other impact angles. A closer look at of Figs. 2 and 4 shows that the SiO_2 thickness is not responsible for the distortion of depth profile, but the amount of
excess Si causes the linear decrease of R_c for impact angles between 0° and 30° and the deviation for 40°.

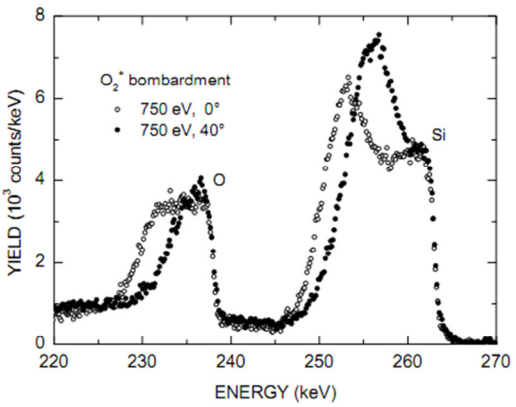

Figure 3. HRBS spectra of the oxide layer formed by 750-eV O_2^+ bombardment at 0° and 40°.

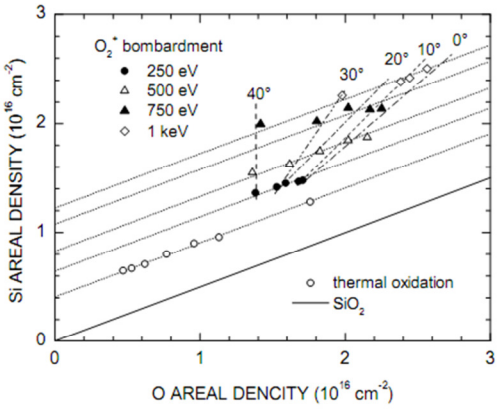

Figure 4. The areal density of oxygen is plotted versus the areal density of silicon.

4. Conclusions

The resolution contrast, R_c, was calculated from the local signal maxima (peak) and minima (valleys) in the boron profile of the boron delta layers. On the basis of the variation in R_c, the dependence of depth resolution on oxygen bombardment conditions was investigated. From HRBS measurements under a channeling condition, the thickness of the SiO_2 layer formed by oxygen bombardment and the amount of excess Si in the interface region between Si single crystal and the SiO_2 layer was determined. The results imply that variation in the SiO_2 thickness is not responsible for the distortion of depth profile but the amount of excess Si is closely correlated with depth resolution.

References.

[1] K. Wittmaack, J. Vac. Sci. technol. A8, 2246 (1990).
[2] K. Wittmaack and S. F. Corcoran, J. Vac. Sci. Technol. B16, 272 (1998) [3] Z. X. Jiang and P. F. A. Alkemade, J. Vac. Sci. technol. B16, 1971 (1998) [4] K. Wittmaack, Philos. Trans. R. Soc. London, Ser. A 354, 2761 (1996)

O19 ToF-SIMS depth profiling of nanometric Mg/Co/Zr stacks

M.-H. Hu[1], K. Le Guen[1], J.-M. André[1], S. K. Zhou[2], H. Ch. Li[2], J. T. Zhu[2], Z. S. Wang[2], A. Galtayries[3] and P. Jonnard[1]

anouk-galtayries@chimie-paristech.fr (corresponding author)

[1] *Laboratoire de Chimie Physique – Matière Rayonnement, UPMC Univ Paris 06, CNRS UMR 761, 11 rue Pierre et Marie Curie, F-75231 Paris cedex 05, France*
[2] *Institute of Precision Optical Engineering, Department of Physics, Tongji University, Shanghai 200092, P.R. China*
[3] *Laboratoire de Physico-Chimie des Surfaces, Ecole Nationale Supérieure de Chimie de Paris (Chimie ParisTech), CNRS UMR7045, 11 rue Pierre et Marie Curie, F-75231 Paris Cedex 05, France*

Nanometric Al/Mo/SiC and Mg/Zr/Co periodic multilayers, deposited through magnetron sputtering, have been studied in order to correlate their optical performances in the Extreme UV (EUV) range to their chemical and structural quality. To that purpose, we have developed an experimental methodology based on a combination of characterization techniques, including Time-of-Flight Secondary Ions Mass spectrometry (ToF-SIMS) in the depth profiling mode, having the great advantage of giving a fast chemical information on such multilayers stacks, at high depth resolution (<1 nm). First performed on the Al/Mo/SiC system [1, 2], for example $[Al(11.5\ nm)/Mo(1.3\ nm)/SiC(3.8\ nm)]_{15}$, we have obtained a new set of results with the $[Mg(13\ nm)/Co(2.5\ nm)/Zr(1.5\ nm)]_{30}$ periodic multilayered stacks. The EUV reflectivity measured at ELETTRA synchrotron facility gives evidence that Mg/Co/Zr stacks, with different elemental permutations, possess high optical reflectivity (> 40.0%). To optimize the multilayer order in the system, the Mg/Co, Mg/Zr/Co, Mg/Co/Zr and Mg/Zr/Co/Zr periodic layered samples have been prepared and characterized.

The depth profiles are obtained using a dual beam of Cs^+ (1 keV) sputtering ions and Bi^+ (25 keV) primary ions. The Co^- depth profiles of Mg/Co and Mg/Co/Zr multilayers present a symmetrical shape, corresponding to sharp interfaces, without intermixing at the Zr-on-Co interface. The comparison with Mg^+ depth profiles of the Mg/Zr/Co sample confirms this result. However, in the case of the Mg/Zr/Co and Mg/Zr/Co/Zr samples, the Co^- depth profiles present an asymmetrical shape, characteristic of a chemical modification at the interface.

Nuclear Magnetic Resonance (NMR) additional measurements have nicely completed the information brought by the ToF-SIMS depth profiles, confirming the absence of interfacial compound between Co Mg or Zr in Mg/Co and Mg/Co/Zr multilayers, and also proving that Co atoms have lost their metallic character in Mg/Zr/Co and Mg/Zr/Co/Zr, due to the interaction with the Zr layers. X-ray Emission Spectroscopy (XES) results have shown that the Mg atoms remain in the metallic state in Mg/Co/Zr and Mg/Zr/Co/Zr multilayers.

From these results, we have been able to justify the best the reflectivity value of about ~ 50.0% obtained with the Mg/Co/Zr system [3].

References.

[1] Nanometer designed Al/SiC periodic multilayers: characterization by a multitechnique approach, A. Galtayries, M.-H. Hu, K. Le Guen, J.-M. André, P. Jonnard, E. Meltchakov, C. Hecquet, F. Delmotte, Surf. & Interface Anal., 42, 997, (2010).

[2] Optical, depth and surface characterization of Al/Mo/SiC periodic multilayers,M.-H. Hu, K. Le Guen, J.-M. André, P. Jonnard, E. Meltchakov, F. Delmotte, A. Galtayries, Optics Express, 18, numéro 19, 10 pages, (2010).

[3] Introduction of Zr in nanometric periodic Mg/Co multilayers, K. Le Guen, M.-H. Hu, J.-M. André, P. Jonnard, S. K. Zhou, H. Ch. Li, J. T. Zhu, Z. S. Wang, N. Mahne, A. Giglia, S. Nannarone, Appl. Phys. A 102, 69 (2011).

I 10. Using MEIS to probe segregation effects in bimetallic nanoparticles

C J Baddeley[1], J Gustafson[1]*, A R Haire[1], A G Trant[1], T E Jones[1], A Murdoch[1], T C Q Noakes[2], P Bailey[2]

[1]EaStCHEM School of Chemistry, University of St Andrews, St Andrews, Fife, KY169ST, UK

[2]MEIS facility, Daresbury Laboratory, Daresbury, Cheshire, WA4 4AD, UK

*Current address: Lund University, Division of Synchrotron Radiation Research, Sweden

The near monolayer depth resolution of medium energy ion scattering is utilized to develop probe of the depth dependent composition of bimetallic nanoparticles supported on planar oxide supports [1]. The approach fits spectra of scattered ion intensity versus ion energy at well-defined scattering angles taking into account the asymmetric line shape in such spectra and also the depth dependent loss processes encountered as incident ions travel through the bimetallic particles.

This methodology is used to establish the depth dependent composition of Au/Pd nanoparticles grown on thin silica films on Si(100) as functions of Au/Pd composition, total metal loading and annealing temperature [2]. We show that, despite the fact that Au is deposited prior to Pd, the surface of the particles is generally enriched in Au compared to the bulk composition. The extent of this Au enrichment decreases with annealing temperature. This bimetallic system was selected as a model of oxide supported Au/Pd catalysts employed in the industrial synthesis of vinyl acetate monomer from acetic acid and ethylene. We examine the influence of the adsorption of acetic acid on the surface composition of Au/Pd particles grown on thin alumina films on NiAl(110). We find that acetic acid causes limited segregation of Pd to the bimetallic surface of relatively Au-rich particles. We compare our findings with analogous measurements acquired on single crystal AuPd surfaces [3].

References

[1] J. Gustafson, A.R. Haire, C.J. Baddeley, Surface Science **605** (2011) 220.

[2] A.R. Haire, J. Gustafson, A.G. Trant, T.E. Jones, T.C.Q. Noakes, P. Bailey, C.J. Baddeley, Surface Science **605** (2011) 214.

[3] T.G. Owens, T.E. Jones, T.C.Q. Noakes, P. Bailey, C.J. Baddeley, Journal of Physical Chemistry B **110** (2006) 21152.

O20 Nanostructures characterization using the MEIS technique.

M. A. Sortica[1], P. L. Grande[1], C. Radtke[2]

mau_ufrgs@yahoo.com.br

[1] *Institute of Physics, Universidade Federal do Rio Grande do Sul, Brazil*
[2] *Institute of Chemistry, Universidade Federal do Rio Grande do Sul, Brazil*

Medium energy ion scattering (MEIS) is a powerful tool for nanostructures characterization [1] and is a unique technique for depth profiling inside of nanostructures with size smaller than 5 nm [2]. For that reason, we developed a Monte Carlo simulation software (PowerMeis) that considers the geometry, size distribution, and density of nanostructures [3]. The software also considers the asymmetry of the energy-loss distribution [4].

We used our method to characterize several systems of nanoparticles near the surface in order to get the best depth resolution of the MEIS technique. Here we show two systems: gold nanoparticles adsorbed in a polyelectrolyte multilayer film (PEM) and core-shell characterization of CdSe/ZnS quantum dots.

The first system consists in a multilayered film, built by the deposition of 20 layer-by-layers (LbL) of poly(allylamine hydrochloride) (PAH) and poly(acrylic acid) (PAA), as shown in Figure 1-(a). This deposition is made by electrostatic interaction between the polycations PAH and the polyanions PAA. The film is immersed in a colloidal solution of gold nanoparticles stabilized by the citrate method (Figure 1-(b)). Depending of the pH value in both colloidal gold solution and PEM films, different morphological structures can be obtained from monolayer or bilayer of the gold nanoparticles [5]. The modeling of the interface polymer-NPs was obtained with MEIS, as shown in Figure 2. The MEIS simulation reveals features that are not observed by microscopy like, for exemple, the gold bi-layer modeling showed in Figure 2-(i) reveals that one of the gold layers are totally immersed in the PEM film. Mreover, changing the configuration of the arrangement of nanoparticles on the surface can also significantly affect the optical preoperties of the matrix. For this kind of of layer-by-layer system the combination of optical multi-layer films and plasmonic structures allows the design of specific optical responses in photonic devices [6].

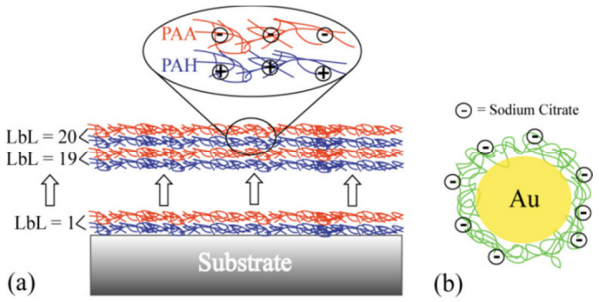

Figure 1: (a) Schematic of the synthesis of the 20 layers of LbL using PAH/PAA. (b) Schematic configuration of a gold nanoparticle stabilized with citrate.

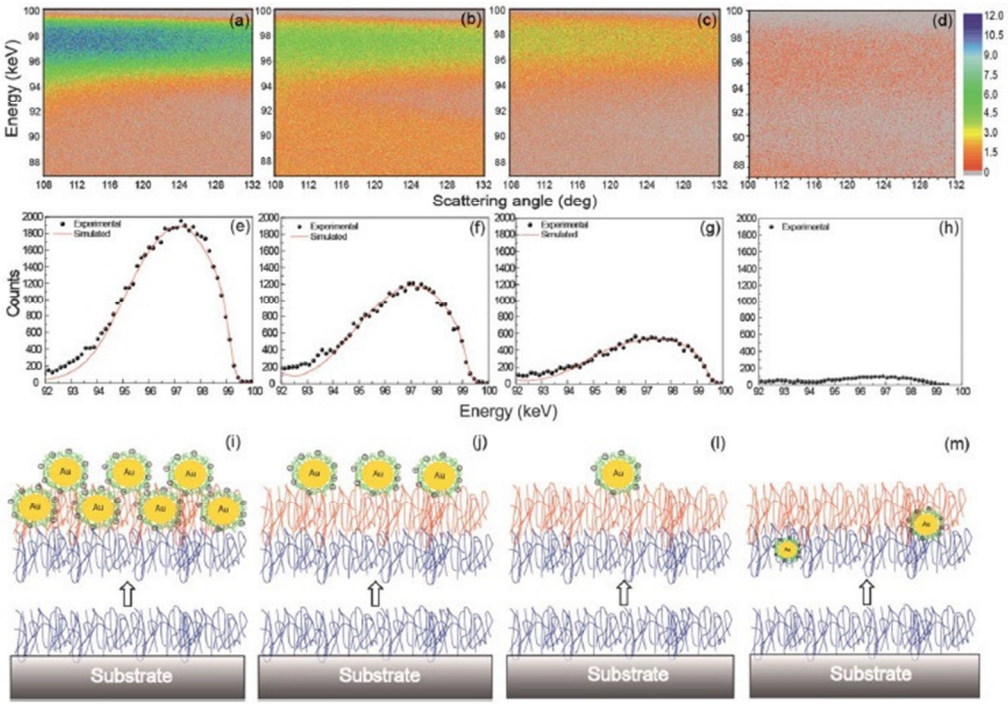

Figure 2: MEIS spectra of the gold nanoparticles on the film surface, with the fitting at 120 degrees of scattering angle.

The second system consists of the commercial core-shell EviDots – Maple Red-orange quantum dots, from Evident. We are studying the core-shell characteristics of this system, such as the size and composition of the core and the shell parts, through MEIS simulation, as shown in Figure 4. First we dilute the QDs solution in toluene, in order to control the concentration of the QDs and then we spread a drop of the solution on a silicon oxide surface and wait until the toluene dries. We obtain a surface like the one shown in the Figure 3. That sample is then analyzed by MEIS.

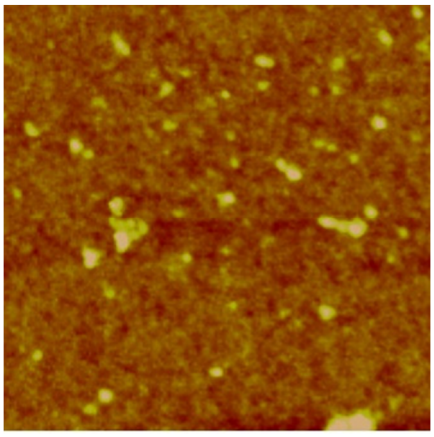

Figure 3: QDs on silicon oxide surface.

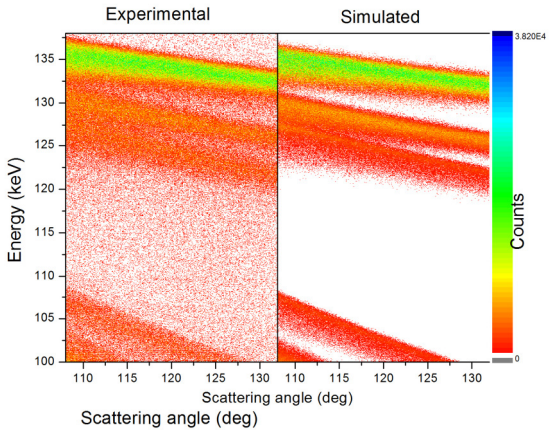

Figure 4: Meis spectrum fitting of CdSe/ZnS QDs.

At the present, we can show that de CdSe nucleus is composed by Cd_6Se_4 and the shell thickness is about 0.5 nm.

References.

[1] Determination of the number and size of inhomogeneities in thin films by ion beam analysis, J. P. Stoquert,T. Szörenyi, Phys. Rev B 66 (2002) 144108.

[2] Au(core)/Pd(Shell) structures analyzed by high-resolution medium energy ion scattering, H. Matsumoto, K.Mitsuhara, A. Visikovskiy, T. Akita, N. Toshima, Y. Kido, Nucl. Instr. and Meth. in Phys. Res. B, (2010) DOI 10.1016/j.nimb.2010.03.032 .

[3] Characterization of nanoparticles through medium-energy ion scattering, M. A. Sortica, P. L. Grande, G. achado, L. Miotti, Journal of Applied Physics 106 (2009) 114320.

[4] An analytical energy-loss line shape for high depth resolution in ion-beam analysis, P. L. Grande, A. Hentz, R. P. Pezzi, I. J. R. Baumvol, G. Schiwietz, Nucl. Instr. and Meth. In Phys. Res. B 256 (2007) 92-96.

[5] Structural control of gold nanoparticles self-assemblies by layer-by-layer process, G. Machado, A. F. Feil, P. Migowski, L. Rossi, M. Giovanela, J. S. Crespo, L. Miotti, M. A. Sortica, P . L. Grande, M. B. Pereira, R. R. B Correia, Nanoscale, 3 (2011), 1717.

[6] O. Soltwedel, O. Ivanova, M. Höhne, M. Gopinadhan, C. A. Helm, Langmuir, 26 (2010), 15219-15228.

O21 Structural characterization of buried nanostructured materials through Medium Energy Ion Scattering technique

D. F. Sanchez[1], F. P. Luce[1], M. A. Sortica[1], C. Marin[1], J. Leveneur[2], Z. E. Fabrim[1], F. Kremer[1], P. F. P. Fichtner[1], P. L. Grande[1], J. Kennedy[2], G. Kellermann[3]

dario@if.ufrgs.br (corresponding author)

[1] *Instituto de Física, Universidade Federal do Rio Grande do Sul, Porto Alegre – Brazil*
[3] *National Isotope Centre, GNS Science, Lower Hutt - New Zealand*
[4] *Departamento de Física, Universidade Federal do Paraná, Curitiba - Brazil*

Medium energy ion scattering (MEIS) is an ion beam characterization technique capable to determine with subnanometric depth resolution elemental composition and concentration–depth profiles in thin films. MEIS measurements were recently used as an additional tool for the characterization of shape, composition, size distribution and stoichiometry from surface located Pt–Rh [1] and Au [2] nanoparticle systems, as well as of InAs–GaAs quantum dots [3]. Other promising MEIS applications are the determination of depth distributions of different elements in a single nanoparticle [4]. We have developed a Monte Carlo simulation and fitting software, the PowerMeis [5], that considers any geometry, size distribution, composition and density of the nanostructures and also the asymmetry of the energy loss-distribution.

We have explored the MEIS characterization potentiality to investigate a buried 2-dimensional NP system. Its synthesis has attracted interest in connection e.g. with plasmonic [6–8] or magnetic [9–11] applications. For both, the NP system properties are strongly dependent on size, shape, number density and spatial order of the NP set.

We use a condensed arrangement of Pb NPs located under a silica layer as a model case system [12]. The samples were synthesized by Pb^+ ion implantation into a 200 nm thick silica film over a Si (001) substrate. The implantation energy of 300 keV was selected in order to place the implanted ions in the central region of the film. The Pb ions are implanted to a fluence of $\Phi_1 = 0.5\times10^{16}$ atoms/cm^2 and $\Phi_2 = 1.0\times10^{16}$ atoms/cm^2, and submitted to a combination of a two-step annealing: (i) a low temperature long time aging treatment performed at 200 ºC for 100 h in open atmosphere, and (ii) a high vacuum furnace annealing (FA) for 1 h at 1100 ºC. RBS measurements and TEM observations from aged and FA samples show the formation of a dense Pb NP system exclusively at the interface, while the silica film recovers its pristine aspect [13,14]. The shape of the interface located NPs from aged and FA samples were characterized by plan-view and cross-section TEM observations, which show that the NPs have a nearly hemispherical shape in the SiO_2 side and a pyramidal frustum shape in the Si matrix. Moreover, the pyramidal frustum facets are parallel to the (001) Si plane. For the Φ_2 sample, the symmetry expected for this structure is confirmed by GISAXS measurements performed at different azimuthal angles. Complementary microstructural information comprising shape, mean size and number density of NPs were determined through analysis of the MEIS spectra. To avoid effects such as energy-loss straggling and multiple scattering in the MEIS analysis, part of the SiO_2 layer was removed by chemical etching with HF solution. Through the 2D MEIS spectra (energy and angle), we have studied the nanostructure geometry, number density and mean NP size of such systems, and compared to TEM measurements.

In order to investigate the geometrical shape of the NPs for the Φ_1 sample, the system was modeled in two different ways: i) as a hemisphere in the SiO_2 side on a pyramidal frustum in the Si matrix side (further referred as PF) and ii) as a sphere, half in the SiO_2 and half in the Si matrix.

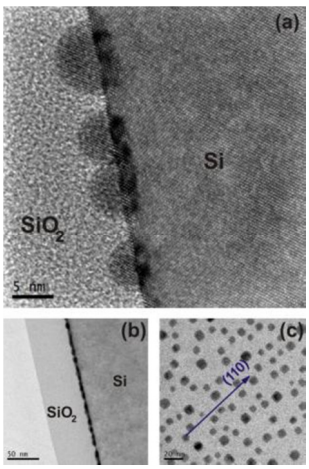

(1)

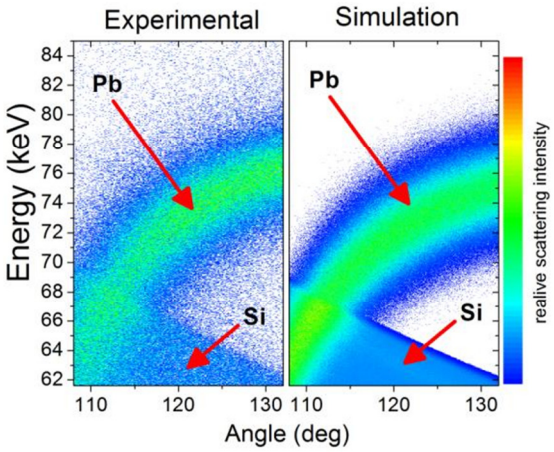

(2)

Fig. 1. *(1-a) HRTEM micrograph from a [011] oriented sample presenting a cross-section view of the NPs partially embedded in the Si matrix; (1-b) Bright-field two-beam image, underfocus, demonstrating that the NPs are exclusively located at the SiO2/Si (100) interface. (c) Plan-view image (bright field, in focus) close to the (001) zone axis, showing square based NPs preferentially aligned parallel to the (011) planes of the matrix. (2) Experimental and simulated 2D MEIS spectra. Figures extracted from Ref. [12].*

Simulations were performed with different densities for both geometrical models, constrained to the same amount of Pb per area, namely $(Nt)_{Pb,MEIS} = 2.26\times10^{15}$ atoms×cm^{-2}, value obtained by the MEIS and RBS measurements. The number density obtained for the PF shape is $(4.2\pm1.6)\times10^{11}$ cm^{-2}, and, $(5.3\pm1.7)\times10^{11}$ cm^{-2} considering the spherical shape. These values of densities correspond to the values of radii of (3.7±0.5) nm for PF shape and (3.2±0.4) nm for spherical shape. The result for PF shape agrees better to the value obtained by TEM, namely radius of (4±1) nm and number density of 3.7×10^{11} cm^{-2}. HRTEM images show that the PF shape is in better agreement.

For the sample Φ_2, the MEIS measurements are compared to GISAXS and also to TEM observations from plan-view and cross-section type samples. GISAXS results provided information about the NPs shape and their pair correlation function. The TEM images show NPs having a nearly hemispherical shape in the SiO_2 side and a pyramidal frustum shape in the Si matrix. Moreover, the pyramidal frustum facets are parallel to the (001) Si plane. The symmetry expected for this structure is confirmed by GISAXS measurements performed at different azimuthal angles of X-rays beam incidence. The results show that the Pb NPs from the Φ_2 sample are larger than the ones from the Φ_1 sample.

The results obtained here show how the MEIS information strongly depends on the overlayer thickness. They also show that, for silica overlayers thinner than ≈ 50 nm MEIS can be used as a valuable non destructive technique providing a combination of micro-structural and elemental characterization.

Other buried NPs system namely Au NPs in SiO_2 was also investigated. The Au NPs were synthesized by sputtering deposition, where Au atoms were deposited with, 1.8×10^{15}, 3.1×10^{15} and 7.4×10^{15} Au/cm^2, over a 200 nm thick silica film over a Si (001) substrate and followed by a deposition of 38 nm thick of SiO_2. The mean size and number density of two dimensional set of Au were characterized through MEIS and TEM.

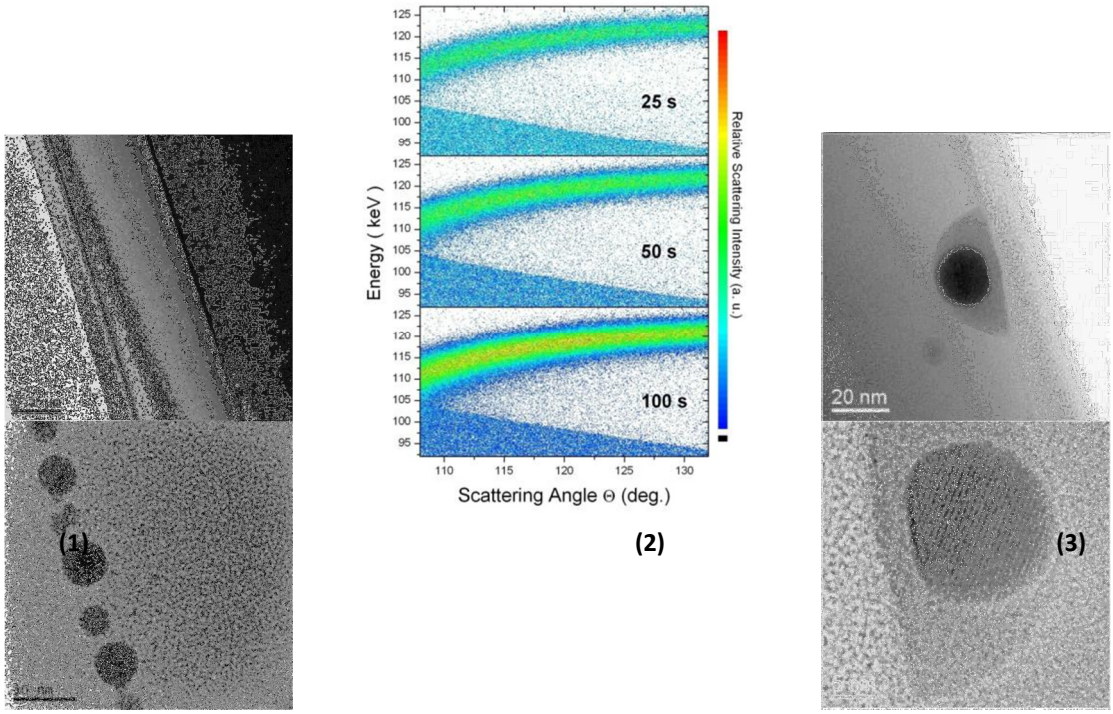

Fig. 1. (1-a) TEM micrograph of Au NPs deposited by sputtering deposition with 7.4×10^{15} *Au/cm*^{2}*, (2) MEIS spectra of Au deposited for a time of 25, 50 and 100 seconds, which corresponds to the three conditions of deposition and (3) core/shell NPs near the surface synthesized by Fe low energy implantation [15], with a core of metallic iron and the core composed by iron, silicon and oxygen.*

Finally we also show first MEIS results of a two dimensional set of core/shell NPs synthesized by low energy Fe^+ implantation followed by electron beam annealing [15]. The composition of the core and the shell were studied through TEM, XPS, XANES and EELS analysis, which revealed that the composition of the core is Fe bbc crystalline phase but does not allowed to reveal clearly the composition of the shell. These techniques in connection with MEIS results allow for the full determination of the NP shell (composition, stoichiometry and density).

Here we have shown the capability of MEIS analysis to characterize buried NPs, which opens new perspectives for nanostructure analysis in situ that can be of great interest.

References

[1] I. Konomi, S. Hyodo, T. Motohiro, J. Catal. 192 (2000) 11.
[2] T. Okazawa, M. Kohyama, Y. Kido, Surf. Sci. 600 (2006) 4430.
[3] P.D. Quinn, N.R. Wilson, S.A. Hatfield, C.F. McConville, G.R. Bell, T.C.Q. Noakes, P. Bailey, S. Al-Harthi, F. Gard, Appl. Phys. Lett. 87 (2005) 153110.
[4] H. Matsumoto, K. Mitsuhara, A. Visikovskiy, T. Akita, N. Toshima, Y. Kido, Nucl. Instrum. Methods Phys. Res. Sect. B 268 (2010) 2281.
[5] M. A. Sortica, P. L. Grande, G. Machado, L. Miotti, Journal of Applied Physics (2009) 106, 114320. [6] Harry A. Atwater, Albert Polman, Nat. Mater. 9 (2010) 205.
[7] G. Xu, M. Tazawa, P. Jin, S. Nakao, K. Yoshimura, Appl. Phys. Lett. 82 (2003) 3811. [8] A.P. Alivisatos, science 271 (1996) 933.
[9] P.R. Krauss, S.Y. Chou, Appl. Phys. Lett. 71 (1997) 3174.
[10] J. Moritz, L. Buda, B. Dieny, J.P. Nozieres, R.J.M. van de Veerdonk, T.M. Crawford, D. Weller, Appl. Phys. Lett. 84 (2004) 1519.
[11] R.P. Cowburn, J. Appl. Phys. 93 (2003) 9310.
[12] D.F. Sanchez, F.P. Luce, Z.E. Fabrim, M.A. Sortica, P.F.P. Fichtner, P.L. Grande, Surface Science 605 (2011) 654–658.
[13] F.P. Luce, F. Kremer, S. Reboh, Z.E. Fabrim, D.F. Sanchez, F.C. Zawislak, P.F.P. Fichtner, J. Appl. Phys. 109 (2011) 014320.
[14] F. P. Luce, F. Kremer, D. F. Sanchez, Z. E. Fabrim, S. Reboh, F. C. Zawislak, P. F. P. Fichtner, Mater. Res. Soc. Symp. Vol. 1308 (2011).
[15] J. Kennedy, J. Leveneur, G. V. M. Williams, D. R. G. Mitchell, A. Markwitz, Nanotechnology 22 (2011) 115602.

I 11. Improvement of sensitivity in high-resolution RBS by reducing detector noise

H. Hashimoto[1], K. Nakajima[1], M. Suzuki[1], K. Sasakawa[1, 2], K. Kimura[1]

kimura@kues.kyoto-u.ac.jp

[1] *Department of Micro Engineering, Kyoto University, Kyoto 606-8501, Japan*
[2] *Kobelco Research Institute, Inc., Takatsukadai 1-5-5, Nishi-ku, Kobe 651-2271, Japan*

High-resolution Rutherford backscattering spectroscopy (HRBS) is a powerful surface analysis technique. It allows quantitative and non-destructive depth profiling of constituent elements with sub-nm depth resolution within a reasonably short measurement time (typically 10 - 20 min.) without any special pre-treatment of the sample. There are, of course, some drawbacks in HRBS. The main drawback is its relatively low elemental concentration sensitivity compared to e.g., secondary ion mass spectrometry (SIMS). The typical sensitivity of HRBS is 100 – 10000 ppm, which is not good enough for some applications. For example, sensitivity better than 10 ppm is required to measure the junction depth in electronic devices. The main factor which influences the ultimate sensitivity of HRBS is the background noise in the energy spectrum. There are two major origins of the background noise. One is stray ions scattered from the inner wall of the spectrometer and the other is the dark noise of the micro channel plate (MCP) used in the focal plane detector of the spectrometer. These noises should be reduced for improvment of the sensitivity. In this presentation, we report improvement of the spectrometer to reduce the background noise. In order to reject the stray ions, several barriers are installed inside the vacuum chamber of the spectrometer and a thin Mylar foil is mounted in front of the detector. The dark noise of the MCP detector is rejected by the coincidence measurement with the secondary electrons emitted from the Mylar foil upon the ion passage. After these improvements, the background noise is reduced by factor 200. The detection limit is improved down to 10 ppm for As in Si at a measurement time of one hour.

O22 A UHV-compatible, demountable heat transfer system.

Paul Bailey, David Teehan, Tim Noakes

p.bailey@dl.ac.uk (corresponding author)

Daresbury Laboratory, Daresbury, Warrington, WA4 4AD, UK

A system is described whereby a good thermal connection may be readily made and unmade to a thermally isolated component (e.g. a sample plate) in vacuum or other extreme environment without disturbing that environment. The design is highly versatile and is compatible with many existing systems. It is particularly suited to cooling samples transferred under vacuum by the attachment of a cold finger. The system requires only the addition of a single mechanical rotary/ linear drive combination, a liquid nitrogen vessel and a modified sample plate.

Since the rms thermal vibration is proportional to the square root of the absolute temperature, a lower sample temperature produces a more static lattice in a single crystal. This can be crucial in certain MEIS experiments [1] where important processes are activated around room temperature.

The system was designed for cooling samples mounted on the HVEE sample transfer holder but could be used with many other items of equipment. The system enables the effective attachment of a cooling system to a sample holder which can be free to be removed from the vacuum system and can rotate in three axes. A typical lower figure of 130 K can be quickly reached. The cooling system does not compromise heating the sample.

A novel solution has been achieved, its operation is shown in video and its performance is described.

References

[1] T. C. Q. Noakes, P. Bailey, and G. van der Laan, Phys. Rev. B, 67, 153401 (2003)

O23 Development of imaging TOF- MEIS and Applications

DaeWon Moon

Korea Research Institute of Standards and Science, Doryong-dong 1, Yusung, Daejeon, Korea 305-600

Medium Energy Ion Scattering Spectroscopy (MEIS) has been successfully applied for compositional and structural depth profiling of nm thick ultrathin films, especially for nm gate dielectrics such as SiOxNy and high k ultrathin films. However, conventional MEIS based on a continuous ion beam and an electrostatic energy analyzer with a broad ion beam is not capable of imaging or point analysis either. Therefore, its applications are limited to uniform ultrathin film analysis Most of surface and nano analysis require spatial resolution for practical applications such as patterned wafer analysis and local analysis of inhomogeneous specimen.

A time-of-flight nano medium energy ion scattering (TOF-nano MEIS) was developed using a pulsed focused ion beam and a TOF delay line detector (DLD) of a large area. Using a bright rf ion source generating proton, He, and Ne of 70~100 keV and a deflector for ion beam pulsing, micro meter level spatial resolution and MEIS energy resolution of 5x10-3 were obtained. Scattered ions are collected by a DLD with a diameter of 120 mm to maximize the collection efficiency. The DLD gives the two dimensional spatial information and flight time of scattered protons, which can provide elemental composition and geometrical structure information simultaneously. nm HfO2 high k thin film on Si and CdSe/ZnS quantum dots were analyzed with TOF-MEIS and compared with the results from a conventional electrostatic MEIS system.

The special feature of TOF-MEIS free from ion survival probability due to the collection of both ionic and neutral scattered ions is utilized to increase the sensitivity of MEIS by using Ne ions. Preliminary results on depth profiling of ultrashallow junctions will be presented. Further possible applications of TOF-MEIS to biomolecule analysis will be also discussed.

High-Resolution Depth Profiling

June 27th - 30th, 2011

Poster abstracts

P1 Study of Nitrogen Concentration in Ancient Sword

H.C. Santos, N. Added

hsantos@dfn.if.usp.br

Instituto de Física da Universidade de São Paulo – Departamento de Física Nuclear

The nuclear reaction analysis (NRA) has been used to determine absolute concentration of some elements as well as its depth profile. In this work, NRA technique was used to measure the concentration of nitrides in a Damascus blade, trying to explain its dependence with hardness, supplied by our collaborator researcher Diogo Emiliano. This depth profile will be obtained using the resonances in production of γ rays (4.43 MeV) for the reaction $^{15}N(p,\alpha\gamma)^{12}C$. In parallel to this work, the characterization of the Damascus blade and standard samples were done with PIXE (Particle Induced X-rays Emissions) for a future comparison with other ancient sword.

The irradiation was performed in external beam setup installed at Lamfi accelerator, from São Paulo University that uses a 2.6 MeV proton beam to probe the samples. The system of detection is composed by one NaI(Tl) scintillation detector (7% resolution in Co region) for γ rays, and one Si(Li) detector for x-rays. The acquisition system allows the simultaneous PIXE and NRA measurements. The beam charge was estimated by x- rays coming from an Au foil, placed immediately after the output window in the external beam line.

Even with the low precision obtained, it was possible to differentiate between the absolute nitrogen concentration in edge and a thick part of blade, suggesting difference in the treatment of this part.

P2 Study of Cs aggregation in metal-organic samples after ion bombardment

K.Q. Ngo[a], P. Philipp[a], Y. Jin[b], M. Shtein[b], J. Kieffer[b], T. Wirtz[a]

ngo@lippmann.lu

[a] *Department "Science and Analysis of Materials" (SAM), Centre de Recherche Public – Gabriel Lippmann, 41 rue du Brill, L-4422 Belvaux, Luxembourg*

[b] *Department of Materials Science and Engineering, University of Michigan, Ann Arbor, Michigan 48109-2136*

In secondary ion mass spectrometry, Cs^+ primary ion beams are widely used as they enhance the negative secondary ion yields and provide quantitative analyses through MCs^+ secondary ion detection. A proper interpretation of produced depth profiles and elemental mappings requires often a characterisation of the topography at the crater bottoms. In this study, Cs aggregation in craters after Cs^+ bombardment has been observed and investigated. Cs hillocks appear after exposing the Cs^+ bombarded sample to air, thus changing topography and chemical information. Artefacts in data interpretation can only be avoided when considering this phenomenon.

In the current research, the Cs aggregation is investigated at the crater bottoms for some silver-organic bi-layered samples sputtered by a 500eV Cs^+ beam in both positive and negative mode on a Cameca SC-Ultra instrument. Altogether, two different organic molecules used in organic optoelectronic devices, Tris(8-hydroxyquinolinato) aluminium (Alq_3 – $C_{27}H_{18}N_3O_3Al$) and Copper Phthalocyanine (CuPc – $C_{32}H_{16}N_8Cu$), different layer thicknesses and deposition methods are studied. The roughness both with and without limiting Cs hillocks is investigated as a function of depth and air exposure time. For this purpose, SIMS depth profiles were stopped at different depths: crater 1 at the Ag – organic interface, crater 2 at the middle of the organic layer, crater 3 at the organic – Si interface. Then, after air exposure the surface roughness is measured by AFM. Elemental mapping of the surface before and after air exposure was carried out by SIMS and AES imaging. This allows determining the hillock composition. The different samples are shown in table 1. Inorganic and organic layer have always the same thickness.

Name	Sample	Layer thickness	Depositing system	Sample substrate
A	Ag / Alq_3	30 nm	Angstrom	Room temperature
B	Ag / CuPc	30 nm	Angstrom	Room temperature
C	Ag / CuPc	13 nm	Angstrom	Cooling substrate

Table 1: List of sample and prepared details.

After few days in air, the AFM images taken at the bottom of different craters of sample B show the development of Cs hillocks. There were no Cs hillocks at the surface and in crater 1. In crater 2, the hillocks were dense with a medium grain size of about 125nm. For crater 3, the dots are bigger (to about 200nm) but less dense than in the crater 2 (Fig. 1). Those observations could be explained as follows: Cs metal is highly reactive and very pyrophoric, such that the Cs atoms implanted in the matrix tend to diffuse to the surface and to react with oxygen and moisture immediately after exposure to air. The products from the reaction tend to aggregation to dots. However, these dots can only be seen when the concentration of Cs in the matrix is high enough.

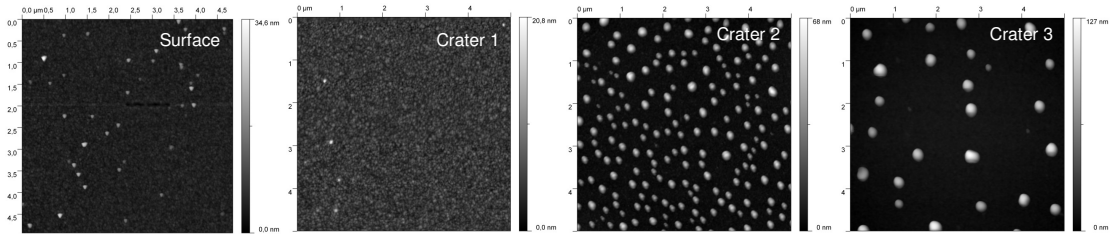

Figure. 1: AFM images (5 x 5 μm^2) at the bottom of craters of sample B, after less than 4 days exposure to air.

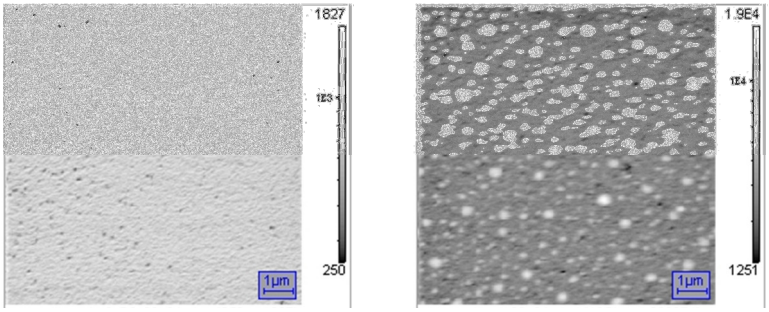

Figure. 2: Oxygen images (10 x 10 μm^2) by NanoSIMS in crater 3 of sample B, before (left image) and after (right image) exposure to air.

For the sample B, the NanoSIMS images of O element in the crater 3 show homogeneous images before exposed to air and O – dots image after exposed to air (Fig. 2). This change proves the surface change after exposing the samples to air and the reaction of Cs with O. Comparable sizes and density of hillocks are also found in the AFM image and in the AES image of Cs which proves that the hillocks are composed of Cs (Fig. 3).

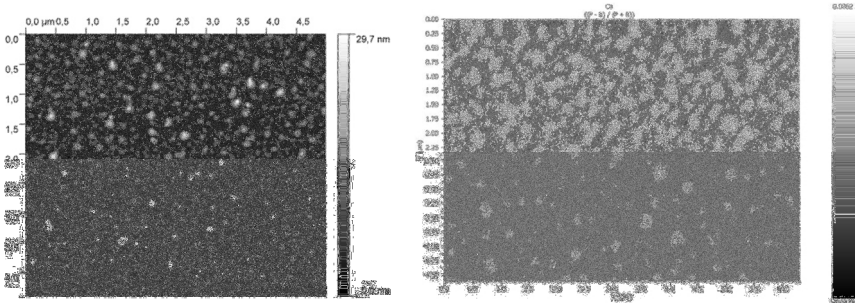

Figure. 3: Crater 2 of sample B: AFM image (5 x 5 μm^2) at the first day in air (left image) and Cs image from Auger (6.25 x 4.6 μm^2), the next day (right image).

However, the formation of Cs hillocks depends on the sample composition and preparation. Samples A and B where prepared in the same way, having the same layer thickness, but contain different organic molecules, Alq_3 or CuPc. While the AFM images of the craters in Alq_3 (sample A) do not show any well-defined Cs hillocks, those in CuPc (sample B) are dominated by such Cs dots (Fig. 4). The absence of Cs hillocks in craters of sample A has been verified for image sizes of 5 x 5 μm^2 (Fig. 4) and 20 x 20 μm^2 (image is not showed here). As Alq_3 contains oxygen atoms in its structure, those atoms could act as a Cs getter and avoid, or at least limit, the Cs diffusion to the surface and its reaction with air. The CuPc molecule contains no oxygen, so the Cs can move easily to surface and react with air.

For the same organic molecule, a few Cs dots appear in crater 2 and some small dots in crater 3 for sample C while the density of Cs hillocks increases largely for both craters of sample B (Fig. 4). The samples B and C have different thickness and were prepared by different methods (deposition at room temperature or using cooling substrate). Those differences between samples B and C could lead to different Cs concentrations in the matrix after sputtering, and explain the difference in the appearance of Cs hillocks.

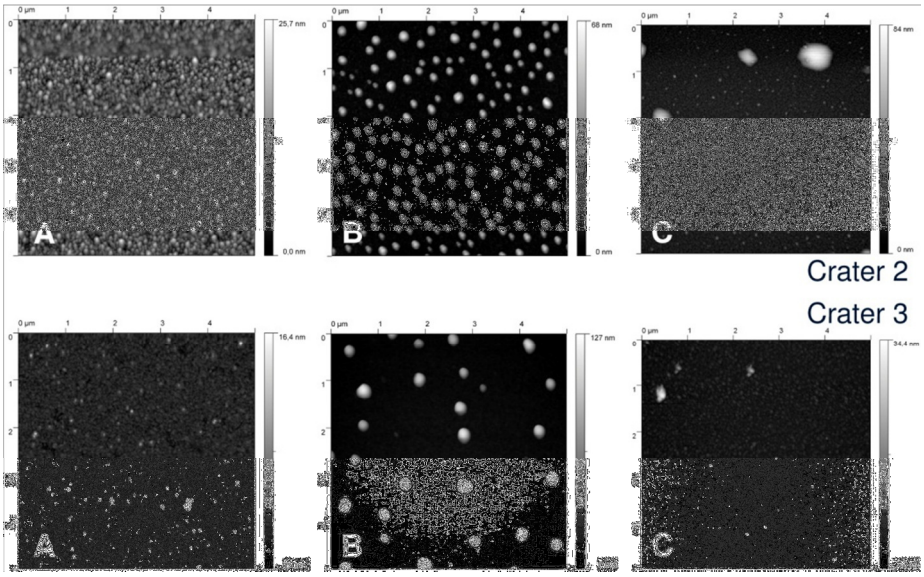

Figure. 4: AFM images 5 x 5 µm^2 of crater 2 (top) and 3 (bottom), of sample A (left), sample B (middle) and sample C (right) (after a few days in air).

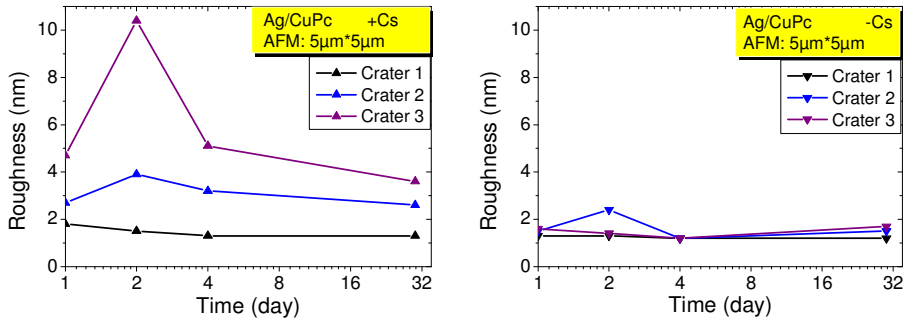

Figure. 5: Development of crater roughness as a function of days in air for sample B, including Cs hillocks (+Cs) (left) and without including Cs hillocks (-Cs) (right).

As shown in Fig. 5, the roughness in crater 1 (Ag-CuPc interface) is almost stable during the first 30 days in air. And there is no contribution of Cs hillocks to the surface roughness (RMS values for +Cs and –Cs are quite close). Otherwise, in crater 3, the roughness including Cs dots increases strongly after 2 days and then decreases afterwards to stabilise more or less after 30 days. The same tendency is seen in crater 2, but is less pronounced than in crater 3. The roughness values excluding Cs dots (-Cs) are rather stable. The –Cs roughness of crater 2 presents a maximum at the 2nd day, and can be influenced by the small Cs hillocks that could not be masked manually.

P3 Depth profiling of Mo/Si multilayers: the effect of Ar-ion energy on layer structure.

E. Zoethout[1], E. Louis[1] and F. Bijkerk[1,2]

E.Zoethout@rijnhuizen.nl (corresponding author)

[1] *FOM Institute for Plasma Physics Rijnhuizen, nanolayer- Surface and Interface Physics department, P.O. Box 1207, 3430 BE Nieuwegein, The Netherlands*
[2] *MESA+, University of Twente, P.O. Box 217, 7500 AE Enschede, The Netherlands*

Periodic molybdenum silicon multilayers can be used as reflecting optical elements for many applications including extreme ultra-violet lithography (EUVL) as a most demanding example. Key task is to develop these artificial Bragg reflectors with properties as close as possible to natural, crystal Bragg reflectors. In the EUVL application the stack of 3 to 4 nm thick layers that forms the multilayer shows a close to perfect reflectance of about 70% with a theoretical limit of 75%, indicating relative small interface thickness compared to the layer thickness. Usually Ar-ion erosion of these structures together with either X-ray Photo-electron Spectroscopy or Auger Electron Spectroscopy is used to investigate the in-depth layer composition, but the erosion process can affect the structure. Therefore, we studied the Ar erosion process in detail.
Variable ion energy was used in the range of 0.25 to 2 keV to erode a molybdenum silicon multilayer. The underlying in-depth concentration profile was reconstructed by using Hoffman's MRI approach [1] and Cumpson's estimate for attenuation lengths [2]. It is shown that the resulting in-depth profile of these multilayers is to a large extent erosion energy dependent. Furthermore, due to this erosion dependency, it is found that the less surface sensitive X-ray Photo-electron Spectroscopy provides a better estimate for the in-depth elemental concentration profile than can be obtained by Auger Electron Spectroscopy.

1. Hofmann, S., *From depth resolution to depth resolution function: refinement of the concept for delta layers, single layers and multilayers.* Surface and Interface Analysis, 1999. **27**(9): p. 825-834.
2. Cumpson, P.J. and M.P. Seah, *Elastic Scattering Corrections in AES and XPS. II. Estimating Attenuation Lengths and Conditions Required for their Valid Use in Overlayer/Substrate Experiments.* Surface and Interface Analysis, 1997. **25**(6): p. 430-446.

P4 Application of Nuclear Resonance Analysis and Narrow Resonance Profiling in understanding porous film growth on aluminium.

A. Baron-W ieche ć [1], P. Skeldon[1], G.E. Thompson[1], J.J.Ganem[2] I.C.Vickridge[2]

Aleksandrawanda.baronwiechec@manchester.ac.uk (corresponding author)

[1] *Corrosion and Protection Centre, the University o Manchester, UK*
[2] *SAFIR, Institut des Nano Sciences de Paris, Université de Pierre et Marie Curie, France*

Porous anodic oxides are of increasing interest for nanotechnological applications, such as photonic crystals, sensors and solar cells, as well as being of continuing importance for protection and functionalization of metal surfaces, eg of aluminium in the aerospace, architectural, and electronic sectors, where energy reduction and environmental compliance are critical considerations. Despite significant previous research, the understanding of porous oxide growth is still subject to much debate. Earlier work on the formation of porous anodic alumina has generally considered that pore initiation follows a first stage of enhanced film growth due to preferential oxidation at certain sites of the aluminum substrate, with the subsequent growth of the major pores being due to dissolution of the alumina accelerated greatly by the electric field. However, more recent evidence has suggested that major pore generation occurs due to flow of the anodic alumina, which is displaced under the stresses of film growth from the barrier layer at the base of the alumina film into the pore walls and electrostriction effect in the porous alumina. The present work utilizes in-depth probing of the mechanism of porous oxide growth by complementary transmission electron microscopy (TEM), scanning electron microscopy (SEM) and ion beam analysis (including nuclear resonance analysis (NRA), Rutherford backscattering spectroscopy (RBS) and narrow resonance profiling (NRP)). Key experiments have involved the use of ^{18}O as a tracer species in the study of the transport of oxygen in the growing oxide films. Since the film morphology changes significantly as the film evolves from an initial non-porous, barrier oxide to a fully porous oxide, microscopy of the oxide at the various stages of film growth is essential for the interpretation of the tracer data.

A first layer of anodic film was produced on specimens of electropolished aluminium by anodizing to 20 V at 5 mA/cm^2 in 0.4 M phosphoric acid electrolyte enriched in ^{18}O to 10%. Specimens were then further anodized to selected voltages in 0.4 M phosphoric acid electrolyte containing ^{18}O at the natural abundance. The voltage-time response was recorded during the anodizing process. The morphology and thickness of the cross-sectioned specimens were examined by TEM and SEM. The amounts of ^{18}O, ^{16}O, Al and P in films were determined by NRA, RBS, and NRP.

Morphologies of films. Transmission electron micrographs of the development of the film during anodizing to different voltages in the phosphoric acid are shown in Fig. 1. The film produced by anodizing to 20 V (specimen S20 - formed in enriched electrolyte only) is a barrier-type oxide layer. Increase of the anodizing voltage to 100 V (sequentially anodized specimen S100) results in formation of embryo pores; the film thickness is 160-170 nm and the metal/oxide interface is flat. SEM micrographs of plan views of the non-anodized and anodized surfaces indicated that nucleation of the embryo pores is related to the surface texture of the substrate. Following anodizing to the maximum voltage at approximately 140 V, the metal/oxide interface becomes scalloped and major pores are developing (specimen Smax). Thereafter, the voltage decreased slowly and attained a steady value of about 107 V

(specimen Sconst- anodized for 385 s); the film morphology was typical of porous anodic alumina, with major pores of length of 850 nm and a barrier layer at the base of the pores about 150 nm thick. The dependence of the film thickness on the time of anodizing suggested two linear regions, with slower growth for anodizing times up to 75 s, followed by an increased growth rate at longer times.

Composition of the films. The analysis of the specimens by RBS determined the amount of aluminium oxygen and phosphorus in the films. An example of an experimental spectrum is given in Fig. 2. Table 1 summarizes the results of the data fitting using SIMNRA. The atomic ratios derived from the fitting procedure were used to express the average compositions of the sequentially formed films as $Al_2O_3.xAlPO_4$, which reflects the presence of phosphorus as units of aluminium phosphate in the amorphous alumina structure.

Table 1 Results of NRA and RBS measurements of the oxygen contents of anodic films formed on aluminium at 5 mA cm^{-2} in 0.4 M phosphoric acid at 20°C.

Specimen	Potential	Anodizing time	O RBS	^{16}O NRA	^{18}O - natural O18	Al RBS	$^{16}O+^{18}O$ NRA	P/Al
	V	s	10^{15} at/cm^2					
S20	21	16	127	127	11.69	80	138	0.052
S40	41	35	270	258	11.51	165	270	0.05
S100	101	91	738	708	11.46	448	720	0.051
Smax	140	149	1360	1289	11.4	821	1300	0.057
Sconst		385	3809	3407	11.03	2305	3418	0.058

The ^{16}O and ^{18}O contents of the anodic films were determined by NRA, using the $^{16}O(d,p_1)^{17}O$ and $^{18}O(p,\alpha)^{15}N$ reactions. The resulting oxygen contents for specimens sequentially anodized to the selected final voltages are presented in Table 1. The findings show that the amounts of ^{18}O in the films do not change significantly with increasing time of anodizing during the evolution of the film between the barrier and porous stages in the non-enriched electrolyte. The ^{18}O enrichment in S20 was 9.7 ± 0.4%, which is slightly below the enrichment of the water, due mainly to the presence of phosphate ions in the films.

Distributions of oxygen tracer. The distributions of the ^{18}O through the thicknesses of the anodic films were determined using the $^{18}O(p,\alpha)^{15}N$ reaction by probing the films with the resonance at a proton energy of 151 keV. The dependence of the yields of alpha particles from the resonance reaction on the energy of the ion beam is shown in Fig. 3 for the various specimens. The findings show that in the early stages of the texture-dependent pore development, a large fraction of ^{18}O is located in a layer near the metal/film interface. However, toward the end stages of anodizing, the ^{18}O is distributed between an inner region, an intermediate region, and an outer region of the film in proportions 0.55:0.20:0.25. The ^{18}O distribution near the film surface does not change greatly with an increase in the anodizing time and is clearly associated with the texture-dependent porous region. Following the establishment of the major pores in the 850 nm thick film of Sconst, most ^{18}O was located in the outer half of the film, but ^{18}O was also present in a 25 nm-thick layer near the film base. In comparison with specimen S100, the proportion of the total O^{18} in the barrier layer has reduced from ~55 to ~17% due to the transfer of ^{18}O to the cell walls.

Conclusions

As a result of the transport processes within the barrier layer, the order of oxygen tracer species in the film is not conserved. Further, the oxygen tracer species are retained within the

anodic films. The behaviour is suggested to be due to instability of the barrier layer, which leads to local flow of material between the inner and outer film regions as a consequence of composition, current density and stress gradients in the films. The flow of material enables the eventual attainment of a stable film morphology associated with the establishment of the major pores of the film. Due to the flow of the material, oxygen tracer species introduced into the initial barrier layer are retained within the film during the development of the pores and are located in the walls of the final pores.

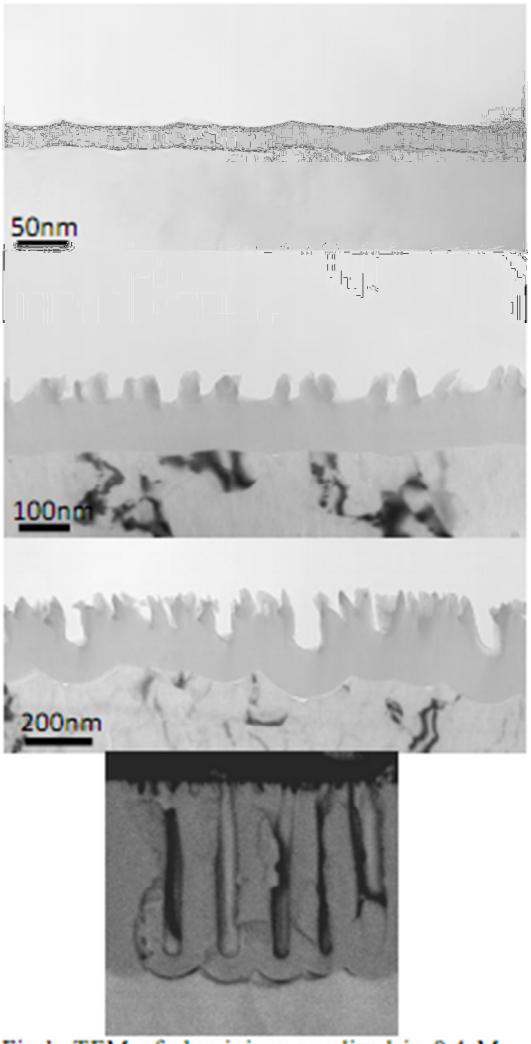

Fig.1. TEM of aluminium anodized in 0.4 M H_3PO_4 to (a) 20 V (S20), (b) 100 V (S100), (e) 140 V (Smax). (f) SEM of 107 V (Sconst)

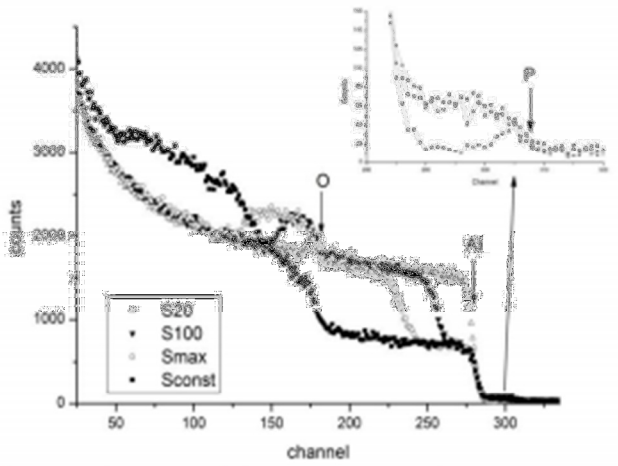

Fig. 2. RBS spectra of S20, S100, Smax, Sconst

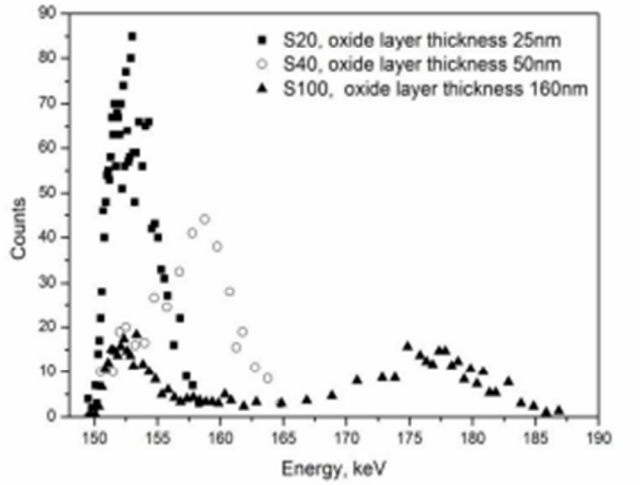

Fig. 3. Comparison of the excitation curves, determined using the resonance at 151 keV of the ^{18}O (p,α)^{15}N reaction for S20, S40, S100.

References

[1] ^{18}O tracer study of porous film growth on aluminum in phosphoric acid. A. Baron-Wiechec, J.J. Ganem, S.J. Garcia-Vergara, P.Skeldon,G.E. Thompson, I.C. Vickridge, JES 157 (2010) pp C399-407.

[2] Tracer studies relating to alloying element behaviour in porous anodic alumina formed in phosphoric acid S.J. Garcia- Vergara, H. Habazaki, P. Skeldon G.E. Thompson. Electrochim. Acta 55 (2010) pp 3175-3184.

[3] The contribution of stable isotopic tracing, narrow nuclear resonance depth profiling, and a simple stochastic theory of charged particle energy loss to studies of the dry thermal oxidation of SiC. I. C. Vickridge, J. J. Ganem, I. Trimaille, and J.-L. Cantin. Nucl. Instr. and Meth. B 232 (2005) 272-279.

[4] A study of the oxygen growth laws of anodic oxide films on aluminum and tantalum using nuclear microanalysis of O^{16} and O^{18}. J. Siejka, J. P. Nadai,G. Amsel. JES. 118 (1971) pp 727-737

Acknowledgements

The work was supported by EPSRC (U.K.) Programme Grant: LATEST2 and the 7th European Community Framework Programme, Grant agreement no. PIEF-GA-2008-219913.

P5 Elemental depth profiling of ultra thin high-k material stacks for 32 nm node devices by ToF-SIMS, pAR-XPS and HRBS

M. Py[1], R. Boujamaa[1, 2], H. Grampeix[1], R. Gassilloud[1], C. Roukoss[3], B. Pelissier[3], K. Nakajima[4], K. Kimura[4], N. Gambacorti[1], F. Bertin[1]

Matthieu.py@cea.fr

[1] *CEA-Leti, MINATEC Campus, 17 rue des Martyrs, 38054 GRENOBLE Cedex 9, France*
[2] *STMicroelectronics, 850 rue de Jean Monnet, 38926 Crolles, France*
[3] *LTM-CNRS/CEA-LETI, 17 rue des Martyrs, 38054 GRENOBLE Cedex 9, France*
[4] *Department of Micro Engineering, Kyoto University, KYOTO 606-8501, Japan*

32 nm and below technological nodes require extreme dimension scaling which is impossible to obtain with classical materials for CMOS integration. High-k materials, with their enhanced mobility and reduced EOT, are considered as one of the answers to this problem [1]. Further performance improvement can be achieved by combining the high-k technologies and SiGe based mobility enhancement technologies [2]. However the electrical properties of these materials greatly depend of their stoichiometry and of the in-depth distribution of its different elements [3]. Accurate concentration depth profiling of these materials is thus demanded.

Although HRBS and AR-XPS already proved their ability in this domain [4], SIMS or ToF-SIMS characterization of high-k material stacks is hampered by matrix effects [5]. However we developed a protocol for ToF-SIMS data treatment (the Full Spectrum protocol), based on pioneer work by Ferrari *et al*. [6]. We have very recently shown that this protocol allowed reduced matrix effects and permitted quantitative profiling of high-k stacks [7].

In this work we focused on two series of samples: a first series involving ultra thin high-k stacks on Si bulk substrate, and a second series involving high-k stacks on SiGe strain engineered channels with different activation anneals. Comparison of the profiles obtained by all techniques brings comprehension on their accuracy, both in terms of chemical composition quantification and in terms of depth resolution. It proves the accuracy of the Full Spectrum data treatment for ToF-SIMS and shows a good agreement between techniques (see Figure 1). This study also reveals ToF-SIMS, and to a lesser extent HRBS limits in depth resolution for interfacial layers that parallel AR-XPS is able to resolve, although the same pAR-XPS does not enable analysis of thick stacks superior to ~10 nm.

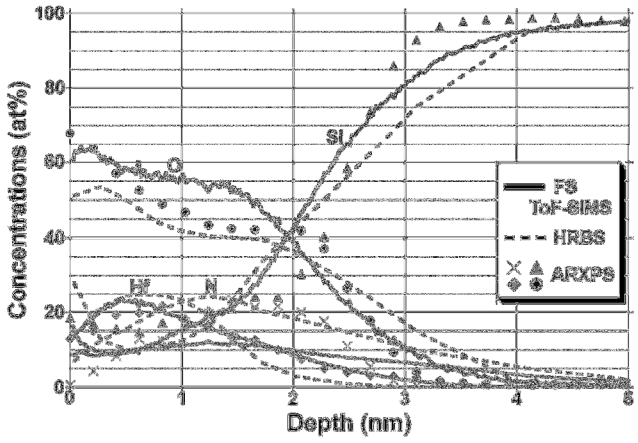

FIGURE 1. Overlaid Full Spectrum ToF-SIMS, HRBS and pAR-XPS profiles of a 1.7 nm HfSiON / 1.5 nm SiON / Si sample.

References.

[1] E.P. Gusev, V. Narayanan, M.M. Frank, IBM J. Res. Dev. 50, 2006, 387-410.
[2] O. Weber, Thesis work, INSA Lyon, 2005.
[3] R. Katamreddy, R. Inman, G. Jursich, A. Soulet, C. Takoudis, Thin Solid Films 516, 2008, 8498-8506.
[4] K. Kimura, K. Nakajima, M. Zhao, H. Nohira, T. Hattori, M. Kobata, E. Ikenaga, J.J. Kim, K. Kobayashi, T. Conard, W. Vandervorst, Surf. Interface Anal. 40, 2008, 423-426.
[5] W. Vandervorst, J. Bennett, C. Huyghebaert, T. Conard, C. Gondran, H. De Witte, Appl. Surf. Sci. 231-232, 2004, 569-573.
[6] S. Ferrari, M. Perego, M. Fanciulli, Appl. Surf. Sci. 203-204, 2003, 52-55.
[7] M. Py, J.P. Barnes, R. Boujamaa, M. Gros-Jean, K. Nakajima, K. Kimura, C. Roukoss, B. Pelissier, N. Gambacorti, accepted for publication in J. Vac. Sc. Technol. B (2011).

Acknowledgments: This work was partially supported by the European EUREKA/CATRENE program in the frame of the CT206 UTTERMOST project and by the National Research Agency (ANR) through the French "Recherche Technologique de Base" Program.

P6 A high depth resolution MEIS investigation of ultra thin STO/TiN layers on Si for DRAM MIM capacitors

J. A. van den Berg[1], M.A. Reading[1], P.C. Zalm[1], P. Bailey[2], T.C.Q. Noakes[2], C. Adelmann[3], M. Popovici[3] and H. Tielens[3].

j.a.vandenberg@salford.ac.uk (corresponding author)

[1]*Materials & Physics Research Centre, University of Salford, Salford, M5 4WT, United Kingdom*
[2]*STFC Daresbury Laboratory, Daresbury, WA4 4AD, United Kingdom*
[3]*IMEC. Kapeldreef 75, 3001 Leuven, Belgium*

The ongoing scale reduction in microelectronics is driving a renewed interest in high-k materials for metal-insulator-metal capacitors (MIMcap) in Dynamic Random Access Memory (DRAM) devices, not only in the form of planar but notably in high aspect geometries [1]. Because of its high electrical constant (k~150-300) and the ability to deposit good conformal thin layers by Atomic Layer Deposition (ALD) [2], $Sr_xTi_{1-x}O_y$ (STO) has emerged as a promising dielectric material. The application of TiN electrodes represents a low cost and more easily manufacturable alternative to Pt or Ru, previously investigated. Deposition and thermal processes have to be controlled in order to tailor the layer composition and thickness and especially to understand metal / dielectric interface effects.

The physical characterisation of these compound multi layers of a few nm thick, represents a considerable analytical challenge. Medium energy ion scattering (MEIS) combined with energy spectrum simulation has been applied to the STO/TiN layer system in view of its demonstrated capability of yielding quantitative information on the structure and composition of ultra thin layers with sub-nm depth resolution at the surface [3]. Factors that affect the quantification of MEIS information such as neutralization, Andersen correction and changing energy bin width across the energy spectrum have been assessed and the potential effect of an asymmetric energy loss function is considered.

Layer structures analysed included individual, 3 nm thick TiN and STO insulator layers (Sr rich and stoichiometric) on IMEC cleaned Si(100) as well as combinations of these layers, building up to a full MIMcap structure consisting of a 2 nm TiN top electrode, a 3 nm STO insulator layer and a 3 nm TiN bottom electrode. In particular the effect of annealing at 650°C in N_2 was investigated. MEIS conditions used were 100 keV He^+ ions in the double alignment configuration with the ion beam incident along the [-1-11] direction and the analyser aligned with either the [221] direction, yielding a scattering angle of 90°.

Further to a determination of the composition and thickness of the layers investigated, which are in good agreement with HR-RBS results, MEIS studies have enabled the monitoring of interface behaviour, providing information on thermal processing and interface issues such as the effect of the TiN sputter deposition process, the near-surface Sr enrichment of the uncapped Sr rich STO layer, Ti interdiffusion into the Sr rich STO upon annealing and the apparent higher thermal stability of the stoichiometric STO/TiN system against Ti diffusion.

References.

[1] J. A. Kittl et al., Microelectron. Eng. 86 (2008) 1789
[2] N. Menou et al., J. Appl. Phys. 106 (2009) 106
[3] M. A. Reading et al., J. Vac. Sci. Technol. B 28 (1), (2010) C65-70

P7 Energy loss of protons in $SrTiO_3$ on Si(001) studied by medium energy ion spectroscopy

S.N. Dedyulin, W.N. Lennard, L.V. Goncharova

sdedyuli@uwo.ca

Department of Physics and Astronomy, University of Western Ontario, London, ON, Canada

The energy loss (EL) concept is a central idea in the interaction of a beam of charged particles with solid matter. Relevant to EL are the stopping power, S, and stopping cross-section, ε, which for the thin film target may be defined as $\frac{\Delta E}{\Delta x}$ and $\frac{\Delta E}{N\Delta x}$ respectively, where ΔE is the energy lost by the energetic ion in traversing the path Δx, when there are N atoms (or molecules) per unit volume of the stopping medium. Since the original paper of Bragg [1] ε for the compound is usually found as simply the sum of the atomic ε for the elements taken with stoichiometric coefficients; thus for a two-element compound A_nB_m:

$$\varepsilon(A_nB_m) = n\varepsilon(A) + m\varepsilon(B). \quad (1)$$

The deviation from the Bragg's rule as applied to inorganic compounds (eq. 1) is presumed to be either due to the chemical effect (modification of the atomic electronic density in the compound) or due to the physical effect (if atomic ε is obtained for the different physical state than that of the compound) and is defined as follows [2]:

$$\Delta\varepsilon = \varepsilon_{compound} - \sum \varepsilon_{atomic}. \quad (2)$$

It has been shown recently that for stopping of protons in binary oxides, the maximum for $\Delta\varepsilon$ occurs below the maxima of the compounds and the mixtures (<100 keV) [3]. An alternative approach considers $\varepsilon_{compound}$ to be the sum of stopping from the structural blocks (not necessarily atomic) and the chemical bonding in between the blocks and is believed to be more accurate than Bragg's rule [4,5]. Unfortunately, the latter approach is limited to organic compounds only due to the absence of systematic studies of stopping in inorganic materials forming the same class.

The current research is focused on the EL of 55 - 170 keV protons in a ternary oxide compound $SrTiO_3$ (STO) measured by medium energy ion spectroscopy (MEIS). MEIS has been chosen for two main reasons: i) high energy resolution ($\frac{\Delta E}{E} < 10^{-2}$) that allows one to detect slight changes in the EL of the compound and ii) the MEIS energy range coincides with the region where the chemical effects (eq. 2) for the protons are most pronounced.

Epitaxial 4 nm thick STO films on Si (001) were deposited by molecular beam epitaxy following the procedure described elsewhere [6].[1] A series of amorphous samples were grown by pulsed laser deposition.[2] Thickness and crystallinity were characterized by Rutherford backscattering spectroscopy (RBS) (500 keV He^+ ions) in random and aligned geometries. In order to test eq. 2 and compare the results of MEIS for STO with those available in the literature for the amorphous elemental targets [7], the MEIS spectra of protons in the energy range

[1] STO films were provided by T. Gustafsson (Rutgers U., USA) and prepared by D.G. Schlom group (U.Cornell, USA).

[2] Pulsed laser deposition growth was done in collaboration with F. Razavi (Brock U., Canada).

55-170 keV were recorded by inclining the samples away from the STO specific crystalline directions to maximize the yield. EL and the corresponding ε's were calculated in the surface-energy approximation by measuring the shift in the Si edge position as a function of energy, and using STO thickness values as obtained by RBS. The results were compared with the sum of atomic ε-values: $\varepsilon(Sr) + \varepsilon(Ti) + 3\varepsilon(O)$ (see the first approach above), as well as with the sum of the ε-values for the possible structural blocks: $\varepsilon(SrO) + \varepsilon(TiO_2)$ (see the second approach above) in the entire energy range studied.

References

[1] W. H. Bragg and R. Kleeman. Philos. Mag. 10 (1905) pp. 318–340.
[2] D. I. Thwaites. Nucl. Instrum. Methods Phys. Res. B 12 (1985) pp. 84–89.
[3] P. Bauer, R. Golser, D. Semrad, P. Maier-Komor, F. Aumayr and A. Arnau. Nucl. Insrum. Methods Phys. Res. B 136-137 (1998) pp. 103–108. [4] D. Powers. Acc. Chem. Res. 12 (1980) pp. 433–440.
[5] J. F. Ziegler and J. M. Manoyan. Nucl. Instrum. Methods Phys. Res. B 35 (1988) pp. 215–228.
[6] J. Lettieri, J. H. Haeni and D. G. Schlom. J. Vac. Sci. Technol. A 20 (2002) pp. 1332–1340.
[7] J. F. Ziegler, J. P. Biersack and U. Littmark. The stopping and range of ions in matter. Pergamon Press, Inc., Toronto, 1985.

P8 Hydrogen detection by medium energy N^+ and Ne^+ impacts

Kei Mitsuhara, Hideki Okumura, Anton Visikovskiy and Yoshiaki Kido

Corresponding author: k-mitsu@se.ritsumei.ac.jp

Department of Physics, Ritsumeikan University, Kusatsu, Shiga-ken 525-8577, Japan

The absolute amounts of H on the Si(111)-1×1-H and hydroxylated rutile TiO_2(110) surfaces were determined by elastic recoil detection using medium energy N^+ and Ne^+ ions[1]. The singly ionized fraction of recoiled H depends on emerging energy and strongly on emerging angle. Figure 1 shows a typical ERD spectrum observed for 102 keV Ne^+ impact on Si(111)-1×1-H along the [1$\underline{1}$1]-axis. The H^+ ions recoiled to 70° with respect to surface normal were detected by a toroidal electrostatic analyzer. The relatively broad width originates from the Doppler effect and a degraded system energy resolution at low energies. The H^+ fractions observed are strongly dependent on emerging angle, as shown in Fig. 2. This is attributed to the fact that H atoms are located protuberantly on the top layer Si and thus a long path length along the surface is required for recoiled H atoms to be equilibrated in the charge state distributions. More detailed discussion will be also given about the energy dependent H^+ fractions and the Doppler broadening in terms of the zero-point energy of the Si-H oscillating system.

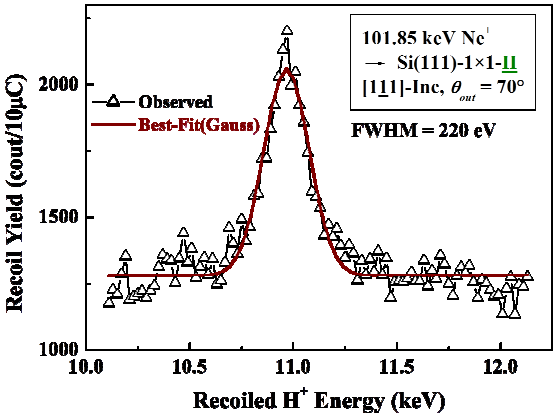

Fig. 1. Typical ERD spectrum observed for 102 keV Ne^+ impact on Si(111)-1×1-H.

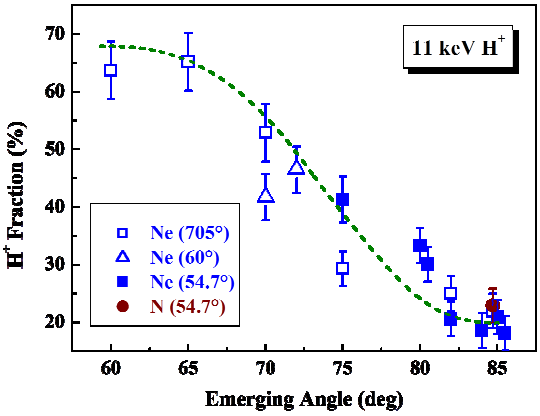

Fig. 2. H^+ fractions for recoiled H with an energy of 11 keV as a function of emerging angle.

[1] K. Mitsuhara, T. Kushida, H. Okumura, H. Matsumoto, A. Visikovskiy and Y. Kido, Surf. Sci. **604** (2010) L48.

P9 Complex Investigation of Properties of Seeds with Micro-RBS-PIXE Techniques

A. Lagutin[1], H. Gorodecka[2]

lagutin_ae@mail.ru (corresponding author)

[1] *Belarusian State Agrarian Technical University*
[2] *Central Botanical Garden of the National Academy of Sciences of Belarus, helgorod2003@mail.ru*

Nuclear microscopy is a generic term referring to a large panel of ion beam analysis techniques carried out using light ion microbeams in the MeV energy range (typically H^+ and He^+) [1]. Numerous applications in biological samples take advantage of its versatility and easy operation, either at the tissue or individual cell scale. PIXE is the basic method employed for routine elemental mapping. In addition, micro-PIXE and other microbeam techniques complement each other to offer unique information. The use of the nuclear microprobe in conjunction with Rutherford backscattering spectrometry with electrostatic analyzer represents a powerful technique for imaging the spatial and depth distribution of sample layers [2].

To study the efficiency of propagation of ions through the capillaries and capillary systems the special experimental setup has been developed and manufactured. The schema of the experimental setup designed for studying the transmission of accelerated ions through capillaries and capillary systems is shown in Fig. 1.

In this review, different examples of investigation will be presented with emphasis placed on agricultural plants. The response of seed germination characteristics of some important agricultural plants to treatment in low pressure plasma of a capacitive coupled radio frequency (rf) discharge and in rf electromagnetic field has been studied. It has been shown that the pre-sowing plasma and radio-wave treatment of seeds contributes to their germination enhancement and sowing quality improvement.

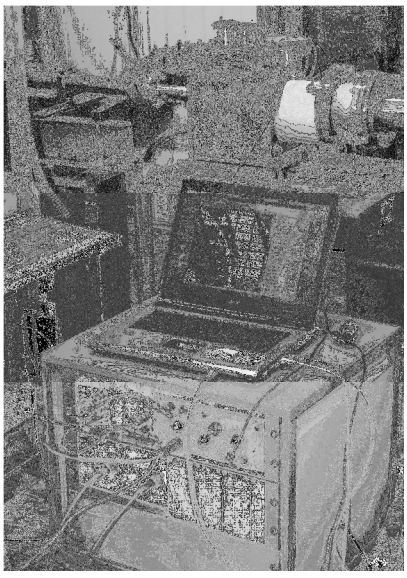

Figure 1: Experimental setup

References.

[1] Investigation of Properties of Seeds with Device on the Basic of Micro Insulating Capillaries. A. Lagutin, H. Gorodecka. Book of Abstracts 12th ICNMTA2010, P.60.

[2] Device on the Basic of Insulating Capillaries for RBS and Other Applications. A. Lagutin. Book of Abstracts 19th International Conference on Ion Beam Analysis 2009, P.187.

P10 A comparison of *i*-AlPdMn and *i*-AgInYb quasicrystals using medium energy ion scattering

T.C.Q. Noakes[1], P. Bailey[1], C.F. McConville[2], C.R. Parkinson[2], M. Draxler[2], J.A. Smerdon[3], J. Ledieu[3], P.J. Nugent[3], J. Parle[3], H.R. Sharma[3], R. McGrath[3]

tim.noakes@stfc.ac.uk (corresponding author)

[1] *STFC Daresbury Laboratory, Daresbury Science and Innovation Campus, Keckwick Lane, Daresbury, Warrington, Cheshire, WA4 4AD, UK*
[2] *Department of Physics, University of Warwick, Coventry, Warwickshire, CV4 7AL, UK*
[3] *Surface Science Research Centre and Department of Physics, University of Liverpool, Liverpool, L69 3GH, UK*

Over the last decade there have been many surface science investigations of aluminium based ternary alloys exhibiting face centred icosahedral structure [1]. *i*-CdYb also exhibits five fold periodicity, but with primitive icosahedral structure; this material is not ideal for surface science studies because of the high vapour pressure exhibited by cadmium. Recently, a new quasicrystal has been produced which is isostructural to *i*-CdYb but with the Cd sites occupied by a 50:50 mixture of Ag and In, allowing the direct comparison of the surface and near surface structure and chemistry of this material with face centred icosahedral materials such as *i*-AlPdMn [2].

The sensitivity of the MEIS technique to the structure can be demonstrated using VEGAS simulations [3]; the same blocking dips can be seen but the relative amplitudes for each sample are different. Observing these differences experimentally is complicated by the limited number and reduced amplitude of dips compared to crystalline materials and the tendency for quasicrystals to damage quickly under ion irradiation. For *i*-$Al_{71}Pd_{20}Mn_9$ the surface region of the material can be seen to be Al rich, but as the sample is annealed closer to the decomposition temperature Mn segregates to the surface. High temperature anneals have been found to be necessary to form an atomically smooth surfaces [4]. For *i*-$Ag_{42}In_{42}Yb_{16}$ the surface terminates at densely packed Yb rich planes and annealing close to the decomposition temperature leads to further Yb enhancement and significant roughening of the surface. For samples prepared using optimal conditions both materials showed essentially bulk like surface structure.

References

[1] R. McGrath, J.A. Smerdon, H.R. Sharma, W. Theis and J. Ledieu, Journal of Physics: Condensed Matter 22 (2010) 084022
[2] H.R. Sharma, M. Shimoda, K. Sagisaka, H. Takakura, J.A. Smerdon, P.J. Nugent, R. McGrath, D. Fujita, S. Ohhashi and A.P. Tsai, Physical Review B 80 (2009) 121401(R)
[3] J.F. Frenken, J.F. van der Veen and R.M. Tromp, Nuclear Instruments and Methods in Physics Research B 17 (1986) 334
[4] J. Ledieu, A.W. Munz, T.M. Parker, R. McGrath, R.D. Diehl, D.W. Delaney and T.A. Lograsso, Surface Science 433-435 (1999) 666

P11 Test of SRIM 2010 stopping power data using TOF-ERDA spectra

I.Bogdanović Radović[1], Z. Siketić[2,1], Ž. Pastuović[3], M. Jakšić[1]

iva@irb.hr

[1]*Ruđer Bošković Institute, P. O. Box 180, 10000 Zagreb, Croatia*
[2]*Jožef Stefan Institute, Jamova c. 39, 1000 Ljubljana, Slovenia*
[3] *ANSTO,Locked bag 2001, Kirrawee DC NSW 2232, Australia*

Knowledge of the accurate stopping power data is one of the most important parameters for precise high resolution depth profiling using heavier ion beams. Accuracy of SRIM 2010 [1] stopping power data when compared to experimental results for ions heavier than lithium in different matrices is around 6%. In cases without experimental stopping data, the SRIM calculation relies on interpolated values from ion-target pairs for which stopping power was measured and therefore the accuracy can be even worse. From that can be concluded that accuracy of such experiments using heavier ions is certainly worse than 6%.

In the present work Time-of-flight Elastic Recoil Detection Analysis (TOF-ERDA) spectra of several samples with well known layer thickness and composition were measured with heavy ions to test how good experimental spectra can be simulated using heavy ion SRIM 2010 stopping power data. TOF-ERDA measurements were performed with different incident ions (Cl, Cu, Au and I) and ion energies impinging under several incident angles toward the sample surface. Experimentally obtained spectra were compared with the simulated spectra calculated using Monte Carlo program CORTEO [2] and SRIM 2010 stopping power data.

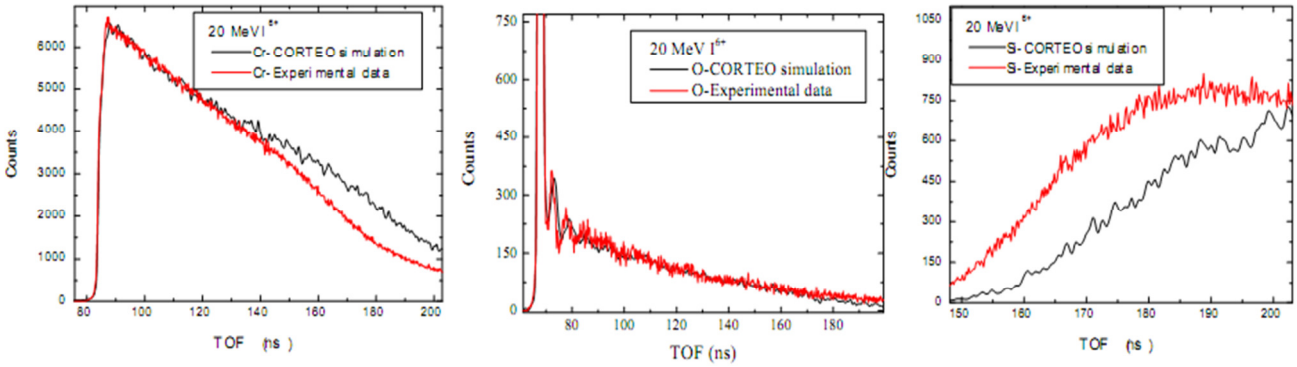

Fig.1 TOF-ERDA spectra of the NIST 2136 standard reference material measured with 20 MeV $^{127}I^{6+}$ beam

Figure 2 displays TOF-ERDA spectra of the same NIST 2136 standard reference material but measured under same conditions with 26 MeV $^{197}Au^{7+}$ ions.

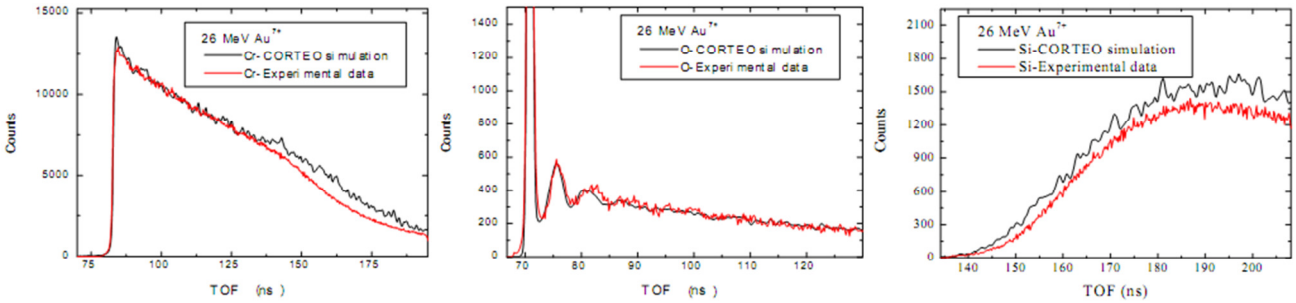

Fig.2 TOF-ERDA spectra of the NIST 2136 standard reference material measured with 26 MeV $^{197}Au^{7+}$ beam

From the figures above can be concluded that discrepancy exist between the experimental and simulated data using SRIM 2010 stopping power values. In case of oxygen spectra, discrepancy is more pronounced for the heavier ion beam used. Also, from the figures can be seen that simulations of the chromium spectra do not reproduce experimental data and certified thickness of the film. The biggest mismatch between experimental and simulated spectra was found for silicon spectra obtained using iodine beam. Performed measurements clearly show that heavy ion stopping power data are essential problem in HI TOF-ERDA. In order to get a more reliable data from the HI ERDA experiments (thicknesses of the thin films) new measurements of the heavy ion stopping powers are needed.

Reference.

[1] J. F. Ziegler, M. D. Ziegler, J. P. BiersackNucl. Instr. And Meth. B 268 (2010) 1818
[2] F. Schiettekatte, Nucl. Instr. And Meth. B 266 (2008) 1880

P12 Performance of the NEC HR-RBS System at CIM-AAMU

C. Muntele[1, 2], R. Givens[1, 2], D. Ila[2]

claudiu.muntele@aamu.edu, claudiu@cim.aamu.edu

[1]*Center for Irradiation of Materials, Alabama A&M University, Normal, AL 35762, USA*
[2]*Physics Department, Alabama A&M University, Normal, AL 35762, USA*

A little more than a year ago we installed a high resolution RBS (HR-RBS) detection system and a terminal potential control system upgrade for our 5SDH-2 Pelletron tandem accelerator from National Electrostatics Corporation. The system consists on a single focusing 90 deg magnet with an angle defining aperture at the entrance and a 100 mm wide position sensitive microchannel plate detector at the exit. The system is installed on the modified original RC43 chamber, with two ports to connect, for forward and back scattering geometries, with the whole assembly seated on a rail track, for easy maneuverability between the two positions. This arrangement is complementary to the original RBS setup using a SSB detector with an 18 keV resolution for the 2 MeV He^+ beam. The new system is designed to reach a resolution of 1 keV for 400 keV He^+ beams.

Since its installation, we have used the HR-RBS system with various energy He^+ beams around 400 keV and various target samples from uniform, single crystal 6H silicon carbide, to highly oriented pyrolytic carbon, graphene sheets on various substrates, and nanolayered multi-sandwich structures for our thermoelectrics convertors program. We will discuss the performance of the system as a function of beam energy, position, sample type and condition, and show results from recent usage on nanostructured research samples.

P13 Molecular Effects in the $^{15}N(p,\alpha\gamma)^{12}C$ Nuclear Reaction Profiling

S. M. Shubeita[1], J. F. Dias[1], P.L. Grande[1], I.C. Vickridge[2], A. L'Hoir[2], I. Trimaille[2], and J.J. Ganem[2]

grande@if.ufrgs.br (corresponding author)

[1]*Instituto de Física da Universidade Federal do Rio Grande do Sul, Laboratório de Implantação Iônica, Porto Alegre, RS, Brazil.*

[2]*Institut des Nanosciences de Paris, INSP, UMR 7588 du CNRS, Université Pierre et Marie Curie, Université Denis Diderot, Paris, France*

In the present work we explore the effects arising from the interaction between ionic molecular beams (H_2^+ and H_3^+) and ^{15}N-enriched Si_3N_4 amorphous target through the Nuclear Reaction Profiling (NRP) technique (Fig. 1). In this case, we used the $^{15}N(p,\alpha\gamma)^{12}C$ resonant nuclear reaction at 429 keV/nucleon (Γ=120 eV). The depth dependent energy-loss ratio R_n due to the vicinage effect and the contribution of the Coulomb explosion to the energy loss straggling are obtained experimentally from a simple fitting model and compared with theoretical results based on Monte Carlo simulations [1].

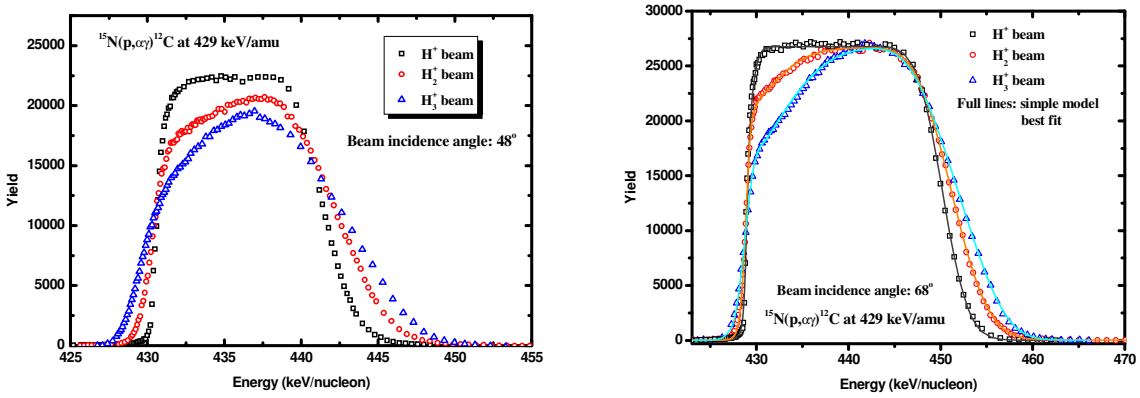

(a) (b)

Figure 1: Normalized excitation curves as a function of the H^+ (black squares), H_2^+ (red circles) and H_3^+ (blue triangles) energy per proton. The H_2^+ and H_3^+ excitation curves show a very different shape compared with the H^+ excitation curve, demonstrating the effects due to the correlated motion of the molecular ionic fragments. (a) Beam incidence angle: 48°. The H_2^+ and H_3^+ excitation curves do not reach the H^+ plateau. (b) Beam incidence angle: 68°. The H_2^+ and H_3^+ excitation curves reach the H^+ plateau. The full lines in (b) represent the best fittings provided by the simple model.

The results obtained for the depth dependent vicinage effects show a strong contribution of the correlated motion among ionic molecular fragments to the fragments energy loss. The contribution of the Coulomb explosion to the energy-loss straggling increases and saturates with the dwell time or penetrated depth. The results agree with theoretical predictions described in [1] and show the importance of multiple scattering and screening effects. On the other hand, the present results open the perspective for an absolute perfilometry of amorphous ultra-thin films, where the energy-loss straggling stemming from the Coulomb explosion grows linearly with depth, and screening and multiple scattering effects are less important.

References

[1] A. L'Hoir, J. J. Ganem, I. Trimaille, I. C. Vickridge, Nucl. Instrum. Methods Phys. Res., Sect. B 268 (2010) 2850-2853

P14 Study of impact-parameter dependence of inelastic energy loss in silicon

O. El Bounagui[1], H. Erramli[2]

elbounagui@gmail.com

[1]*Theoretical Physics Laboratory, Department of Physics, Faculty of Sciences Rabat, Morocco*
[2]*Nuclear Physics and Techniques Laboratory, Department of Physics, Faculty of Sciences Semlalia, University Cadi Ayyad, P. B. 2390, Marrakech, Morocco.*

In this work, we describe a new computer code for the inelastic energy loss as a function of the impact parameter for projectiles. The calculation are performed by using Monte Carlo simulations, each event characterized by choosing the distance between electron and projectile b determined by using the random procedure ξn. We compare simulated data with those obtained by other authors using theoretical and experimental methods.

Keywords*: Charged particles; Monte Carlo simulations; Inelastic energy loss; Impact parameter; Silicon*

P15 Calibration correction of ultra-low energy SIMS profiles based on MEIS analyses for Arsenic shallow implants in silicon.

E. Demenev[1,4], D. Giubertoni[1], M.A. Reading[2], P. Bailey[3], T.C.Q. Noakes[3] , M. Bersani[1] and J.A. van den Berg[2]

demenev@fbk.eu (corresponding author)

[1]*Centro per i Materiali e Microsistemi (CMM) Fondazione Bruno Kessler (FBK) Via Sommarive 18, 38123 Povo-Trento, Italia*

[2]*JMaterials & Physics Research Centre, University of Salford, Salford, M5 4WT*

[3]*STFC Daresbury Laboratory, Daresbury, WA4 4AD, United Kingdom*

[4]*Department of Physics, University of Trento, via Sommarive 14, 38123 Povo (Trento) Italy*

The quantitative analysis by secondary ion mass spectrometry (SIMS) of ultra shallow dopant distribution in silicon is still one of the most challenging applications of dynamic SIMS. Since such dopant distributions are confined to the top few nm of samples, an important fraction of them is contained in the initial SIMS transient width, i.e. the thickness of Si that has to be removed away before a sputtering equilibrium is established. A further complication is due to the presence of native or induced SiO_2 layer at the surface and the related variation of sputtering and ion yields at the SiO_2/Si interface. In this work, we develop previous observations [1,2] related to arsenic profile quantification at the SiO_2/Si interface by SIMS and propose a correction model for SIMS raw data aimed at reducing the artifacts. Profiles of As implanted with energies from 3 to 10 keV through a thin (11nm) SiO_2 layer to fluences of $7x10^{14}/cm^2$, were used to calibrate the model. Note that for 3 keV, almost all As is implanted in the SiO_2. Figure 1 shows the SIMS profiles after applying corrections for the sputtering rate and relative sensitivity factor variations.

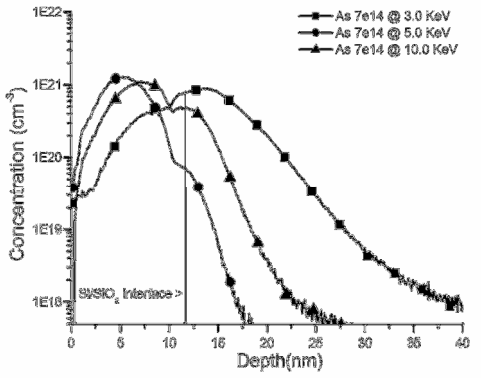

Figure 1.SIMS profile of samples with 11 nm thick SiO_2 layer

The model for correcting SIMS depth profiles of arsenic has been implemented using medium energy ion scattering (MEIS) obtained profile results as reference. MEIS is of great value in ultra shallow depth profiling as it quantitative, gives high depth resolution (< 1nm) and avoids typical SIMS problems (e.g. initial transient width and matrix effects) [3] but the achievable detection limit is always poorer than the one obtained by SIMS. These two techniques have been applied to the characterization of ultra shallow distributions of As in Si obtained by ion implantation with energies ranging from 0.5 to 5 keV and fluences from $1x10^{14}$ to $1x10^{15}$ at/cm^3, in order to develop quantitative model to correct SIMS profiles to the MEIS determined distributions.

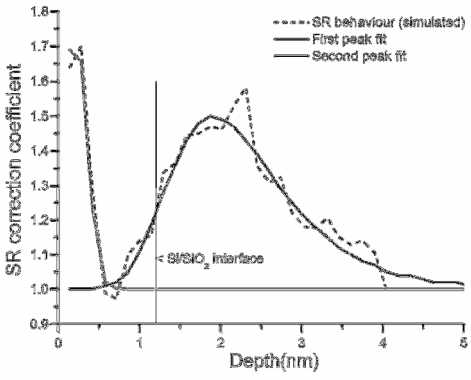

Figure 2 .Sputtering rate behaviour obtained from SIMS to MEIS

Figure 2 presents the sputtering rate behaviour inside the sample during SIMS analysis based on

the comparison with MEIS results obtained on the shallow implants in Si. The curves represent the ratio between sputtering rate in every point to the equilibrium value in Si. Through the use of this correction as well as the correction in the oxide part, ultra low energy SIMS depth profiles can be aligned with the MEIS results but with the important advantage of better detection limit as is clearly demonstrated in Figure 3.

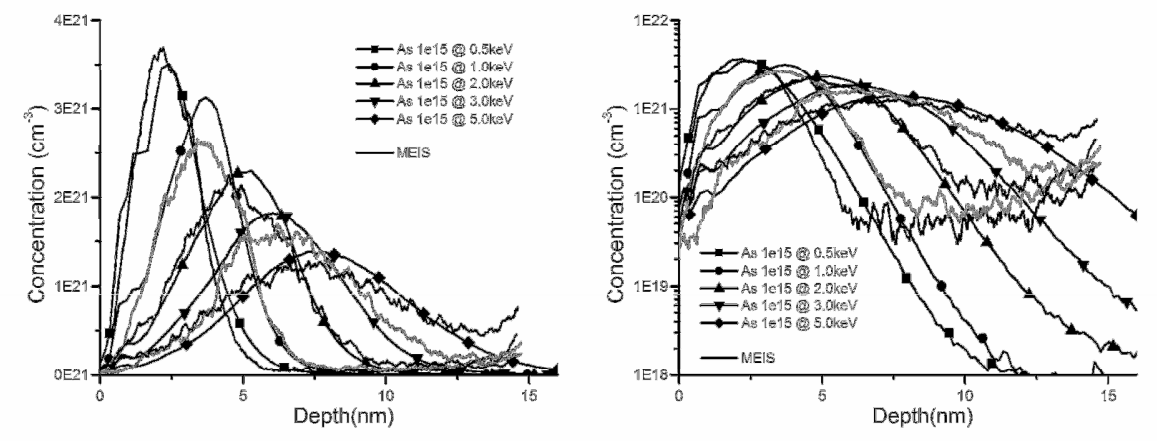

Figure 3. Profiles obtained by SIMS and MEIS for ultra shallow junction of arsenic in silicon on linear (left) and logarithmic (right) scales

In addition, this approach was applied to arsenic implanted samples at 2 keV with different nominal fluences ranging from $1x10^{14}$ to $1x10^{15}$ at/cm^3 in order to evaluate any concentration dependence of the model and the results shown in Figure 4. The un-corrected SIMS profiles (not shown) are 1-2 nm shallower in comparison with MEIS. After applying the model, the As peak position difference with MEIS coincide within 0.4 nm in all samples for depths from 2 to 8 nm as presented in Figures 3 and 4.

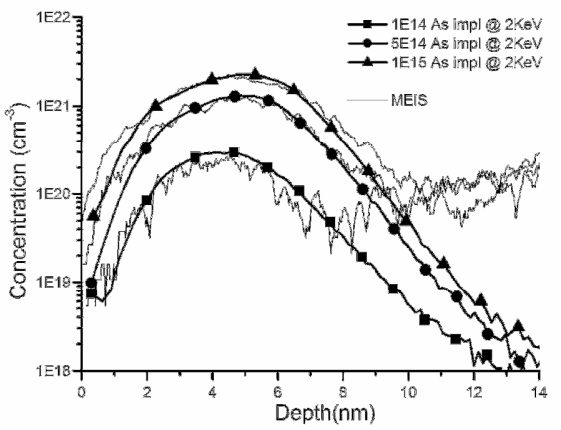

Figure 4. SIMS and MEIS profiles of 2 keV As implanted samples

References.

[1] D. Giubertoni, M. Bersani, M. Barozzi, S. Pederzoli, E. Iacob, J. A. van den Berg, M. Werner, Appl. Surf. Sci. 252 (2006) 7214.

[2] M. Barozzi, D. Giubertoni, M. Anderle and M. Bersani, Appl. Surf. Sci. 231-232 (2004) 632.

[3] A.Merkulov, P.Peres, J.Choi, F.Horreard, H-U.Ehrke, N. Loibl, M.Schuhmacher, J Vac Science Technol. B. 28, C1C48 (2010); doi:10.1116/1.3225588

P16 Electronic stopping of slow hydrogen ions in silicon

D. Roth, S. Rund, D. Primetzhofer, D. Goebl and P. Bauer

dietmar.roth@jku.at (corresponding author)

Institut für Experimentalphysik, Johannes Kepler Universität Linz, Altenbergerstraße 69, A-4040 Linz, Austria

The energy loss of ions propagating in a solid has been under close investigation for many decades. The aim in this field of research is to achieve a profound understanding of ion-target interactions and to obtain valuable information on the deceleration of ions in matter. There are two distinct processes due to which kinetic energy of the projectile is transferred to the target: either by repulsive Coulomb interaction with the nuclei (nuclear stopping) or by excitation of the electrons (electronic stopping). The resulting retardation force $-dE/dx$ is called stopping power S; the electronic stopping cross section ε is related to S via $\varepsilon = (1/n) \cdot S$, where n denotes the atomic density of the target. While for high energy ions electronic stopping is well understood, many unanswered questions still persist when low ion energies are considered.

In the regime of low-energy ion scattering (LEIS), i.e. from 0.5 to 10 keV primary ion energy, for a free electron gas (FEG), S is proportional to the ion velocity v, if the projectile is sufficiently slow compared to the Fermi velocity of the target electrons [1], [2]. Thus, electronic stopping acts on the moving ion like a friction force. For a FEG-like metal, e.g. Al, velocity proportionality for S has been found in both, transmission [3] and backscattering geometry [4]. The situation changes if noble metals like Cu, Ag or Au are investigated: here, S shows a change in its velocity dependence which can be explained by a threshold in the excitation of d-band electrons, located several eV below the Fermi energy [5], [6]. For insulators like KCl and LiF, electronic energy loss vanishes for ions slower than a certain threshold velocity v_{th} [7], [8].

Consequently, band structure effects in electronic stopping processes occurring in semiconductors are an interesting field of research, since this class of material is at the boundary between conductive and non-conductive materials. Like insulators they feature a band gap, but much smaller in magnitude. When it comes to the dominating process of energy dissipation in the deceleration process of a slow ion, the question is whether a semiconductor acts more like a metal or like an insulator.

In the present work, we studied electronic energy loss of hydrogen ions in polycrystalline silicon by means of time-of-flight low energy ion scattering (TOF-LEIS). Measurements were performed with the TOF-LEIS setup ACOLISSA [9]. It permits experiments in a UHV environment (typical base pressure: $8 \cdot 10^{-11}$ mbar) using primary energies from 0.7 to 10 keV in backscattering geometry with a scattering angle of 129°. Mass-separated atomic and molecular beams of hydrogen and deuterium in an energy range of 1–10 keV were used to perform measurements for Si relative to Al, which served as a reference target.

Preparation of polycrystalline samples was done in the following way: Both samples, a piece cut from a commercial Si wafer and a 500 nm ex-situ evaporated Al film, were cleaned thoroughly by means of 3 keV Ar^+-bombardment. Several cycles of sputtering ensured amorphous surface conditions. This is especially important for Si, where one has to overcome the original single crystalline structure. Surface purity was checked by Auger electron spectroscopy. Data analysis was performed following the procedure described in [5].

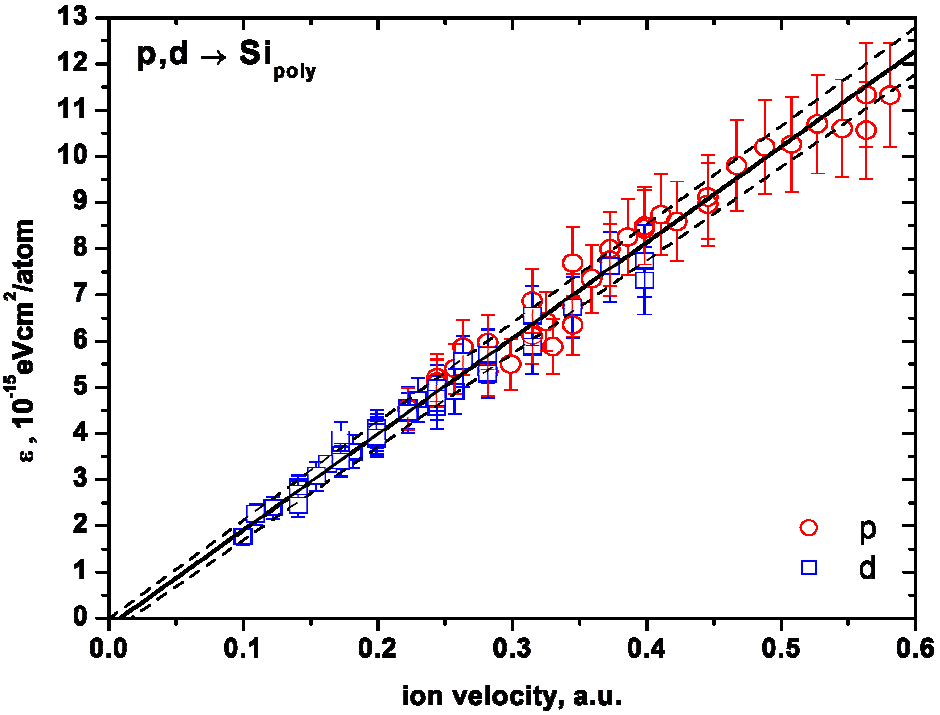

Fig. 1: Electronic stopping cross section ε deduced by relative evaluation with respect to an Al reference target. Data is extrapolating to a threshold velocity of 0.008 a.u. The dashed lines represent one standard deviation of the linear fit.

In Fig. 1, ε for H ions in Si is presented as a function of the ion velocity in atomic units, i.e. in units of the Bohr velocity $v_0 = c/137$. Our results exhibit the following information: S is linear in v; from extrapolation to lower velocities it becomes clear that if a threshold v_{th} exists, it is very small ($v_{th} = 0.008 \pm 0.008$ a.u.). Indeed, a very low threshold might be expected from a comparison of the results for Si and LiF: since the band gap energies E_{gap} differ by a factor of 12.5 (E_{gap} is 14 eV and 1.12 eV for LiF and Si, respectively [10]) a similar factor may be expected for the threshold velocities. Thus, from $v_{th} = 0.1$ a.u. for LiF [7], a threshold of 0.008 a.u. would result for Si. In contrast, when the valence electrons in Si are modeled as a Fermi gas, a threshold velocity of 0.02 a.u. is obtained [11], [12].

Partial support by the Austrian Science Fund (FWF) under Contract No. P19595-N20 is gratefully acknowledged.

References.

[1] R.H. Ritchie. Phys. Rev. 114, 3 (1959). pp 644-654.
[2] N.R. Arista and P. Sigmund. Phys. Rev. A 76, 062902 (2007).
[3] J.E. Valdés, G. Martínez Tamayo, G.H. Lantschner, J.C. Eckardt and N.R. Arista, Nucl. Instr. And Meth. B 73 (1993). pp 313-318.
[4] D. Primetzhofer. Private communication.
[5] S.N. Markin, D. Primetzhofer, M. Spitz and P. Bauer. Phys. Rev. B 80, 205105 (2009).
[6] J.E. Valdés, J.C. Eckardt, G.H. Lantschner and N.R. Arista. Phys. Rev. A 49, 2 (1994). pp 1083-1088.
[7] S.N. Markin, D. Primetzhofer and P. Bauer. Phys. Rev. Lett. 103, 113201 (2009).
[8] L.N. Serkovic Loli, E.A. Sánchez, O Grizzi and N.R. Arista. Phys. Rev. A 81, 022902 (2010).
[9] M. Draxler, S.N. Markin, S.N. Ermolov, K. Schmid, C. Hesch, A. Poschacher, R. Gruber, M. Bergsmann and P. Bauer. Vacuum 73 (2004). pp. 39-45.
[10] W.H.Strehlow and E.L.Cook, J. Phys. Chem. Ref. Data 2 (1973) 163.
[11] R.A. Baragiola, E.V. Alonso and A. Oliva-Florio. Phys. Rev. B 22, 80 (1980).
[12] J.R. Chelikowsky and M.L. Cohen, Phys. Rev. B 10, 5095 (1974).

P17 A study on hydrogen performance in high-*k* stacks by high-resolution ERDA

Ming Zhao[1], Shinji Nagata[1], Tatsuo Shikama[1], Kaoru Nakajima[2], Motofumi Suzuki[2], Kenji Kimura[2]

ming.zhao@imr.tohoku.ac.jp (corresponding author)

[1] *Institute for Materials Research, Tohoku University, Sendai 980-8577, Japan*
[2] *Department of Micro Engineering, Kyoto University, Kyoto 606-8501, Japan*

With a continuous decreasing in the thickness of high-*k* stacks along the advances of semiconductor process technology, negative bias temperature instability (NBTI) has shown its increasing influences in limiting the lifetime of electronic devices. NBTI occurs in *p*-channel MOS devices stressed with negative gate voltage at elevated temperature. It manifests as the absolute drain current I_{Dsat} decrease and the threshold voltage V_T increase. [1]

Currently, two major models have been proposed to explain NBTI. One explanation is referred as a "diffusion-limited" model in which H^+ diffuses to SiO_2/Si interface and reacts with Si-H traps to produce a silicon dandling bond and H_2. The other major explanation can be regarded as a "reaction-limited" model in which holes diffuse to SiO_2/Si interface and reacts with Si-H traps and neutral water-related species to produce H^+. In addition, some of the H^+ ions diffuse from the interface to the oxide layer. However, no explanation of NBTI is firmly accepted because there still lacks an observation of the diffusion of elements in the devices under the NBTI stress.

In this research, we have measured the hydrogen performance in high-*k* stacks by high-resolution elastic recoil detection analysis (ERDA) [2]. The influence of the different kinds of metal layer and the elevated temperature on the hydrogen distribution in metal/HfO_2/SiO_2/Si has been examined. Our results indicate that large amount of hydrogen has been introduced into Si substrate by the deposition of palladium layer.

We acknowledge the support of Japanese Society for the Promotion of Science (Grant-in-Aid No. 22760222). The authors are thankful to the Advance Research Center of Metallic Glasses of Tohoku University. Parts of this work were conducted in Kyoto-Advanced Nanotechnology Network, supported by "Nanotechnology Network" of the Ministry of Education, Culture, Sports, Science and Technology (MEXT), Japan.

References.

[1] Negative bias temperature instability: Road to cross in deep submicron silicon semiconductor manufacturing. Dieter K. Schroder, Jeff A. Babcock. Appl. Phys. Rev. 94(2003) pp 1-18.
[2] Accumulation of hydrogen near the interface between ultrathin SiO_2 and Si(100) under ion irradiation in high-resolution elastic recoil detection. Kaoru Nakajima, Ryo Imaizumi, Motofumi Suzuki, Kenji Kimura. Nucl. Instrum. Methods Phys. Res. Sect. B, 249(2006) pp 425-428

P18 A high-resolution ERDA and RBS facility

A.B. Kramchenkov[1], O.O. Drozdenko[1], V.L. Denisenko[1], V.Yu. Storizhko[1], H.D. Carstanjen[2]

akramchenkov@yandex.ru (corresponding author)

[1] – *Institute of Applied Physics, National Academy of Sciences of Ukraine, 40030, 58, Petropavlivska str., Sumy, Ukraine*

[2] - *Max Planck Institute of Metals Research, D-70569, 1, Heisenbergstrasse, Stuttgart, Germany*

In the Sumy Institute of Applied Physics, National Academy of Sciences, Ukraine we operate the analytical facility, based on the compact 2 MeV electrostatic accelerator (fig.1a) [1]. It consists of four analytical channels: ion luminescense, NRA, scanning nuclear microprobe [2] and high-resolution RBS channel (fig. 1b). Recently a new high-resolution ERDA and RBS channel with precision electrostatic spectrometer was constructed. First tests of the spectrometer are now being carried out.

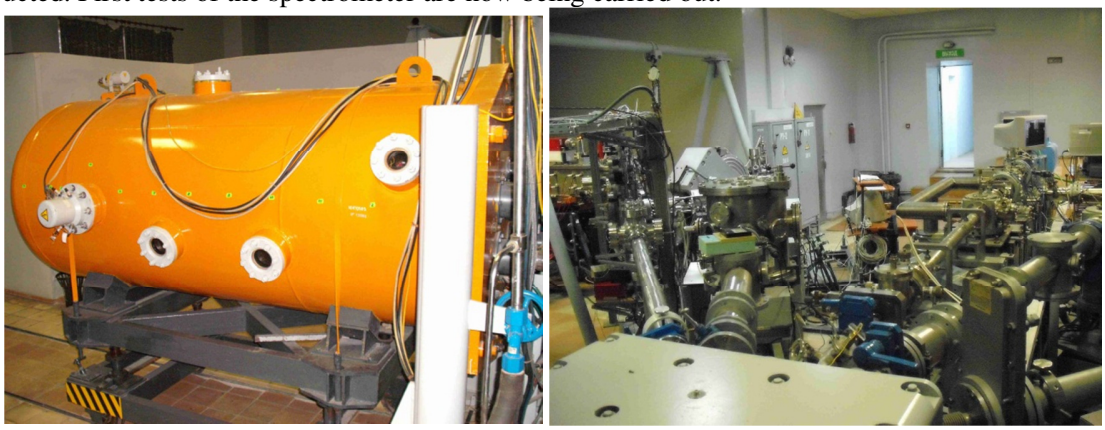

a b

Fig.1a 2 MV electrostatic accelerator. Fig. 1b Five analytical channels of the IAP NASU accelerator facility

A novel channel consists of beamline, scattering chamber and a precision electrostatic spectrometer transferred from the Max Planck Institute for Metals Research, Stuttgart, Germany. It was fully reconstructed and launched at our Institute. The spectrometer and the scattering chamber were adjusted to our beamline requirements. Vacuum, electric and electronic tests were carried out and several defects were repaired.

Beamline provides beam transport from the switching magnet of the microanalytical facility to the scattering chamber. Beam current is measured in front of the scattering chamber (not at the specimen, but before the beam entrance onto the chamber). After installation of the beamline, the scattering chamber and the electrostatic spectrometer in Sumy, laser and ion beam alignment were performed.

Scattering chamber is an improved serial vacuum chamber Varian VT-118 permitting to conduct experiments in ultra-high vacuum (up to 10^{-8} Pa). For ultra-high vacuum pumping the chamber is equipped with ion pumps and titanium sublimation pump, so organic contamination of specimen is excluded. On the top of the scattering chamber there is a 4-axis goniometer providing rotation and three-dimension translation of the specimen. In Sumy the scattering chamber was equipped with a new specimen holder, which allows several targets mounting to avoid frequent loss of vacuum. The electrostatic spectrometer can rotate about z-axis of the interaction chamber, so scattering angles between 0° and 135° are possible.

Electrostatic spectrometer consists of a cylinder type 100° electrostatic analyser (radius: 700 mm, gap width: 20 mm) and a system of electrostatic quadrupole lenses which focus ions emitted from the target parallel to the optical axis onto the entrance slit of the analyser. The analyzed ions are registered with a position sensitive Si-surface barrier detector. The maximum energy of the analyzed singly charged ions is

about 2 MeV. The relative energy resolution ΔE/E of the instrument is better than 3×10-4. For particle identification spectrometer is equipped with TOF system. General view of the spectrometer is presented on the fig. 3. In details the electrostatic spectrometer is described in reference [3].

Fig. 2 General view of the electrostatic spectrometer

The novel high-resolution ERDA and RBS channel is now being tested. In future it will be used for non-destructive hydrogen profiling in solids (construction materials of nuclear reactors, cryogenic materials, biological specimens etc.) by means of 2 MeV He primary beam. Also it may be used for heavy impurities detection in materials using high-resolution RBS and RBS(c) techniques. Blind flanges of the scattering chamber allow to install an X-ray detector, so the new facility becomes a universal instrument for material analysis with IBA techniques.

References.

[1] V.E. Storizhko, A.A. Drozdenko, V.I. Miroshnichenko, A.G. Ponomarev, Int. Conf. “Current Problems in Nuclear Physics and Atomic Energy”, Kyiv,Ukraine, 29.05.-03.06.2006, p. 165.

[2] V.E. Storizhko, A.G. Ponomarev, V.A. Rebrov, A.L. Chemeris, A.A. Drozdenko, A.B. Dudnik, V.I. Miroshnichenko, N.A. Sayko, P.A. Pavlenko and L.P. Peleshuk. Nucl. Instr. and Meth. B 260 (2007), pp 101 - 104.

[3] T. Enders, M. Rilli, H.D. Carstanjen, Nucl. Instr. and Meth. B 64 (1992) pp 817-824.

P19 A comparative study of ion beam based methods for compositional depth profiling of thin solid films

J. Jensen[(1)], S. Schmidt[(1)], A. Furlan[(2)], A. Hultqvist[(2)], H.J. Whitlow[(3)], T. Sajavaara[(3)], M. Laitinen[(3)], R. Kersting[(4)], D. Breitenstein[(4)], M. Fartmann[(4)], T. Grehl[(5)], and L. Hultman[(1)]

jejen@ifm.liu.se (corresponding author)

[1]*Thin Film Physics Division, IFM, Linköping University, SE-581 83 Linköping, Sweden*
[2]*Ångström Laboratory, Uppsala University, SE-751 21 Uppsala, Sweden*
[3]*Department of Physics, PO Box 35 (YFL) University of Jyväskylä, Jyväskylä 40014, Finland*
[4]*Tascon GmbH, Materials Characterisation, D-48149 Münster, Germany*
[5]*ION-TOF GmbH, D-48149 Münster, Germany*

As the functionality of thin solid films depends on their stoichiometry and impurity levels, a detailed compositional analysis is essential for many technological applications. The necessary qualitative or quantitative elemental depth profiling can be performed with a series of analytical techniques, all having their individual drawbacks and advantages.

In this contribution we present a comparison between the compositional analyses of various thin films performed using completely different techniques. The elemental depth profiles were obtained by (i) Time-of-Flight Elastic Recoil Detection Analysis (ToF-E ERDA) and Rutherford Backscattering Spectrometry (RBS), (ii) X-ray photoelectron spectroscopy (XPS) in combination with sputter depth profiling, (iii) Dynamic mode Secondary Ion Mass Spectrometry (ToF-SIMS), and (iv) Low Energy Ion Scattering (LEIS) using static and dynamic depth profiling.

The ToF-ERDA and RBS was performed using 6-40 MeV Cl and I ions as probing beams delivered from a tandem accelerator. XPS depth profiling was done with a PHI Quantum 2000 instrument using monochromatic Al Kα radiation as the probing beam and 2-4 keV Ar ions as the sputtering beam. ToF-SIMS was performed with an ION-TOF TOF.SIMS_5 instrument, using 25-30 keV Bi ions as the probing ions. Finally, the dynamic LEIS depth profiling was carried out with a Qtac100 instrument, using 5 keV He ions as the probing beam and 0.5-2 keV Ar ions as the sputtering beam. Similar to RBS in LEIS the energy of backscattered He ions is analysed, but at much lower energies. LEIS thus enable quantitative elemental analysis of the 1st atomic layer, in contrast to SIMS (which is not inherently quantitative) and XPS, which probes over larger depth.

The samples used in this comparative study were different oxides (e.g. ZnO), nitrides (e.g. CN_x) as well as diamond like carbon (DLC) thin films deposited on Si substrates. All films were grown by magnetron sputtering in an argon atmosphere using different precursor gases.

The methodology of the analytic techniques and their individual and complementary benefits will be discussed. For example the ability to obtain the main chemical composition and identify very low contaminations, the capability of analysing very thin films, in addition to their differences in surface sensitivity and interface resolution. Different features of film morphology and composition, which may influence the analysis, will also be addressed. Particularly, the importance of ion accelerators for calibration and reference materials enabling quantitative analysis with the smaller compact instruments is noteworthy.

P20 The study of the NiO/Au interface structural and electronic properties by MEIS, ab initio calculations and photoemission spectroscopy

A.Visikovskiy, K. Mitsuhara, M. Hazama, H. Yamada, Y. Kido

anton@fc.ritsumei.ac.jp (corresponding author)

Department of Physics, Ritsumeikan University, Kusatsu, Shiga-ken 525-8577, Japan

The role of the metal-oxide interface is an important topic in the field of heterogeneous catalysis. Catalytic activity of gold (Au) clusters is the one example [1]. Charge transfer and induced strain by the support are thought to have a large influence on catalytic properties of Au particles. It is, however, difficult to study the interface in these systems due to the insulating nature of the support and limited interface area. The reversed system, such as a layered oxide grown on the metal surface gives much more freedom for exploration. The layered NiO films on metals also presents interest for magnetic device application. The structure and electronic properties of NiO on silver have been studied extensively [2,3], however, we are not aware of such studies for Au substrate. Here we would like to present the combined MEIS, ab initio and photoemission study of properties of the NiO/Au interface.

We have prepared NiO(111)/Au(111)(10ML)/Ni(111) and NiO(100)/Au(100)(10ML)/Ag(100) with different thickness of NiO. The photoemission spectra show the higher binding energy shift of Au 4f core-level peaks for NiO/Au(100) system and none for NiO/Au(111). This is attributed to the difference in the interface structure of NiO grown on (100) and (111) metal surfaces. The bonding of Au atom with oxygen may results in a charge transfer producing the core-level shifts. We used high- resolution MEIS analysis to find which atoms – Ni or O are bonded to Au and the structure of the interface on (100) and (111) metal surfaces. The tetragonal distortion of the NiO(100) layers on Au(100) depending on the thickness also has been determined. The results have been further analyzed using ab initio calculations.

References.

[1] Catalysis by Supported Gold Nanoclusters. D.W. Goodman. Dekker Encyclopedia of Nanoscience and Nanotechnology. Edited by James A. Schwarz and Cristian I. Contescu, chapter 36, pp 611-620.

[2] Early Stages of NiO Growth on Ag(001) . M. Caffio, B. Cortigiani, G. Rovida, A. Atrei, and C. Giovanardi, J. Phys. Chem. B 108 (2004) pp 9919-9926.

[3] Ultrathin nickel oxide films grown on Ag(001): a study by XPS, LEIS and LEED intesity analysis, M. Caffio, B. Cortigiani, G. Rovida, A. Atrei, and C. Giovanardi, A. di Bona, S. Valeri, Surf. Sci. 531 (2003) pp. 368-374.

P21 A high depth resolution MEIS investigation of ultra thin STO/TiN layers on Si for DRAM MIM capacitors

J. A. van den Berg[1], M.A. Reading[1], P.C. Zalm[1], P. Bailey[2], T.C.Q. Noakes[2], C. Adelmann[3], M. Popovici[3] and H. Tielens[3].

j.a.vandenberg@salford.ac.uk (corresponding author)

[1]*Materials & Physics Research Centre, University of Salford, Salford, M5 4WT, United Kingdom*
[2]*STFC Daresbury Laboratory, Daresbury, WA4 4AD, United Kingdom*
[3]*IMEC. Kapeldreef 75, 3001 Leuven, Belgium*

The ongoing scale reduction in microelectronics is driving a renewed interest in high-k materials for metal-insulator-metal capacitors (MIMcap) in Dynamic Random Access Memory (DRAM) devices, not only in the form of planar but notably in high aspect geometries [1]. Because of its high electrical constant (k~150-300) and the ability to deposit good conformal thin layers by Atomic Layer Deposition (ALD) [2], $Sr_xTi_{1-x}O_y$ (STO) has emerged as a promising dielectric material. The application of TiN electrodes represents a low cost and more easily manufacturable alternative to Pt or Ru, previously investigated. Deposition and thermal processes have to be controlled in order to tailor the layer composition and thickness and especially to understand metal / dielectric interface effects.

The physical characterisation of these compound multi layers of a few nm thick, represents a considerable analytical challenge. Medium energy ion scattering (MEIS) combined with energy spectrum simulation has been applied to the STO/TiN layer system in view of its demonstrated capability of yielding quantitative information on the structure and composition of ultra thin layers with sub-nm depth resolution at the surface [3]. Factors that affect the quantification of MEIS information such as neutralization, Andersen correction and changing energy bin width across the energy spectrum have been assessed and the potential effect of an asymmetric energy loss function is considered.

Layer structures analysed included individual, 3 nm thick TiN and STO insulator layers (Sr rich and stoichiometric) on IMEC cleaned Si(100) as well as combinations of these layers, building up to a full MIMcap structure consisting of a 2 nm TiN top electrode, a 3 nm STO insulator layer and a 3 nm TiN bottom electrode. In particular the effect of annealing at 650°C in N_2 was investigated. MEIS conditions used were 100 keV He^+ ions in the double alignment configuration with the ion beam incident along the [-1-11] direction and the analyser aligned with the [221] direction, resulting in a scattering angle of 90°. For the full MIMcap structure these particular conditions yielded an energy spectrum having well resolved peaks for all layer constituents as shown in Figure 1.

Further to a determination of the composition and thickness of the layers investigated, which are in good agreement with HR-RBS results, MEIS studies have enabled the monitoring of interface behaviour, providing information on thermal processing and interface issues such as the effect of the TiN sputter deposition process, the near-surface Sr enrichment of the uncapped Sr rich STO

layer, Ti interdiffusion into the Sr rich STO upon annealing and the apparent higher thermal stability of the stoichiometric STO/TiN system against Ti diffusion.

References.

[1] J. A. Kittl et al., Microelectron. Eng. 86 (2008) 1789
[2] N. Menou et al., J. Appl. Phys. 106 (2009) 106
[3] M. A. Reading et al., J. Vac. Sci. Technol. B 28 (1), (2010) C65-70

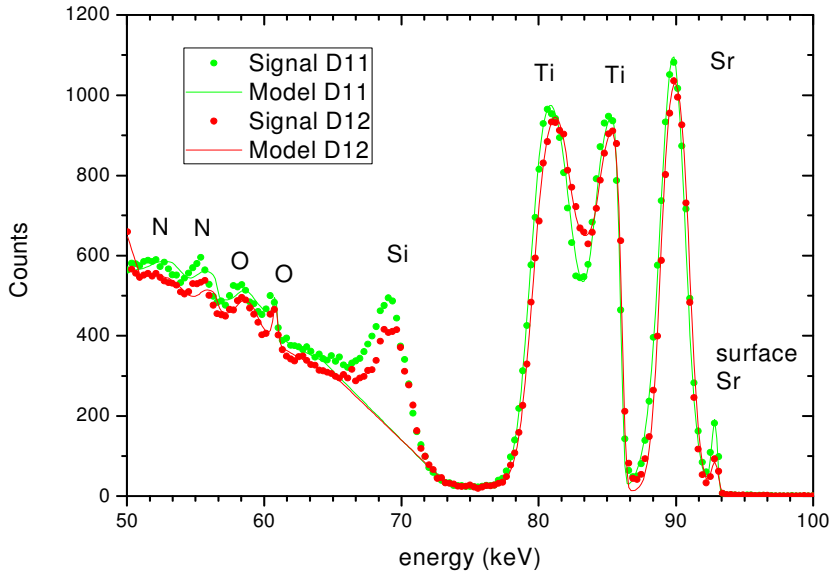

Figure 1. MEIS spectra taken using 100 keV He^+ ions scattered through 90° as well and model simulations of a full MIMcap structure consisting of a 2 nm TiN top electrode, a 3 nm stoichiometric STO insulator layer and a 3 nm TiN bottom electrode before (D11) and after (D12) annealing to 650° C in a N_2 atmosphere.

P22 Ion beam analysis of InAs quantum dots grown by epitaxy on a silicon substrate

D. Pelloux-Gervais[1], B. Canut[1], D. Jalabert[2], A. El Akra[1,3], H. Dumont[3], M. Gendry[3], C. Bru-Chevallier[1]

david.pelloux-gervais@insa-lyon.fr (corresponding author)

[1] *Université de Lyon ; Institut des Nanotechnologies de Lyon INL UMR5270 CNRS INSA de Lyon ; F-69621 ; FRANCE*

[2] *CEA/INAC/SP2M/LEMMA ; 17 rue des Martyrs ; F-38054 ; FRANCE*

[3] *Université de Lyon ; Institut des Nanotechnologies de Lyon INL UMR5270 CNRS Ecole Centrale de Lyon ; F-69134 ; FRANCE*

This work is part of a program which aims the realization of light emitting devices based on InAs quantum dots (QDs) inserted in a silicon matrix. Our contribution to this project is to perform ion beam analysis of the InAs/Si system using Rutherford Backscattering Spectrometry in Channeling geometry (RBS-C) and Medium Energy Ion Scattering (MEIS).

Random and aligned spectra of InAs QDs grown on a (001) silicon substrate by molecular beam epitaxy (MBE) and further encapsulated in silicon are displayed on Figure 1. From the random spectrum, one can state that the average QDs stoichiometry is $In_{0.3}As_{0.7}$ with an homogenous InAs equivalent thickness of 0.3 nm. The expected equivalent thickness value was 0.6 nm. A significant decrease of the As yield is evidenced in the spectrum recorded in channeling conditions along the [001] axis of the substrate, indicating that the major part of the As atoms are in epitaxial relation with Si. Nothing like this can be observed on the In contribution to the spectrum. We deduce from such results the synthesis of dislocated and stoichiometric InAs QDs. Because of some In atom exo-diffusion phenomena, the total amount of matter deposited is lower than expected and the remaining As atoms have spread into the silicon matrix, taking substitutional sites inside the Si crystal. This last effect is responsible for the channeling effect observed on the As signal. Similar observations have been reported by Komarov et al.[1] in InAs nanocrystals formed by sequential ion implantation.

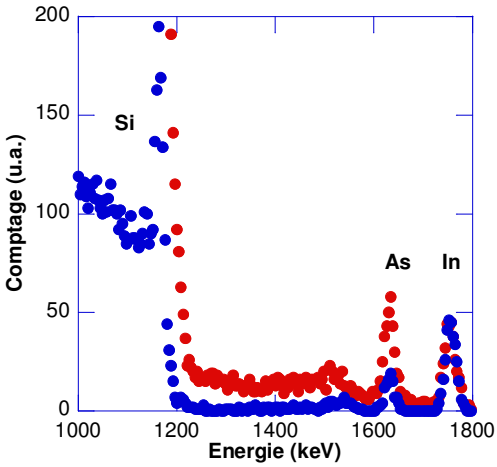

Figure 1: RBS spectra of a Si/InAs QDs/Si system acquired in random geometry (red) and in channeling conditions (blue). Analysis conditions: 2 MeV $^4He^+$; detection angle = 160°.

We aim to present also a comparative study of the QD crystalline quality depending on the amount of monolayer deposited. The Ga addition effect, in order to reduce the lattice mismatch, will be also discussed. The InAs QD system on Si was also characterized using MEIS, whose high depth resolution has made possible to obtain the chemical profile of the QD plane [2]. It will, in a near future, give informations about the strain state of the QDs [3].

References.

[1] Effect of implantation and annealing regimes on ion beam synthesis of InAs nanocrystals. F. Komarov et al. Lithuanian J. Phys. 49 (2009) pp 105-110.

[2] Composition profiles of InAs-GaAs quantum dots determined by medium energy ion scattering. P.D. Quinn et al. Appl. Phys. Lett. 87 (2005) pp153110.

[3] Anisotropic strain relaxation in a-plane GaN quantum dots. S.Founta et al. J. Appl. Phys. 101 (2007) pp 063541.

P23 Cross sections for medium energy He ions scattered from Ni, Hf and Au

Tomoaki Nishimura[1], Kei Mitsuhara[2], Anton Visikovskiy[2] and Yoshiaki Kido[2]

Corresponding author: t-nishi@hosei.ac.jp

[1] *Research Center of Ion Beam Technology, Hosei University, Koganei, Tokyo 184-8584, Japan*
[2] *Department of Physics, Ritsumeikan University, Kusatsu, Shiga-ken 525-8577, Japan*

The Ziegler-Biersack-Littmark (ZBL) potentials have been widely employed to calculate scattering cross sections in the low and medium energy regimes. We calculated the cross sections for medium energy He ions scattered from Si, Ni, Hf and Au atoms using the potentials derived from the Hartree-Fock-Slater wave functions (HF potential), which are compared with those calculated from Moliére, ZBL and Lee potentials, as shown in Fig. 1. It is clearly seen that there are significant inconsistencies between ZBL and HF potentials for heavy Au and Hf atoms. We prepared Ni(3 ML)/Au(5 ML)/Ni(10 ML)/SiC(0001) and Ni(5 ML)/HfO_2/Si(001) and measured the scattering cross sections for medium energy He^+ ions scattered from Ni, Hf and Au. The results are presented at this workshop.

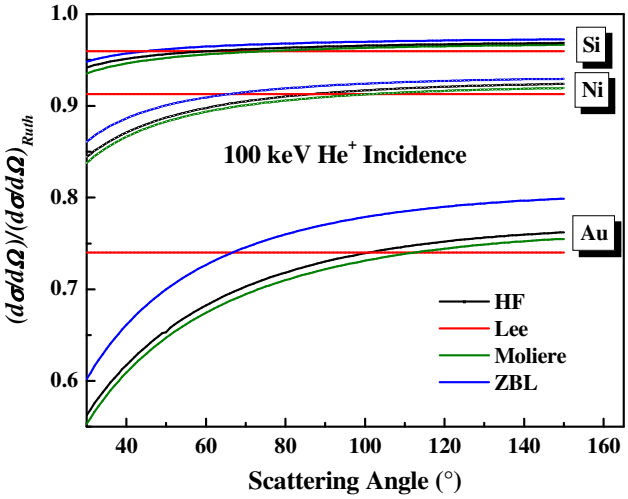

Fig. 1. Scattering cross sections calculated for 100 keV He^+ scattered from Si, Ni and Au, as a function of scattering angle. Black, red, green and blue curves correspond to HF, Lee, Moliére and ZBL potentials, respectively.

[1] J.F. Ziegler, J.P. Biersack and W. Littmark, *The Stopping and Range of Ions in Matter* (Pergamon, New York, 1985).

P24 New beam line for TOF-MEIS in Uppsala, Sweden.

M.K. Linnarsson[1], A. Hallén[1] and G. Possnert[2]

marga@kth.se (corresponding author)

[1] *Royal Institute of Technology, Lab of Materials and Semiconductor Physics, P.O. Box E229, SE-16440 Kista-Stockhom, Sweden*
[2] *Uppsala University, Ångström Laboratory, Dept. of Physics, Ion Physics, P.O. Box 534, SE-751 21 Uppsala, Sweden*

The successful story of MEIS (Medium Energy Ion Scattering) starts in the early 1970's at the FOM institute in Amsterdam. In the 1980's, the pioneering work at FOM results in an instrument commercialized by High Voltage Engineering in the Netherlands. These instruments, using toroidal electrostatic detectors, forms the basis for a large part of the MEIS equipment still used today. The early history of MEIS has been reviewed by van der Veen [1] However, different kind of electrostatic [1] as well as magnetic detectors has been developed [2]. In the mid 2000's, Kobayashi showed a useful way of utilize a time of flight spectrometer in combination with two-dimensional channel plates as detector [3,4].

A new beam line for MEIS has been set up at the Ångström laboratory, Uppsala University, Sweden. This MEIS system is based on a time of flight (TOF) concept [3] and consists of three major sections, the ion source including acceleration stage, the beam line with a chopper system and the experimental end station (scattering chamber). Scattering angle and energy of back scattered ions are then extracted from a time-resolved and position-sensitive detector.

As "ion source", a single stage, air isolated and high current (up to mA), 350 kV accelerator platform from Danfysik is employed. The ion source can be operated in three modes, gas, oven and sputter modes and, in principle, beams of all elements can be produced. However, in general for MEIS experiments hydrogen or helium is mainly utilized. The MEIS beam line is hanging from the ceiling to allow for passage underneath (se Fig.1). Starting from the switch magnet, the beam defining components are one Einzel lens, two sets of slits and one electrostatic quadruple lens. Furthermore, one set of x- and y-plates are included for beam steering. The first slits define the size and shape of the beam and the second slits forms the pulses in combination with another pair of x- and y- deflection plates. A sinus voltage is applied to the horizontal (x-) plates scanning the beam across the second slit. In addition, a gating voltage (countdown) is used switching the voltage from 300 V to 0 V on the vertical (y-) plates. The setup is configured to create pulse frequencies of 1, 1/2, 1/3 or 1/4 MHz. After the second slit, a drift tube buncher is placed to compress the ion packages. This compression will also introduce a variation in energy affecting the resolution. Before entering the scattering chamber, the beam line has a 7° kink to avoid neutrals hitting the sample.

The scattering chamber houses a 6-axis goniometer from Panmure [5], a solid-state detector and a delay line detector (DLD120) from Roentdek [6]. Both detectors can be moved along a circular path with a radius of 300 mm around the scattering point, so that different scattering geometries can be investigated. The main parts of the DLD120 detector are two micro- channel plates

(diameter 120 mm) and two delay-line anodes (x and y). A time-to-digital converter (TDC) is used for determine the flight time between a common start signal from a pick-up monitoring the pulse and the stop signal from the MCP. The combination of the detector and front-end electronics have a temporal resolution < 250 ps. The assignment of the position on the detector is made from the time difference of stop signals appearing at the two ends of each delay-line anode. The time resolution of the used TDC card is <100 ps giving a position resolution <50 μm and data acquisition speed is higher than 100 kHz. The solid angle subtended by the detector is 0.25 sr. The vacuum in the chamber is in the 10^{-10} Torr range. Furthermore, a turbo pumped load-lock is employed for fast samples changes.

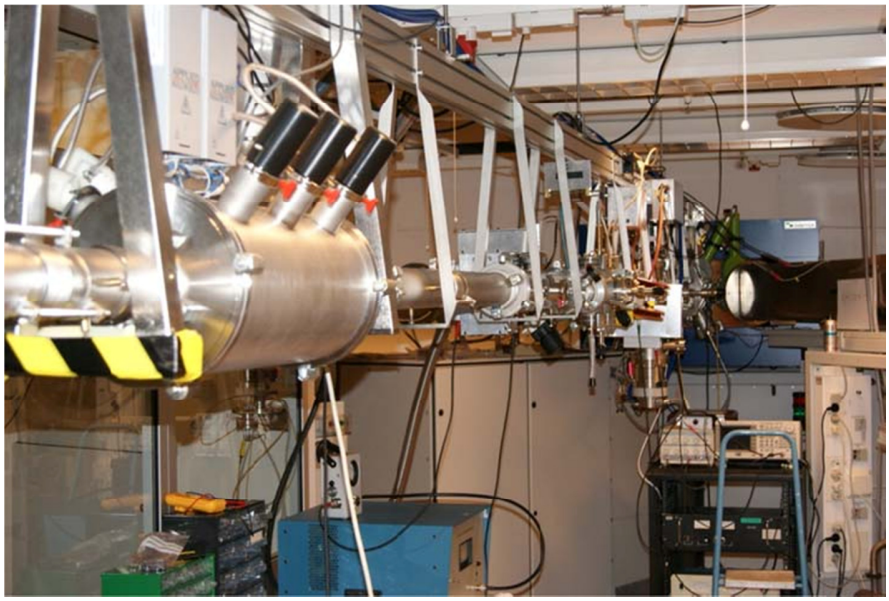

Fig.1. The MEIS Beam Line in Uppsala.

References.

[1] Ion beam crystallography of surfaces and interfaces. J.F. van der Veen, Surf. Sci. Rep. 5 (1985) pp 199-288.

[2] Monolayer analysis in Rutherford backscattering spectroscopy. K.Kimura, K. Ohshims and M. Mannami, Appl. Phys. Lett. 64 (1994) pp 2232-2234.

[3] Development of three-dimensional medium-energy ion scattering using a large solid angle detector. T. Kobayashi, Nucl. Instr. And Meth. B 249 (2006) pp 266-269.

[4] Medium-energy ion scattering spectroscopy with a position-sensitive and time-resolving detector. R. Andrzejewski, H. Baba, Y. Kuwahara and T. Kobayashi, Nucl. Instr. And Meth. B 269 (2011) pp 647-652.

[5] www.panmurescientific.com/

[6] www.roentdek.com

High-Resolution Depth Profiling

June 27th - 30th, 2011

Contents and Author Index

Contents

Author Index

HRDP6

	Monday	Tuesday	Wednesday	Thursday
08h00 - 8h45	*Registration*			
8h45-9h00	***Welcome***			
9h00 - 9h35	I1 Torgny Gustafsson	I4 Lyudmila Goncharova	I8 Wilfried Vandervorst	I10Chris Baddeley
9h35 - 10h00	O1 Primetzhoffer	O7 Deokar	O16 Ngo	O20 Sortica
10h00 - 10h25	O2 Bauer	O8 Py	O17 Meerschaut	O21 Sanchez
10h25 - 10h45	Coffee	Coffee	Coffee	Coffee
10h45 - 11h20	I2 Shutthanandan	I5 Anton Visikovskiy	I9 Esteban Sanchez	I11 Kenji Kimura
11h20 - 11h45	O3 Munnik	O9 Woodruff	O18 Itani	O22 Bailey
11h45-12h10	O4 Chan	O10 Jalabert	O19 Galtayries	O23 Moon
12h10-12h35	Lunch	Lunch	Lunch	Closing Remarks
12h35 - 14h00				Lunch
14h00- 14h35	I3 Didier Blavette	I6 Victor Etgens	***OUTING***	
14h35-15h00	O5 Thevuthasan	O11 Brongersma		
15h00-15h25	O6 King	O12 Goebl		
15h25-15h45	Coffee	Coffee		
15h45 - 18h00	Poster and Sponsor Session	I7 Tim Noakes O13 Bergmaier O14 Ganem O15 Hentz		
		20h00 International Committee Meeting	Gala Dinner	